Pre-Fix

System and Operational Learning Report

July 2024

Electricity Distribution

nationalgrid

Version Control

Issue	Date
1.0	15/07/2024

Publication Control

Name	Role
Greg Shirley – NGED Samuel Jupe – Nortech Andrew Forster – Nortech Mashood Tahir – Nortech	Authors
Paul Morris – NGED	Reviewer
Jennifer Woodruff – NGED	Approver

Contact Details

Email: Nged.innovation@nationalgrid.co.uk

Postal:

Innovation Team

National Grid

Pegasus Business Park

Herald Way

Castle Donington

Derbyshire DE74 2TU

Disclaimer

Neither National Grid, nor any person acting on its behalf, makes any warranty, express or implied, with respect to the use of any information, method or process disclosed in this document or that such use may not infringe the rights of any third party or assumes any liabilities with respect to the use of, or for damage resulting in any way from the use of, any information, apparatus, method or process disclosed in the document.

Contents

Contents

Executive Summary

In line with National Grid Electricity Distribution's (NGED's) robust governance processes, project lessons learned and successes were captured throughout the Pre-Fix project lifecycle. These were captured through a series of on-going reviews with stakeholders and project team members, and were shared in lessons learned dissemination events at the end of the project. This report details the learning captured throughout the development of the system and the operational trial.

The system development learning sections of this report covers:

- Device installation
- Defining and refining device settings
- Learning from the performance of the devices.
- Development of system features
- Common Disturbance Information Platform's (C-DIP) deployment pre-requisites

Key recommendations are given when considering device installation as well as provision of final device settings decided upon within the project.

The operational learning sections of the report covers:

- Performance in the Pre-Fault domain
- Performance in the Post-Fault domain
- Classification of events
- Time to failure predictions
- Verification of results

In-depth analysis of the C-DIP's current capabilities are provided, and extensive examples of the system's accuracy is given. The shortcomings of the system are explained, and the future development required to improve performance and confidence in the system for BaU roll-out is outlined.

Success using the system for both pre-fault and post fault use cases are given. The C-DIP has provided NGED with insight into concerns on the network including, cable anomalies, OHL tree contacts and damaged insulators. The report gives an overview of the processes that have been used to follow up on information gained and interventions that have been made possible through use of the C-DIP.

1. Introduction

In line with National Grid Electricity Distribution's robust governance processes, project lessons learned and successes were captured throughout the Pre-Fix project lifecycle. These were captured through a series of on-going reviews with stakeholders and project team members and were shared in lessons learned dissemination events at the end of the project. Pre-Fix lessons learnt are given in this report in two parts:

Part 1 (System Learning) covers the development of the C-DIP. This includes the required functionality of hardware and software components, and their inter-dependencies. This section also identifies the pre-requisites (such as the carefully considered and judicious selection of device settings to detect and transmit HV defect waveforms), which are needed to deliver operational outputs and benefits.

Part 2 (Operational Learning) covers the application and effectiveness of the C-DIP in determining fault/defect presence, fault/defect location and evolution of defects (pre-faults) to customer-interrupting faults (post-faults). This section of the report also includes avenues of further research identified during the trial phase of Pre-Fix.

The Pre-Fix project team produced two papers for the CIRED 2023 conference and disseminated these at the event. The two papers can be found at the following links:

DELIVERING THE BENEFITS FROM A COMMON DISTURBANCE INFORMATION PLATFORM

APPLYING MACHINE LEARNING TO POWER QUALITY SIGNALS TO DETECT COMPONENT FAILURE SIGNATURES AND PREVENT UNPLANNED HV OUTAGES

In addition, the outputs of Pre-Fix were also presented at the:

- CIGRE UK Conference on "The application of data analytics to enhance power system performance" (London), Friday 27th May 2023
- Ofgem, UKRI and Carbon Trust Workshop on "Market Access and Commercialisation" (On-line Webinar), Tuesday 18th July 2023
- NGED's 26-to-Zero Innovation Showcase event (ICE, London) on 8th February 2024.

Part 1: System Learning

Part 1 (System Learning) covers the development of the C-DIP system during field trials. This includes the required functionality of hardware and software components, and their inter-dependencies. This section also identifies the pre-requisites (such as the carefully considered and judicious selection of device settings to detect and transmit HV defect waveforms), which are needed to deliver operational outputs and benefits.

Learning has been identified by asking the following questions:

1. What worked well and should be repeated?
2. What did not work well and should be changed?

Wherever possible (within scope/time/budget constraints), changes were made during the course of the project as a result of the on-going learning process. However, where changes could not be made during the course of the project (due to scope/time/budget constraints), these have been captured as recommended changes for any follow-on projects by NGED or other GB DNOs.

Operational learning, relating to HV observations (the effectiveness of the system to determine fault/defect presence, fault/defect location and evolution of defects (pre-faults) to customer-interrupting faults (post-faults)) is contained in Part 2 (Operational Learning).

2. Common Disturbance Information Platform (C-DIP) System Overview

2.1. C-DIP Architecture

The conceptual architecture of the Common Disturbance Information Platform (C-DIP) is given in Figure 2.1. The C-DIP architecture was developed in-line with NGED's BaU system (iHost) for field device monitoring of HV and LV networks. iHost is utilised by NGED where it is not financially viable to install traditional Supervisory Control and Data Acquisition (SCADA) Remote Terminal Units (RTUs) to integrate devices directly by this mechanism to PowerOn (the control centre software for real time network management). iHost is NGED's SCADA Data Concentrator layer allowing for fleets of hundreds of hardware devices to be readily integrated using their onboard micro-RTU/modem functionality. The system uses input data from various hardware devices (such as Primary substation relays, Power Quality (PQ) monitors, Cable and Overhead Line Fault Passage Indicators (FPIs) and Autoreclosers) and other software systems (such as NGED's Geographical Information System (GIS) and Integrated Network Model (INM)). These datasets are processed to deliver HV distance-to-fault (D2F), HV distance-to-defect (also termed "pre-fault"), most likely faulted component and probable time-to-failure (giving operational staff insight into the time-to-fix - the urgency with which remedial action needs to be taken).

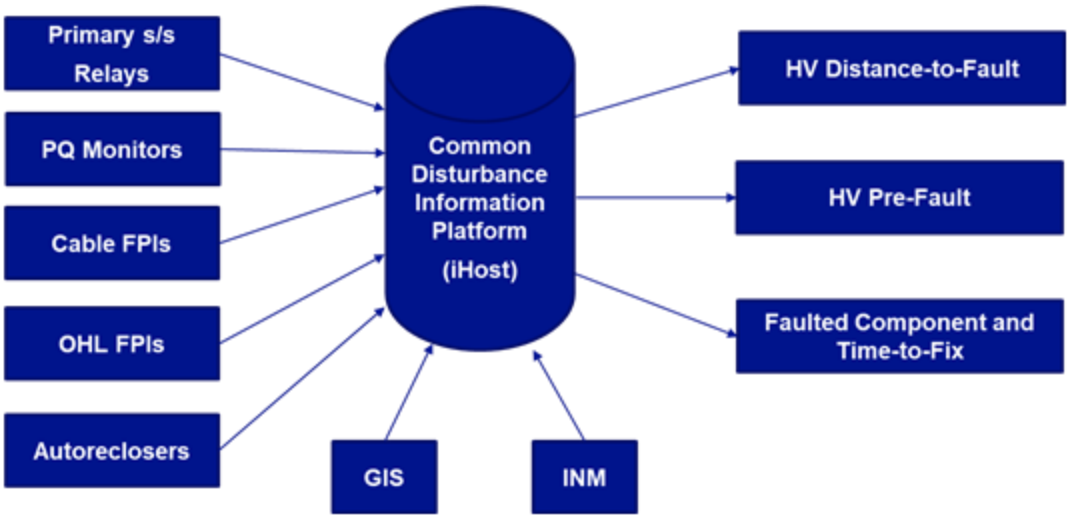

Figure 2.1 – Common Disturbance Information Platform (C-DIP) conceptual architecture

2.2. C-DIP Data Process Flow

The C-DIP data process flow is given in Figure 2.2. The hardware devices (as given in Figure 2.1) are configured to automatically record and transmit binary event and waveform capture data to the C-DIP, relating to network defects (no interruptions to customers) and post-fault events (resulting in interruptions to customers).

Figure 2.2 – Common Disturbance Information Platform (C-DIP) data process flow

The waveform and binary output data is processed to allow the user of the C-DIP to view raw waveforms and timelines of event sequences. As part of the C-DIP, the data from multiple devices on the same HV feeder are brought together, processed and grouped to give the user insight into the occurrence of defect or fault events across time horizons and the network geography. The HV devices are mapped manually onto GIS and subsequently grouped together. The waveform event data is processed to estimate distance-to-defect, calculate distance-to-fault and classify the most likely faulted component. The outputs are displayed to users for both planning decision-making (deciding on what pre-fault remedial action is needed) and operational decision-making (deploying staff more efficiently and effectively to field locations, post-fault, to restore supplies to NGED's customers).

2.3. C-DIP Data Process Flow

The C-DIP is a complex system with many dependencies on the input data integrity to deliver a trusted and actionable output. The dependencies map for distance-to-defect estimations is given in Figure 2.3.

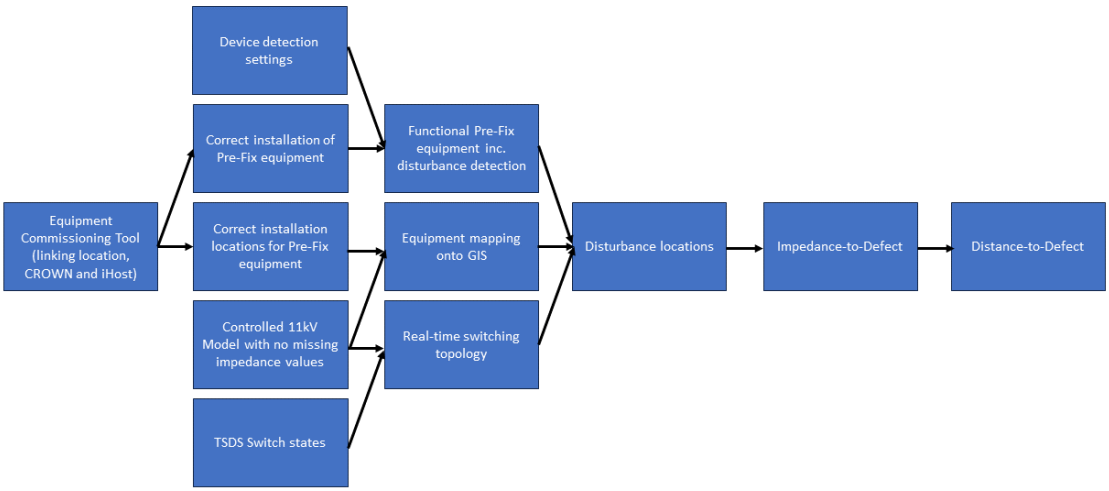

Figure 2.3 – Common Disturbance Information Platform (C-DIP) dependencies map

The dependencies map given in Figure 2.3, together with the C-DIP conceptual architecture given in Figure 2.1, can be used for functional/process gap analysis by other DNOs looking to adopt Pre-Fix as an HV fault intervention solution. Specific learning relating to each of the dependencies is given in Section 5 of this report.

3. C-DIP Devices

3.1. Device Hierarchy

The enabling hardware for Pre-Fix is a variety of devices that can be procured from different manufacturers. Different devices have different use cases within the Pre-Fix system, as described in Table 3.1

Device Category	Description	Examples
Category I / Class 1	Devices that can capture three phase current and voltage waveforms (at a suitable sampling rate) and broadcast the information in operationally useful timescales.	Protection Relays Power Quality Monitors
Category II / Class 2	Devices that can capture three phase current waveforms (at a suitable sampling rate) and broadcast the information in operationally useful timescales. (note, in the future, this could be expanded to devices that capture three phase voltage, but not current, waveforms such as LV monitors)	Smart FPIs such as OHL Smart Navigator 2.0 and the NX44 cable FPI devices
Category III / Class 3	Devices that are sensitive to current passage, voltage presence or circuit status, but do not capture waveforms, but can broadcast information in operationally useful timescales.	LV monitors Connected FPIs HV Autoreclosers

Table 3.1 - Pre-Fault device hierarchy

3.2. Device Installation

3.2.1. Site Selection

The sites selected for installation were in NGED's East Midlands and South West licence areas. The number of Primary substations selected for installation of Pre-Fix devices was based on the worst performing circuits in both areas as well as the number of devices purchased within the project.

The sites selected were based on availability of Current Transformers (CTs) and Voltage Transformers (VTs) within both transformer incomer and individual feeder breaker panels. For downstream monitoring of Ring Main Units (RMUs), sites where individual CTs are present were preferred. However, it was determined that within NGED's network, only around 25-30% of RMUs have individual CTs which limits installations of this type. Where core-balanced CTs are present, there is no possibility to monitor phase to phase activity, which is essential for pre-fault monitoring. Furthermore, during fault conditions, there is no way to determine which phase has been impacted.

At the start of the project, sites were selected where there was a 230V AC supply available within Primary substation feeder circuit breaker and transformer incomer circuit breaker panels which aimed to limit the impact on substation protection supplies. The power quality monitors used within this trial, PQubes, can be powered directly from 24V DC or from 230V AC or 110V DC with an additional power manager module. The cable FPIs used in the trial, NX44s, can be powered directly from 24V DC supply or also adapted to be powered from 230V AC or 110V DC supply. As will be discussed in later sections of the report, the preferred power supply for devices is now 110V DC or 24V DC to ensure no interruption to device power during certain fault conditions. To date only 230V AC and 110V DC supplies have been used within the Pre-Fix trial.

Under fault conditions, the CTs of feeder breakers may saturate (depending on fault current) whereas the CT's for transformer incomer breakers will not. It was also observed that transformer CT's were not sensitive enough to pick up pre-faults on individual feeders. Based on this information, cable FPIs (Class II device) were placed within the feeder breakers and power quality monitors were situated within the transformer breaker panel. As will be discussed in section 3.3, cable FPIs can be set to be more sensitive to pre-fault disturbances where CTs will not saturate. As a result, cable FPIs within feeder breaker panels were used to identify and measure pre-fault activity, while in the post fault domain could still provide binaries to indicate which feeder the fault had occurred on. The power quality monitors in the post fault domain are used to capture information for the fault and are utilised for distance to fault calculations.

3.2.2. Site Surveys

Site surveys were conducted for all sites where devices were installed. Throughout the trial a full list of pre-installation survey requirements was developed to include:

- Confirm adequate 4G Phone Signal
- Confirm required VT and CT connections can be accessed
- Confirm VT ratios
- Confirm CT ratios
- If multiple transformers were on site, confirm if they are running parallel or not.
- Confirm where communication antenna is or determine where it will be located
- Determine acceptable location for Class 1 and Class 2 devices within or near panels.

- Confirm acceptable route for cabling.
- Confirm type and location of power supplies for all devices.

Surveying sites prior to device installation is highly recommended to confirm that there is sufficient mobile coverage for device-to-C-DIP communications. Ensuring sufficient mobile coverage helps to improve/maintain the availability of devices contributing to C-DIP. Where signal strength at the device installation location is low, it is recommended that an external antenna is fitted and located to optimise mobile signal strength.

3.2.3. Installation Process

For the project trial Class 1 and Class 2 devices were installed. PQube power quality monitors were installed to monitor the transformer incomers and NX44s were installed to monitor the HV feeders. Additional Class 2 devices, NX44s and Smart Navigators were installed at strategic locations downstream on the HV feeders. The locations for these were selected to separate the HV feeders into manageable search zones. The number of these installed depended on the length and topology of the feeder being monitored and ranged from 1 up to 7 per feeder for the Pre-Fix trial.

Other Class 1 and Class 2 devices along with Class 3 LV monitors were tested during the project; however, these were not installed as part of the Pre-Fix trial. Details on the testing of other devices is given in more detail in later sections of this report.

In order to deliver a cost-effective solution, Class 1 Power Quality Monitors (PQMs) were installed on the secondary side of one (of two or three) Primary transformers. During the Pre-Fix trial, the team identified three different possible installation locations for PQMs (i) within transformer control panels; (ii) within switchgear riser panels; and (iii) within transformer 11kV circuit breaker panels.

The installations were carried out in accordance with the Standard Technique for Retrofit Power Quality Monitoring Equipment that was pioneered in NGED's fore-running project "Primary Network Power Quality Analysis". The PQM enclosures were magnetically mountable for ease of retrofit and installed in-line with NGED best practice (isolating power temporarily for safe installation). For optimal data acquisition, PQMs should be installed in panels where the three individual phase voltage and current signals are available.

The magnitude of monitored fault infeed was multiplied by the number of transformers running in parallel to represent the total fault infeed (for distance-to-defect calculations), meaning that only one Class I device was installed to monitor one transformer. This approach is appropriate and valid if the normal running arrangement of the Primary substation is with the Primary transformers running in parallel and assuming that the transformer infeeds are equal. However, if the transformers are not running in parallel, the fault infeeds need to be independently monitored (i.e. with the installation of two or more Class 1 devices).

The device installation architecture of Pre-Fix also deployed Class 2 devices (NX44s for the purpose of capability demonstration) into feeder breaker panels at the head end of each HV (11kV or 6.6kV) feeder, powered from the 110V DC supply integral to the panel. Introducing the capability of Class 2 devices to be able to clip onto the existing secondary wiring of CTs can significantly increase the number of sites where Class 2 devices can be retrofitted as well as reducing commissioning costs. This cost-effective approach allows the electrical current disturbances seen by the Class 1 device to be attributed to a particular feeder for circuit localisation and distance-to-defect assessments. This approach reduced the cost of installation to a point that is scalable across the network and removes any requirement to recommission circuit breakers. However, to establish the 110V DC supply to the devices, a short circuit outage was occasionally required. Utilising this approach meant that up to 3 NX44s could be installed in one day. For the purposes of the Pre-Fix trial, the field staff carrying out the retrofit installations favoured the mounting of the NX44, DC:DC power supply units and the fuse on the same magnetically-mounted board within the feeder breaker panel. This will be re-visited as part of wider

roll-out plans to integrate the 110V DC PSU within the NX44 and power multiple NX44s from a fused spur. An entirely new Standard Technique for Retrofit of Feeder Breaker Monitoring Equipment was pioneered as part of Pre-Fix.

It is recommended that for RMU sites where there is no automation, the NX44s are powered utilising the 230V AC supply. Where RMU automation is present, the NX44s should be powered from the 110V AC supply and as the CTs are already utilised for automation purposes, clip-on current sensors should be connected to the secondary automation wiring. At Primary feeder breakers, it is recommended that that NX44s are powered from the 110V DC supply.

Where the NX44s were powered directly from 110V DC supply, the back-up batteries were removed from the units to mitigate fire risk. Where NX44s were installed in downstream RMUs and external to the switchgear, the back-up batteries remained in place which ensured a better capture rate of pre-fault activity.

To ensure that future RMUs are readily able to be integrated to C-DIP, it is recommended that they are specified and procured with individual phase CTs on both switches.

3.2.4. Installation Issues

The OHL FPI's used within the trial have an optional setting of LED indicators when they experience fault current passage to aid operational staff in locating faults[1]. However, early on during the Pre-Fix trial, the NGED control room received several calls from customers about flashing lights on OHLs. As the control room was receiving notifications direct from the FPIs, the decision was made to turn-off the local LED indications to prevent unnecessary calls into the control room and instead rely upon the fact that these units would provide the information to the control room.

In order to optimise the device monitoring system through limiting as far as possible the noise in the signal-to-noise ratio and CT saturation, it is recommended that the Primary-side rating of the transducer is matched to the secondary CT ratio of the circuit/component being monitored (e.g. a 2000/5 CT in the substation is monitored using a 5A rated transducer and a 2000/1 CT is monitored using a 1A rated transducer). In addition, the cabling of the current sensors should be shielded to prevent noise contamination from other electro-magnetic compatibility (EMC) sources within the substation as this was found to cause unwanted device triggers, therefore filling up device memory buffers.

The starting premise of the device installations was to make use of feeder breaker relays for VT and CT availability. However, upon beginning the network installations it was found that the majority of HV feeder breakers were legacy electro-mechanical devices meaning that there were CTs present but no VTs in the electromechanical feeder breaker panels.

Regarding installation of Class 2 devices on RMUs, NGED's BaU process for monitoring is to retrofit a split-core core-balanced CT around all three conductors to detect residual out-of-balance current during earth fault conditions. This does not provide information as to which phase faulted and does not allow the earth fault waveform to be captured for distance to fault calculations or classification.

The use of three individual phase CTs was explored but was not included as many legacy RMUs do not have three individual phase CTs. This informed the requirement for retrofit FPIs to use clip-on current sensors at automation sites. Where possible, FPIs were installed at RMU sites using existing individual phase CTs. However, many of these were in non-optimal locations.

Significant health and safety risks and customer interruption risks associated with retrofitting split core CTs on individual RMU phases, as well as resource cost, meant that this was not taken

[1] The LED indicator feature of the OHL FPIs are intended in normal operation to provide a visual indicator to facilitate faster line patrols.

forwards as a viable option in the project. Therefore, the preferred method during the project was to utilise clip-on CTs.

It is possible for NX44 units to have an opposite polarity depending on which way around the manufacturer installed the CT's in the ring main units, if these are present. Whilst this can be rectified in the Pre-Fix software, it is recommended that there is a polarity check step during installation within RMUs.

For distance-to-defect assessments in earth fault conditions, it is vital that all three voltage signals (corresponding to L1, L2 and L3 respectively) are monitored. (In some legacy installations, the L2 phase is grounded and so the voltage signal corresponding to an earth fault on L2 is not able to be monitored). The recommendation in these instances is to install a Class 1 device with two-phase system and use Root Mean Square (RMS) voltage and current to calculate earth fault loop impedance (accepting the limitation that the instrumentation does not exist to capture earth fault waveforms on L2).

Throughout the trial, on a number of occasions, it was found that some devices were recorded against the incorrect feeder number or recorded as being installed in the incorrect location. This issue was experienced more for OHL FPIs. Therefore, a key recommendation resulting from Pre-Fix is the development of commissioning tools that support the robust capture and record keeping of metadata associated with device installations. The distance-to-defect assessment process builds on the foundation of being able to trust that data from device 'x' is representative of the location in which device 'x' is installed on the network. Any errors in equipment location records or equipment serial number records propagate through the analysis system and lead to errors and uncertainties in system outputs, such as distance-to-defect assessments.

3.3. Device Settings

3.3.1. Initial Settings

Based on pre-fault activity observed during the Pre-Fix project, the magnitude and duration of defects fall below the trigger settings of standard protection equipment on the network, meaning devices must be more sensitive to events than protection equipment. However, this needs to be balanced with not making the device so sensitive that it triggers consistently on minor waveform deviations during peak loading. This balance has been experimented with for both Class 1 and Class 2 devices.

Class I

Prior to Pre-Fix, the Class I power quality monitoring device (the PQube3) was designed to capture network disturbances based on voltage distortion triggers (this was, and still is, appropriate for harmonic/power quality assessment applications such as those specified in Engineering Recommendation G5/5). As part of Pre-Fix, the functionality of the PQube3 disturbance detection trigger was adapted to trigger on current, rather than voltage. This is because latent or evolving network defects exhibit an observable current signal disturbance that is not necessarily present in the corresponding voltage waveform signal.

A level of either 100A or ~5% of the Primary 1ph RMS break rating residual error for 10% of a cycle has been found to be a suitable level for class 1 devices. The sampling rate of the devices used needed to be sufficient to observe short distortions in waveforms and a sampling rate of 256 samples per cycle was sufficient for Class 1 devices. Sampling rates lower than these values were not tested.

Class II

At the beginning of the project FPIs were designed and configured to detect and indicate only when an actual fault or fault pick-up occurred and did not have the ability to detect pre-fault

activity. Before deployment on to the network, settings of both OHL and cable FPIs were adjusted to enable detection of pre-fault activity.

Cable FPIs before the project contained fault trigger elements that armed for waveform capture when a specified current threshold was exceeded and began waveform capture if the threshold was exceeded for a specified length of time.

For Pre-Fix, additional changes were made to these Cable FPIs settings, which included:

- New triggers with similar functionality to the existing fault trigger elements that can be configured for lower current thresholds (A) and minimum time durations (ms)
- New triggers that operate based on the difference in phasor currents from one cycle to the next. If the difference exceeds the configured threshold, the trigger will fire.
- New waveshape change triggers. Per-sample, the difference (error) between the magnitude of the sample for this cycle and the same sample from the previous cycle will be calculated, then the root mean square error between the two cycles is found.

OHL FPIs before the project began only reported a pickup when a certain current threshold was exceeded and reported a fault if the threshold remained exceeded for a certain length of time. In this way Earth Faults and Phase to Phase Faults were detected.

For Pre-Fix, additional changes were made to these settings, which included:

- 3 new triggers (I>, I>> and I>>>) that can be individually enabled and configured for lower current thresholds (A) and minimum time durations (ms) by remote configuration update.

It should be noted that the FPIs referred to here, are NX44s and SN2.0s. Other similar Class 2 FPIs or other devices may require different settings.

The pre-fault detection settings of Class 2 devices can be even more sensitive than Class 1 devices, as Class 2 devices will typically be installed in locations with a lower load current where it is easier to discriminate between pre-fault activity and natural load changes on the network. In this case, a 20A residual error between samples at the same point on the cycle has been a suitable trigger condition.

Initial trials using a 5A distortion for 25% of a cycle and using 25A inrush triggers to make the power quality monitor as sensitive as the feeder breaker Class 2 devices were unsuccessful. In times of peak loading, the normal power fluctuations of the network were enough to trigger captures that had no (pre-)fault condition. These were so frequent that they would fill the memory banks of the power quality monitor and prevent further captures from being made, causing some fault events to be missed.

For Class II devices, where the thresholds were reached for post fault, a post fault indication or binary is produced. Where the threshold settings for pre-fault activity were reached but the current or voltage measurements did not exceed the post fault thresholds, the event is classed as pre-fault with a pre-fault binary produced. These binaries facilitated the categorisation of the event as either pre-fault or post fault within the C-DIP, as discussed further in section 4.7.

It was found that a sampling rate of 32 samples per cycle was sufficient for Class 2 cable FPIs and 40 samples per cycle for OHL FPIs. Sampling rates lower than this have not been tested.

3.3.2. Settings Refinement

Class I

Following development and deployment, the use of current-based distortion triggers within the PQube3 led to enduring device communications (as device lock-ups from excessive waveform capture volumes were avoided) and this led to consistently reliable waveform captures for electrical current disturbances.

A waveform distortion trigger was therefore developed which compares each current waveform cycle with the previous one and triggers an event and a waveform capture when the residual error between the two cycles exceeds a certain value.

Class II

A key learning outcome from Pre-Fix was to use signal distortion-based triggers for waveform captures, rather than simpler magnitude-duration threshold crossing settings. The use of distortion-based triggers inherently filters out changes in electrical current signals as a result of natural network activity (for example, motor start-up or load shift) and focuses on the disturbance of the underlying power transfer waveform due to defective network equipment (cables, transformers, overhead lines and the associated integrity of their insulation). We have also learnt that overcurrent triggers fill up the memory buffers but triggers based on current and voltage distortion rather than overcurrent allows more discriminatory noise rejection.

For the purposes of Pre-Fix, the same set of configuration settings were applied to all devices of the same type (for example Cable FPIs or OHL FPIs) to ensure consistent behaviour across the population of devices and avoid the overhead of managing different device settings across the fleet of devices. Tailoring device settings, for example adjusting settings to make those devices electrically further from the Primary substation more sensitive to disturbances, would need to be balanced against the benefit and the increased overhead of specifying, applying and maintaining bespoke device settings.

This device sensitivity can be applicable to feeders of differing length but also differences in topology. It has been observed during the project trial that settings for OHL and cable networks may have to be different when compared to circuits of mixed OHL/Cable topology. To date during the project trial there has been insufficient data to fully understand the differences in accuracy of locating pre-fault events on purely OHL or cable circuits compared to circuits of mixed topology when using the same settings sensitivities.

The project has had success in capturing OHL pre-fault events including tree brushes/contact and sufficiently damaged insulators before they have progressed to failure. It should be noted that at this stage it is not clear as to what minimum device sensitivity is required to capture minor damage to insulators such as chips or hairline cracks. Further testing and analysis is required to understand what level of damage would cause concern operationally and therefore if device settings should be made more sensitive.

3.3.3. Verification of Value Stacking

One of the main aims of the Pre-Fix project, was to ensure that existing HV devices could be adapted to be utilised for detecting and recording pre-fault activity while maintaining their existing functionality.

It was shown that for the Class I devices used during the trial, PQubes, where the settings were adapted to trigger on a signal distortion basis for pre-faults, the existing functionality (i.e power quality monitoring) could not be maintained. However, with the more recent direct triggering method of Class I devices from Class II NX44s, where settings do not have to be altered, the existing power quality monitoring functionality can be maintained.

Cable and OHL FPIs were able to achieve value stacking. Settings were adapted for them to be able to trigger on waveform distortion and record pre-fault activity, while maintaining the ability to record and transfer post-fault binaries.

3.3.4. Final Settings and Recommendations

As part of Pre-Fix, a device settings philosophy document was produced to document recommendations and to specify required device functionality. This allows any third-party vendors, looking to align their product with the goals of C-DIP, to understand the specific requirements and device performance required.

The key recommendation from Pre-Fix is to use waveform distortion triggers in order to detect and capture all pre-fault activity. Figure 3.3.4.1 shows a typical pre-fault waveform (both current magnitude and duration) that is required to be captured using the correct device triggers. Ensuring the correct triggers are in place is essential to capture the necessary pre-fault data to inform the best action to take.

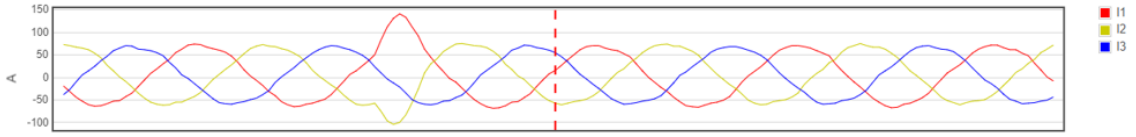

Figure 3.3.4.1 Typical Pre-Fault Waveform

The selection of device pre-fault settings requires a trade-off and needs to be made such that devices are sensitive enough to capture pre-fault activity but not so sensitive that device memory storage becomes overloaded and/or so much data is captured that a significant burden is put on the data processing requirements of C-DIP. Wherever possible, devices should be developed with the capability to pre-filter repetitive noise or underlying current harmonics so that triggers capture defect (pre-fault) events and it is only these events that are transmitted to C-DIP for system-wide processing.

Recommended present best practice is that COMTRADE files or other device waveform captures are transmitted in Combined COMTRADE file format (.cff) to avoid the header and data files being separated in transit and then not being able to be parsed within C-DIP for waveform visualisation and further analysis. During the Pre-Fix trial, where the header and data files were processed separately, a failure to parse issue was experienced resulting in some waveform captures not being visualised correctly within C-DIP. COMTRADE was selected for use in C-DIP for alignment with other power quality monitoring standards published by the ENA such as ERECs G99 and G5/5. It is acknowledged that emerging standards such as MQTT could provide an alternative communications protocol and transfer mechanism for waveform files as the use of this standard matures. It has also been recommended that the use of overcurrent or current in-rush (motor start-up) triggers be avoided due to avoid device memory being saturated. The device settings philosophy document outlines the preferred triggers for manufacturers to use.

Moreover, it is vital that each type of device (and the associated system architecture) is developed to support over-the-air firmware deployment and reconfiguration. This allows device settings to be adjusted without the need for time-intensive and cost-intensive site visits.

3.4. Device Performance

3.4.1. Pre-Fault

The functionality of C-DIP was enhanced to analyse the harmonic content of waveform captures and thereby distinguish genuine pre-fault activity (such as cable pecks, tree branch brushes) from noisy signals (as a result on an underlying power quality issue or where signal-to-noise ratios were too low to distinguish sensor signal from noise). High harmonic content on current waveforms would have resulted in high rates of waveform captures resulting in device memory being filled and therefore potentially missing genuine pre-fault activity. Using this filtering technique, a population of 10,000 waveform captures was reduced to 3,000 meaningful waveforms for further analysis. The waveforms were independently checked for validation and confirmation that the filtering algorithm was behaving as expected. Of the 129 feeders monitored, 10 were found to exhibit

significant power quality / high noise-to-signal ratios and so these were excluded from automated data processing and analysed offline post-event. The cause of this noise is still under investigation and once determined will be considered in recommendations for device settings. Further analysis will be taken to understand what the issue is and if this can be solved at source or if it something that the C-DIP system will have to handle. It is recommended that the source of all noise is accounted for and filtered out to allow for real time analysis of all pre-fault activity.

During the trial, we have also witnessed on 5 occasions where Class I devices (i.e PQubes) across all Primary distribution sites being monitored, have triggered during faults on higher voltage networks, once during a fault on the 33kV network and four times during a fault on the 132kV network. On all occasions we have seen both the current and voltage waveforms be disturbed on the 11kV network suggesting that the 11kV network may be contributing to the fault infeed of these events. The level of disturbance on the current and voltage waveforms at each of the Primary sites varies depending on the proximity to the fault location on the higher voltage networks. Further analysis is planned to understand how these faults impact interaction between the various voltage levels. One key learning point from this, is that these events are discounted from analysis of pre-fault activity of the HV feeders. This could be achieved automatically if the Pre-Fix system is integrated with wider NGED systems, where real time switching/protection operation can be accounted for or ensuring that the Pre-Fix system can analyse these events by comparing the voltage and current characteristics during the upstream fault. The best method to discount these upstream events from pre-fault analysis will be determined during future C-DIP development activity.

3.4.2. Post-Fault

During the project trial, it was observed that when a fault occurred which was close the Primary substation or phase to earth in nature, the PQube device's 230V AC supply was interrupted. As a result, during these events, the PQube was not able to record and a distance to fault calculation was not possible. To overcome this, the recommendation in the context of the installation of Class 1 devices is to power them from the 110V DC uninterruptible power supply of the Primary substation.

Direct triggering of the Class 1 (PQube) from Class 2 devices (NX44s) was tested in Q4 2023 along with the supply of the devices from an 110V DC supply to prevent the loss of data during phase to earth faults. Based on early installations, the time taken for this installation method is 1 day to install 1 PQube and 2-3 NX44s.

The direct trigger solution is achieved by a cross-trigger pilot wire that runs between Class 2 devices in the feeder breaker panel and Class 1 devices located on the transformer incomer(s). In this context, Class 2 devices need to have the functionality to send a binary output signal to Class 1 devices (with a binary state change on Class 2 device disturbance capture) and for the corresponding Class 1 device to have the capability of triggering a disturbance capture from a binary input signal received. Since Class 1 devices are installed (as previously noted) on one of several parallel infeeds, this also overcomes the limitation that the Class 1 devices only see ½ of the fault infeed contribution (or 1/x of the fault infeed, where x is the number of transformers running in parallel) and therefore they need to be configured to be more sensitive. This, in turn, can lead to challenges in the device discriminating between defects and natural network activity (such as load fluctuations) which ultimately results in unwanted and unnecessary additional waveform captures.

3.5. Device Functional Specifications and Integration Blueprint (for third party devices)

A fundamental premise of Pre-Fix was to design the C-DIP in such a way that third party devices could be integrated to stack value on top of existing equipment and its existing functionality.

As part of Pre-Fix, Powerside PQube3 Power Quality Monitors, Horstmann Gmbh Smart Navigator 2.0 overhead line FPIs and Nortech NX44 cable FPIs have all been integrated into the C-DIP to demonstrate the pre-fault and post-fault analysis capabilities of the platform with Class 1 and Class 2 device types.

In addition to this, compatibility of C-DIP has been tested with LV monitors (Category III) and demonstrated on the bench with three different types of HV technologies: (i) Siemens' SIPROTEC relay (Class 1); (ii) Schneider T300 Ring Main Unit (Class 1); and (iii) Schneider's ADVC3 autorecloser (Class 3). Further bench testing was completed on the Schneider T300 RMU, to determine if the existing settings would be sufficient for both pre-fault and post-fault waveform capture purposes. While it was found that based on existing settings that the T300 could detect and capture multicycle pre-fault disturbances as well as post-fault events, it is not able to capture sub-cycle pre-fault disturbances. The testing has informed what alterations would be required to the device in order to make it C-DIP ready. The testing report for the Schneider T300 RMU is given in Appendix A.

As mentioned before, the project has produced an equipment settings philosophy document which outlines setting requirements for capture devices as well as laying out the expectations for third-party vendors wishing to enhance the functionality of their equipment. This would allow further devices to be compatible with the philosophy of Pre-Fix and be 'C-DIP-ready'. As part of Pre-Fix, the enhancement and adaption of equipment functionality was demonstrated by Powerside, the vendor of the PQube3 power quality monitoring equipment. In this case, the functionality of the PQube3 was enhanced to deliver electrical current distortion-based triggers (rather than overcurrent triggers or voltage distortion-based triggers). This meant the PQube3 was more readily able to discern and distinguish between natural load changes on the network and disturbances due to pre-fault network activity. Learning captured regarding the embodiment of the settings design philosophy is given in Section 5.1.

4. C-DIP Features

This section of the report describes key aspects of the work carried out in Pre-Fix in order to act as a best practice guide and knowledge transfer mechanism for any DNOs looking to replicate the C-DIP and its rich feature set. The basis of the C-DIP development and features was the C-DIP technical specification which can be found on the Pre-Fix project website.

4.1. Device Data Ingestion

The enabling hardware for Pre-Fix is a variety of Pre-Fix-compatible devices that can be procured from different manufacturers. Different devices have different use cases within the Pre-Fix system, as described in Table 4.1.

Table 4.1 - Pre-Fault device hierarchy

Device Category	Description	Examples
Category I / Class 1	Devices that can capture three phase current and voltage waveforms (at a suitable sampling rate) and broadcast the information in operationally useful timescales.	Protection Relays Power Quality Monitors

Category II / Class 2	Devices that can capture three phase current waveforms (at a suitable sampling rate) and broadcast the information in operationally useful timescales. (note, in the future, this could be expanded to devices that capture three phase voltage, but not current, waveforms such as LV monitors)	Smart FPIs such as Smart Navigator 2.0 and the NX44 devices
Category III / Class 3	Devices that are sensitive to current passage, voltage presence or circuit status, but do not capture waveforms, but can broadcast information in operationally useful timescales.	LV monitors Connected FPIs HV Autoreclosers

4.2. Third Party Device Integration

A fundamental premise of Pre-Fix was to design the C-DIP in such a way that third party devices could be integrated to stack value on top of existing equipment and its existing functionality.

Illustrative waveforms demonstrating the compatibility with third party devices are given in Figures 4.2.1 and 4.2.2 for Powerside's PQube3, Siemens' SIPROTEC relay and Schneider T300 Automation RMU respectively. In this particular example, ingestion of SIPROTEC relay waveforms allowed for the system to separate what initially appeared as a phase-to-phase fault (when observed from the transformer incomer) into two simultaneous phase-to-earth faults (when observed from a relay) for analysis.

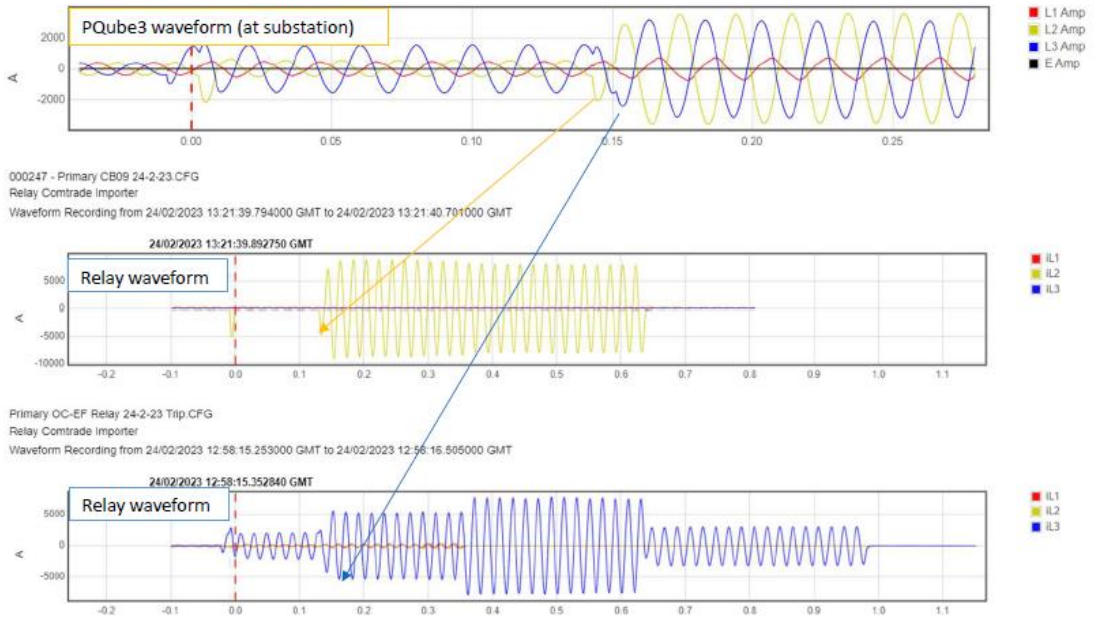

Figure 4.2.1 – Third Party Device Integration within C-DIP (Powerside PQube3 and Siemens SIPROTEC relay)

Figure 4.2.2 – Third Party Device Integration within C-DIP (Schneider T300 RMU Automation)

The ability of relays to provide waveform disturbance data into C-DIP platform is shown in more detail within the technical paper 'Delivering the benefits from a common disturbance information platform to prevent unplanned outages', published in CIRED 2023.

Relays need to fit into (or replace) existing 11kV panels within the Primary substation to monitor the 11kV data feed from 33/11kV transformers. The relays trigger on network disturbances to record waveforms associated with fault and pre-fault activity. Where the capability exists, relays need to generate and remotely communicate to PowerOn impedance-to-fault information. To date, we have shown how COMTRADE files can be manually extracted from existing relays and uploaded onto the C-DIP. As part of work streams separate to Pre-Fix, NGED engineers are considering the development of the digital substation that would enable this type of transfer.

As mentioned previously, only the PQube, NX44 and SN2.0 devices were fully integrated into the C-DIP to provide pre-fault and post-fault data.

4.3. HV Network Model Ingestion

The Single Line Diagram (SLD) feature within the C-DIP, embedded fundamental building blocks for the operational use of the system by ingesting NGED's HV models (in SINCAL[2] source format). This allows users to interact with the SLDs to mark-up locations as a planning tool for the escalation fit of equipment. The SLD data (combined with topological and coordinate data) also acted as the fundamental building block allowing users view geographical plots of potential defect locations, automatically generated post-fault fault flow (based on FPI alarms and distance-to-fault estimations) and automatically generated distance-to-fault network location estimations. The SINCAL model ingestion and conversion process is shown in Figure 4.3.

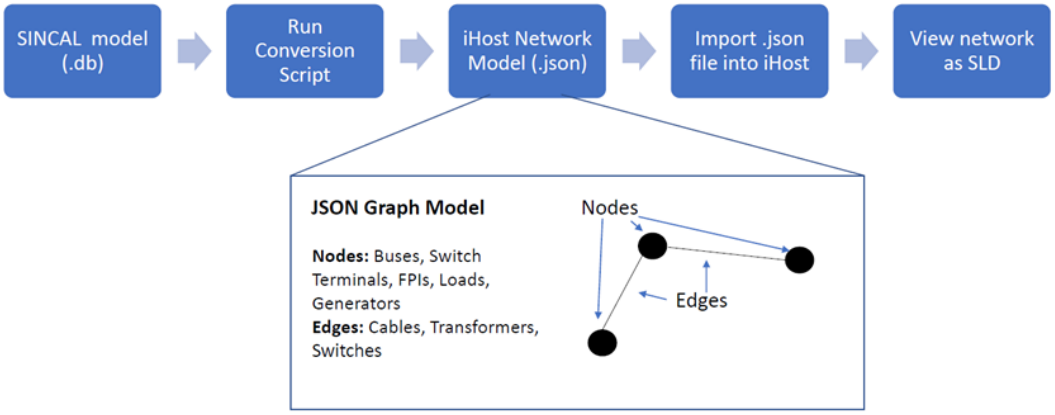

Figure 4.3 - The SINCAL model ingestion and conversion process

At the beginning of the Pre-Fix project, the intention was to utilise the Integrated Network Model (INM)[3] to determine network impedances and real time network topology. However, as the model was not going to be sufficiently developed in the timescales that the project required the decision was made to utilise SINCAL models, the chosen format for NGED's 11kV models. The main use for these models is in network design studies, such as fault level studies.

Some initial issues were discovered with the SINCAL models when converting them to a format suitable for use within the C-DIP. The cable radii within the SINCAL models were defined through a derivative methodology resulting in a number of excessive nodes which would have been difficult to represent correctly within the C-DIP single line diagrams as well as attributing suitable impedances to these small sections. Therefore, an algorithm was developed to cleanse these radii nodes to represent the network correctly.

Where no impedance information was available for circuit sections within the SINCAL models, a zero impedance was attributed to that section rather than assuming an average impedance based on other circuit sections. This would have caused inaccuracies within both the distance to defect and distance to fault predictions. Therefore, where sections of zero impedances were present, an average impedance was assigned. Later releases of SINCAL models have seen the data quality improve within models.

However within later models, a change in the geographical database was observed which caused a shift of approximately 100m when the models were ingested into the C-DIP. This was manually corrected but this is something that should be considered when selecting model formats to be used.

---

[2] PSS Sincal – power system planning and analysis software developed by Siemens
[3] The INM merges data from NGED's PowerOn network model, GIS and Asset Register (CROWN)

Another limitation of the SINCAL model format is that network switching points are not present. As a result, when network reconfigurations take place, pre-fault activity may be missed or assigned to the incorrect feeder. If any backfeeds are in place, without real-time switching statuses, the impedance to defect calculations may mean that the location would be incorrect. Integration of switch locations and real time statuses into C-DIP is planned for future improvements of the system.

It is recommended that where available the Integrated Network Model should be used, however the pre-fix trial has shown that using SINCAL HV network models can produce accurate results and useful insights although manual checks are required to ensure the accuracy of the models are sufficient for use in both pre-fault and post-fault calculations.

4.4. Device Activity Report

The C-DIP allows user-defined reports to be generated. One such report – the Device Activity Report – proved to be a powerful tool for gaining insight into the level of pre-fault and post-fault activity across the HV feeders within the trial networks. An illustration of the Device Activity Report output is given in Figure 4.4. For each class of device that saw activity within a user-defined period, the report returned the type of device, its serial number, network location, communications health status and the number of events (binaries and waveforms) recorded. This dataset could then be used as the basis for further analysis to determine the criticality of HV feeders (for example, ranking them by total number of events recorded during a given period).

	A	B	C	D	E	G	H	K
1	Device Type	Device Serial Number	Substation Name	Group Name	Group Path	Comms Late	Last Communication	Number of Event Recordings (B
23	NX44	50442561	930047_Walsgrave_08_NX44	8	East Midlands/Coventry 132kV/Coventry North 33kV/930047 - Walsgrave/8	N	01/03/2023 00:59:55	21
25	NX44	50442560	930047_Walsgrave_05_NX44	5	East Midlands/Coventry 132kV/Coventry North 33kV/930047 - Walsgrave/5	N	28/02/2023 05:47:59	17
26	NX44	50442567	930047_Walsgrave_09_NX44	9	East Midlands/Coventry 132kV/Coventry North 33kV/930047 - Walsgrave/9	N	28/02/2023 20:37:29	15
27	NX44	50442493	940040_Sandy Lane_13_NX44	13	East Midlands/Coventry 132kV/Coventry North 33kV/930040 - Sandy Lane/13	N	28/02/2023 17:45:14	12
28	NX44	50442550	940040_Sandy Lane_15_NX44	15	East Midlands/Coventry 132kV/Coventry North 33kV/930040 - Sandy Lane/15	N	28/02/2023 11:23:26	11
29	NX44	50442737	930048_Claverdon_04_NX44	4	East Midlands/Warwick 132kV/Warwick 33kV/930048 - Claverdon/4	N	28/02/2023 20:47:13	11
30	NX44	50442673	930041_Spon Street_04_NX44	4	East Midlands/Berkswell 132kV/Coventry South 33kV/930041 - Spon Street/4	N	28/02/2023 08:48:48	10
31	Smart Navigator 2.0	46386	34TB25_SN2	18	South West/306005 - Exeter Main SGP/340001 - Newton Abbot BSP/340011 - Chudleigh Knighton/18	N	01/03/2023 00:59:49	8
32	NX44	50442804	930041_Spon Street_14_NX44	14	East Midlands/Berkswell 132kV/Coventry South 33kV/930041 - Spon Street/14	N	28/02/2023 03:38:46	7
33	Smart Navigator 2.0	46404	34CAH1_SN2	11	South West/306005 - Exeter Main SGP/340001 - Newton Abbot BSP/340011 - Chudleigh Knighton/11	N	01/03/2023 00:59:51	6
34	Smart Navigator 2.0	46428	34CD18_SN2	11	South West/306005 - Exeter Main SGP/340001 - Newton Abbot BSP/340011 - Chudleigh Knighton/11	N	01/03/2023 00:59:44	6
35	NX44	50442558	930047_Walsgrave_18_NX44	18	East Midlands/Coventry 132kV/Coventry North 33kV/930047 - Walsgrave/18	N	28/02/2023 21:48:38	4
36	Smart Navigator 2.0	46410	31NN1_SN2	24	South West/306005 - Exeter Main SGP/310001 - Exeter City BSP/310016 - Folly Bridge/24	N	28/02/2023 22:20:33	4
38	NX44	50442552	940040_Sandy Lane_11_NX44	11	East Midlands/Coventry 132kV/Coventry North 33kV/930040 - Sandy Lane/11	N	01/03/2023 00:18:46	2
39	NX44	50442735	930048_Claverdon_03_NX44	3	East Midlands/Warwick 132kV/Warwick 33kV/930048 - Claverdon/3	Y	08/02/2023 08:20:55	2
40	Smart Navigator 2.0	46407	31BF1_SN2	23	South West/306005 - Exeter Main SGP/310001 - Exeter City BSP/310016 - Folly Bridge/23	N	01/03/2023 00:59:55	2
41	NX44	50442551	940040_Sandy Lane_07_NX44	7	East Midlands/Coventry 132kV/Coventry North 33kV/930040 - Sandy Lane/7	N	28/02/2023 19:09:21	1
42	NX44	50442478	930045_Whitley 11kV_06_NX44	6	East Midlands/Coventry 132kV/Whitley 33kV/930045 - Whitley 11kV/6	N	28/02/2023 12:51:07	1
43	NX44	50442479	930045_Whitley 11kV_07_NX44	7	East Midlands/Coventry 132kV/Whitley 33kV/930045 - Whitley 11kV/7	N	28/02/2023 06:07:35	1
44	Smart Navigator 2.0	46398	31NN47_SN2	24	South West/306005 - Exeter Main SGP/310001 - Exeter City BSP/310016 - Folly Bridge/24	N	01/03/2023 00:59:48	1
45	NX44	50442541	930031_Cox Street_10_NX44	10	East Midlands/Berkswell 132kV/Coventry Central 33kV/930031 - Cox Street/10	Y	12/01/2023 02:29:21	0
46	NX44	50442537	930031_Cox Street_11_NX44	11	East Midlands/Berkswell 132kV/Coventry Central 33kV/930031 - Cox Street/11	Y	04/01/2023 14:54:05	0
47	NX44	50442546	930031_Cox Street_12_NX44	12	East Midlands/Berkswell 132kV/Coventry Central 33kV/930031 - Cox Street/12	Y	14/02/2023 09:26:49	0
48	NX44	50442543	930031_Cox Street_13_NX44	13	East Midlands/Berkswell 132kV/Coventry Central 33kV/930031 - Cox Street/13	Y	12/02/2023 20:02:26	0
49	NX44	50442540	930031_Cox Street_14_NX44	14	East Midlands/Berkswell 132kV/Coventry Central 33kV/930031 - Cox Street/14	Y	05/01/2023 05:29:42	0
50	NX44	50442547	930031_Cox Street_15_NX44	15	East Midlands/Berkswell 132kV/Coventry Central 33kV/930031 - Cox Street/15	Y	15/08/2022 16:56:17	0
51	NX44	50442538	930031_Cox Street_16_NX44	16	East Midlands/Berkswell 132kV/Coventry Central 33kV/930031 - Cox Street/16	Y	21/01/2023 15:35:05	0
52	NX44	50442545	930031_Cox Street_03_NX44	3	East Midlands/Berkswell 132kV/Coventry Central 33kV/930031 - Cox Street/3	Y	07/02/2023 02:45:12	0
53	NX44	50442548	930031_Cox Street_04_NX44	4	East Midlands/Berkswell 132kV/Coventry Central 33kV/930031 - Cox Street/4	Y	22/12/2022 13:00:46	0
54	NX44	50442542	930031_Cox Street_05_NX44	5	East Midlands/Berkswell 132kV/Coventry Central 33kV/930031 - Cox Street/5	Y	12/02/2023 00:19:47	0
55	NX44	50442533	930031_Cox Street_06_NX44	6	East Midlands/Berkswell 132kV/Coventry Central 33kV/930031 - Cox Street/6	N	28/02/2023 17:37:30	0

Figure 4.4 – Automated email report which outputs a .csv file to aid identification and location of feeders hosting anomalies

The device activity report aids the user in understanding the overall performance of the system as well as the overall health of the circuits under observation. Through regular reports, the communication status can be checked across the population of devices either by individual devices or for a Primary substation. This report gives a view to which circuits have had an increase in activity within any given period. This will aid in any decisions for escalation fits of additional equipment, such as OHL FPIs, in order to further refine the source of the activity.

The device activity report is also used to inform the pre-fault wireframe report, where anomalies on feeders are identified and ranked based on key indicators and to highlight anomalies that are progressing in severity and criticality. This wireframe report is described in more detail in section 4.14 and its use is discussed in section 6.

It is also now forming the basis of an OHL feeder watchlist, which is giving NGED helicopter patrols strategic and tactical HV circuits to survey for defect detection confirmation. The use of this watchlist and the results from OHL pre-fault analysis is discussed in section 8.

4.5. Device Health Report

The Device Health Dashboard feature is illustrated in Figure 4.5. This gives business users insight into the communications health of the fleet of devices contributing to the automated analysis and decision-informing within C-DIP.

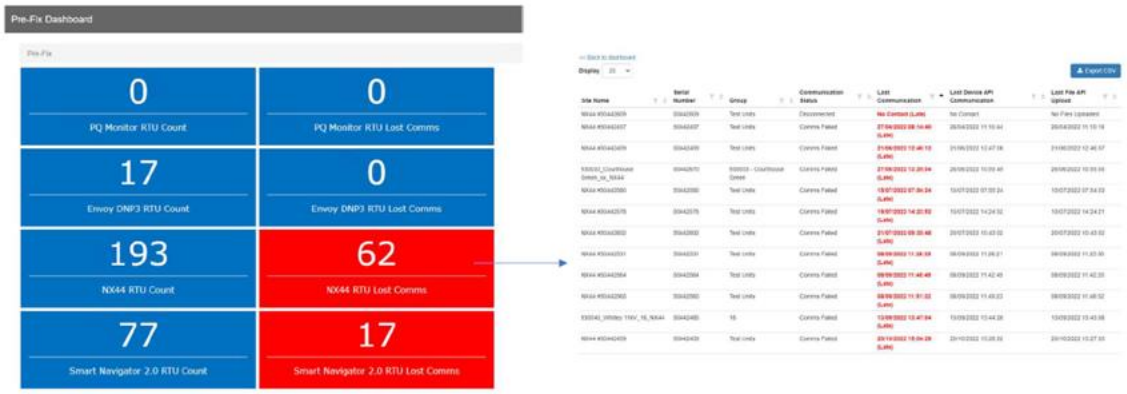

Figure 4.5 – Device Health Dashboard

The device health dashboard highlights device issues and permits the timely diagnosis and potentially repair of any device communication issues over the air. This saves on site visits and therefore resource where issues can be fixed over the air. The dashboard also allows the user to understand, during a post-fault event, if any devices were not active. This information can be used to factor in the device location during the fault event.

4.6. Waveform Viewer

Functionality was developed within the C-DIP to allow system users to view source waveforms generated by the various classes of devices. Furthermore, the suite of features within the C-DIP enabled users to both manually and automatically merge and synchronise different waveform files (for example, where different devices capture the individual phase waveforms associated with the same disturbance event, or devices along an HV feeder all observe the same disturbance event and the user wishes to compare waveforms). Examples of the Waveform Viewer functionality are given in Figure 4.6.1 (Class I Device, PQube3 waveform viewer), Figure 4.6.2 (Class II Device, Smart Navigator 2.0 waveform viewer, including the automatic synchronisation and merging of waveforms) and Figure 4.6.3 (showing the manual synchronisation of waveforms).

Prior to Pre-fix, there was little-or-no real-time visibility of defect (pre-fault) or post-fault waveforms. The waveform viewer was used extensively during the data collection and analysis phase of the project to build up a library of pre-fault and post-fault waveforms. These waveforms were then analysed to give distance-to-(pre-) fault network locations as well as classification of faulted components. Ultimately, this allowed the performance of the system to be evaluated (by confirming distance between actual and predicted fault locations, and alignment of predicted versus actual faulted components (see Part 2 of this Learning Report for performance evaluations). In future, the waveform classifier will continue to be used to view source waveforms and identify new failure signatures that were not captured within the temporal and geographical constraints of the Pre-Fix trial.

The waveform viewer through facilitating visualisation and interrogation of the waveform features, will permit the user to manually reclassify the waveform based on a known fault cause confirmed from the field. This manual classification will inform the machine learning of the waveform classification module within C-DIP, as discussed in section 4.15.

The waveform viewer will be a useful feature for any devices that may be integrated into the C-DIP in the future. When waveform captures are processed and uploaded from other devices, the

waveform viewer can be used to confirm that the capture meets the necessary requirements in terms of capture window, synchronisation, and sampling rate and that all various types of waveform disturbances are being recorded.

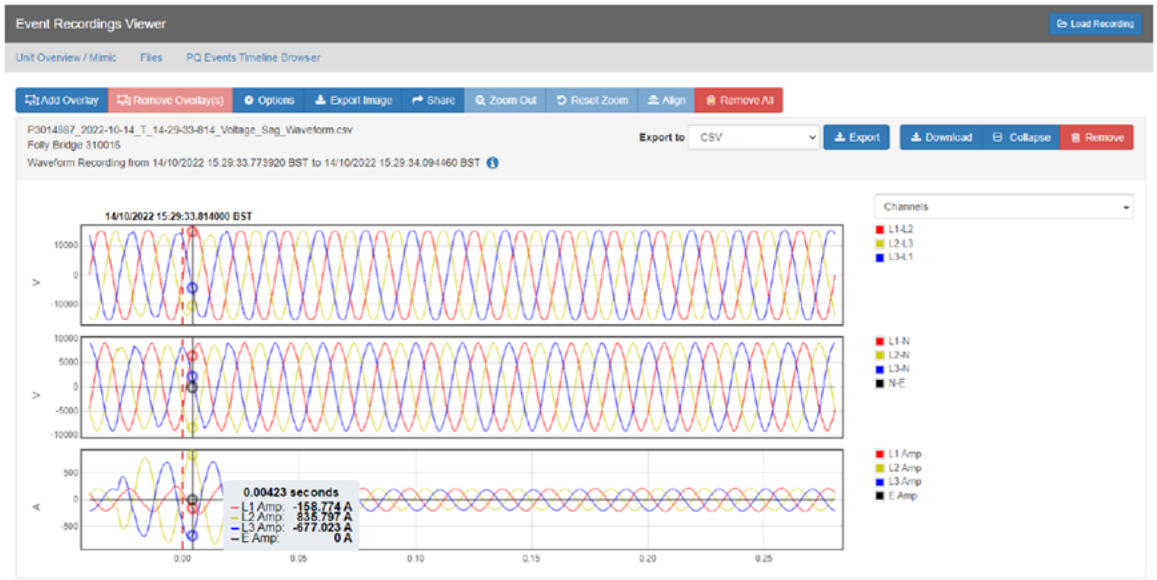

Figure 4.6.1 – Class I Device, PQube3 waveform viewer

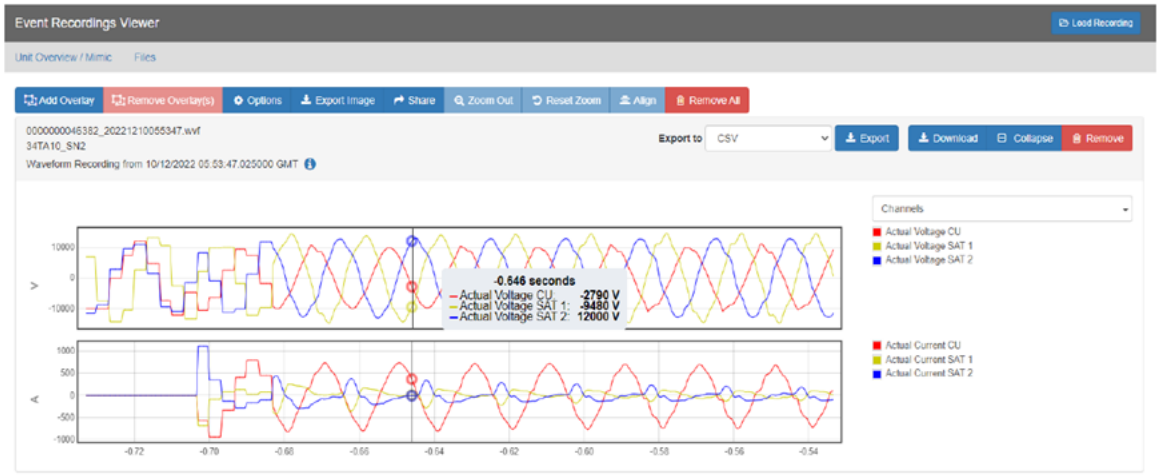

Figure 4.6.2 – Class II Device, Smart Navigator 2.0 waveform viewer, including the automatic synchronisation and merging of waveforms

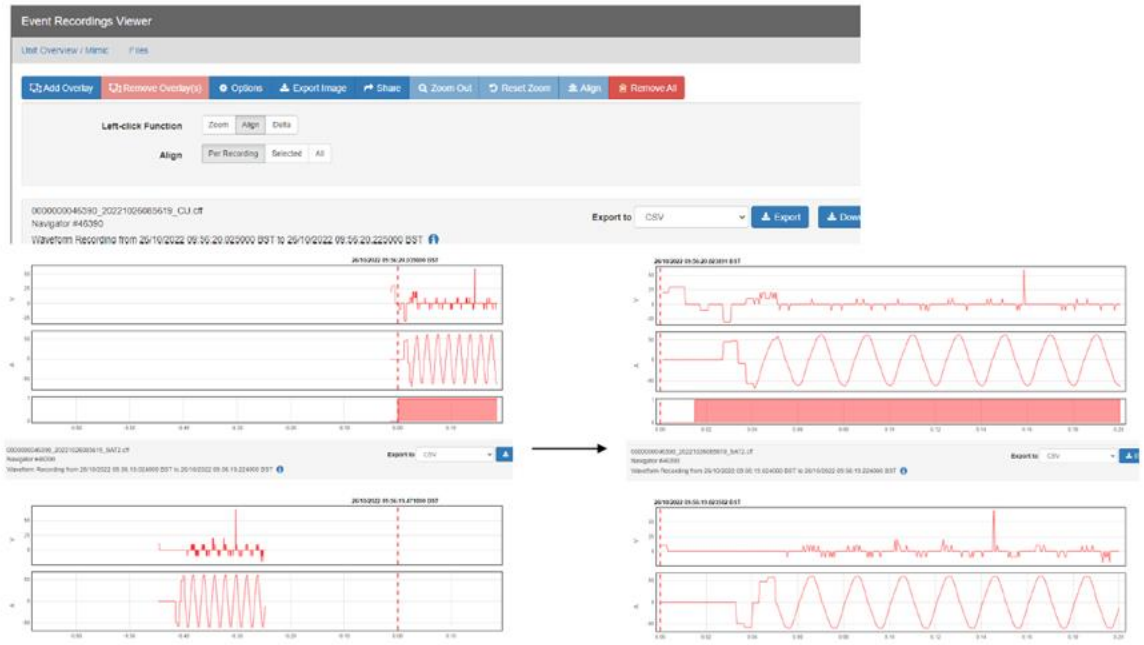

Figure 4.6.3 – Manual synchronisation of waveforms

The recommended capture window for devices is 16 cycles for Class I devices, 10 cycles for OHL FPIs and 5 cycles for cable FPIs. It is essential that the waveform recording begins a few cycles before the event to ensure that the entire event is captured and that the impedance to defect or distance to fault calculations can be performed correctly. The waveform capture should ensure that the fault event or pre-fault activity is captured. Through the trial, separate multicycle disturbances have been observed so the waveform capture length should ensure that these are captured. For a fault event, the fault waveform may last longer than the capture window, however as long as the beginning of the fault event is captured and a sufficient number of cycles is captured, this will enable distance to fault calculations and event classification to be completed.

From using the waveform viewer functionality, it was shown that for the same event on a particular feeder, simultaneous waveform captures from different devices is possible. These events, from for example two cable FPIs, will be grouped together and presented within the network fault browser which is discussed in section 4.7. It has been found that for two simultaneous events, any one particular device will only trigger and record a waveform for the first event. If the waveform recording stops before the second event, then the device will trigger based on the second event and record a separate waveform. For example, if there are two tree brushes that happen simultaneously, then a waveform will only be captured for the first tree contact with the OHL. If however, there is a downstream device present, between the location of the first and second tree brush events, then the two devices will both capture the resulting waveform and will group and upload these to the network faults browser.

When it comes to the processing and communication of waveform captures from several devices, both at the Primary substation and downstream on the feeder, the C-DIP is configured to account for latency within devices. Devices are grouped together by Primary and when a PQube observes an event, there is a 2-minute delay to allow other devices, both cable and OHL FPIs, to call in if they have observed the event. This helps account for the inherent latency of various devices, so that all waveform captures associated with any one event will be grouped and uploaded to the C-DIP for further visualisation and analysis.

In order to group network events together effectively, the monitoring devices within Pre-Fix require periodic synchronisation to a global clock (this recommendation is included in the Device Settings Philosophy Document). If periodic synchronisation does not take place, the internal clock within devices can drift relative to the global clock and therefore report an event happening at a different

time compared to the actual (GPS-stamped) time. Over time, the internal clock of devices could drift to the extent that the event is no longer considered within the configurable validity time window (i.e. a window that allows tolerance in different devices detecting the same event but reporting the timestamp of the event to iHost at different relative times). For post-fault activity the validity window was configured to be 2 minutes from the first reported network disturbance (due to operational timescales needed to inform post-fault response decisions). For pre-fault activity, the validity window was configured to be 24 hours as the timescales for planning pre-fault responses align with NGED's network planning timescale horizons.

4.7. Network Fault Timeline Browser

The Network Faults Timeline Browser feature within C-DIP provides business users with an overview of device activity, grouping by substation and pre-defined time windows as well as pre- and post-fault activity. The feature provides a drilldown so that groups of events can be analysed with greater granularity as and when required. The timeline browser dashboard allows a drill-down to view event grouping initially over a 28 day period with 1 day grouping, then a 7 day period with 3 hour grouping, then a 1 day period with 30 minute grouping. The matrix also provides the distinction between pre-fault and post-fault events allowing the user to filter the matrix depending on their analysis priorities.

The Network Faults Timeline Browser and drill-down interfaces are given in Figures 4.7.1 and 4.7.2 respectively.

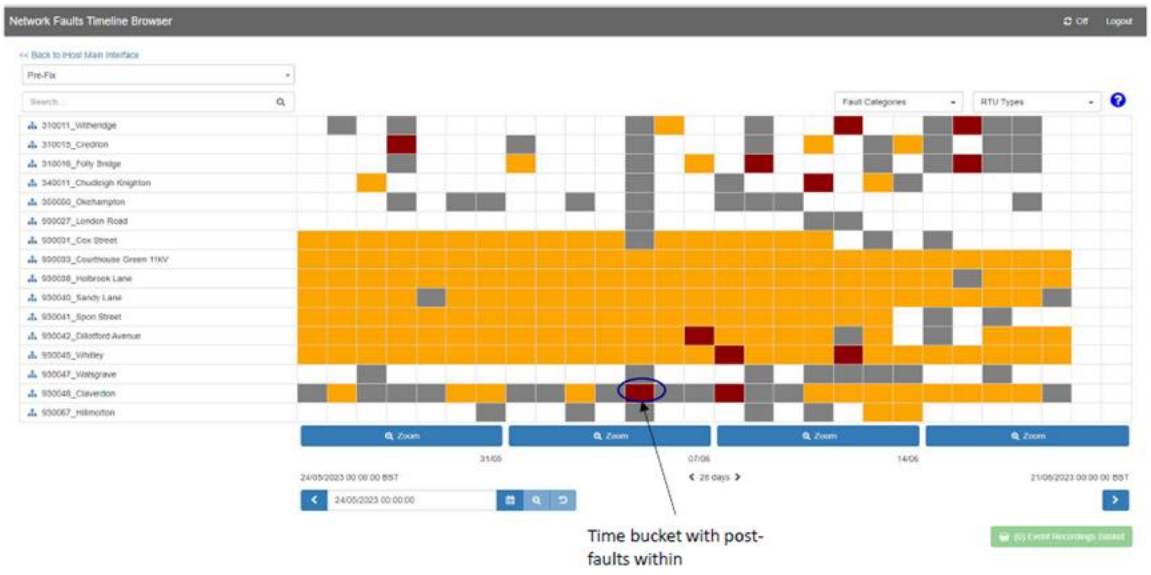

Figure 4.7.1 – Network Faults Timeline Browser

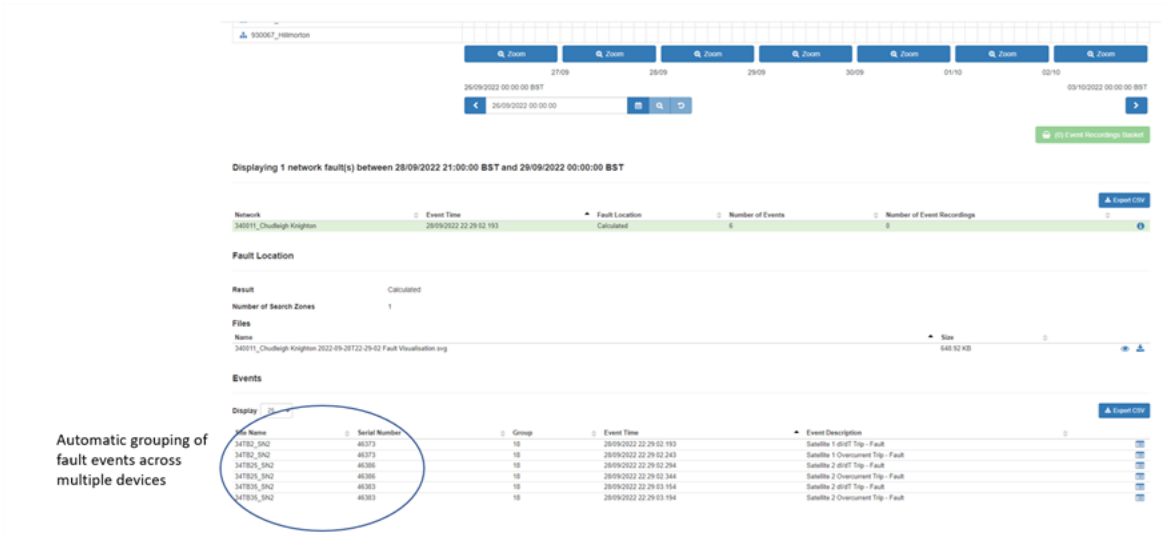

Figure 4.7.2 – Network Faults Timeline Browser – Activity Drill-down

Each cell represents a time bucket for events associated with a particular Primary substation. White cells indicate no activity, amber cells indicate pre-fault activity, dark red cells represent post-fault activity and grey cells represent indeterminate activity. By clicking on a bucket of activity, the user is able to view all the devices and disturbances that underpinned the event, automatically grouped together when the devices have observed the disturbance within 10 minutes of the first device triggering. The user can also access waveform viewing features as described in the preceding sections. The interface is interactive and the user can navigate backwards and forwards in time to determine what, if any, pre-fault activity took place before a post-fault event. The time-geography representation of events also allows the business user to determine if a network-wide event has occurred, simultaneously affecting multiple primaries and/or HV feeders.

Feeders with high pre-fault activity are screened to filter out noise and load pickups, allowing for easier analysis of distinct events. This is done using a Fourier series analysis of the waveforms uploaded to iHost by devices in the field and a rule-based algorithm that considers signal to noise ratio and waveform RMS during the capture time period. This method, on two occasions has appeared to filter out genuine pre-fault activity on feeders were there have been a large number of three phase swells that appear as a small increase in current for a few cycles and occur regularly on the feeder. Pre-fault activity is still recorded by these devices, when memory is not full, but is not added to the networks fault browser. This will be improved once the cause of these three phase swells is fully understood so that these events can be filtered out and only genuine pre-fault activity is recorded.

For events classified as post-faults (red boxes within figure 4.7.1), the logic uses both Pqube and FPI recordings. The event will have had to cause the current to increase beyond protection setting thresholds within the waveform capture from the PQube and a post-fault binary will have to be recorded within the FPI.

Where there is no FPI binary recorded, the event will be classed as indeterminate. One downside to this, is if the cable FPI is not communicating correctly at the time of a fault then a post-fault event will be recorded as indeterminate. In addition to this, is if the feeder affected by the fault is not instrumented with FPIs then no post-fault binaries will be possible and the event will be classed as indeterminate. Where no FPI post-fault binary is recorded the fault waveform will still be captured by the PQube and therefore a distance to fault calculation can still be completed. FPIs from other feeders may also be impacted by the fault event and record what seems to be a pre-fault event and where no FPI recordings are present for the affected feeder, the event will be classed as a pre-fault. To overcome these issues integration with other network control systems,

such as Advanced Distribution Management System (ADMS), is recommended, where information on protection operations can be passed to the C-DIP system to aid with classification of post-fault events.

Another recommendation is to perform distance to fault calculations on every PQube waveform recorded. In the instance where there is a fault, the locations from the impacted feeder can be taken from the geographical plots of predicted fault locations within the C-DIP single line diagrams or map viewers at the time of the fault. This removes the need for FPI binaries to trigger a distance to fault calculation. The implementation of this is planned for future updates to the C-DIP.

For pre-fault classifications where either the FPIs or PQube record events that do not reach the necessary current thresholds the event will be classified as a pre-fault.

4.8. SLD Annotator and Interactive Editor

The Single Line Diagram viewer feature is shown in Figure 4.8.1 and the Single Line Diagram interactive editor is shown in Figure 4.8.2.

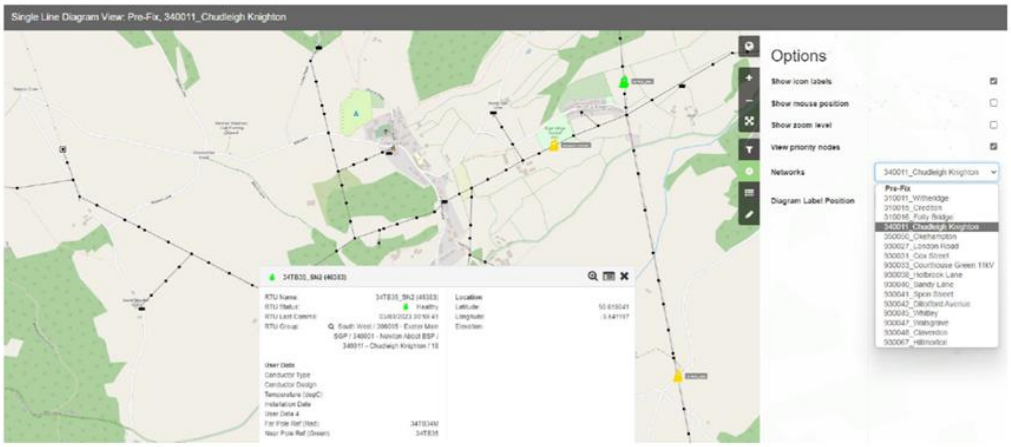

Figure 4.8.1 – Single Line Diagram Viewer

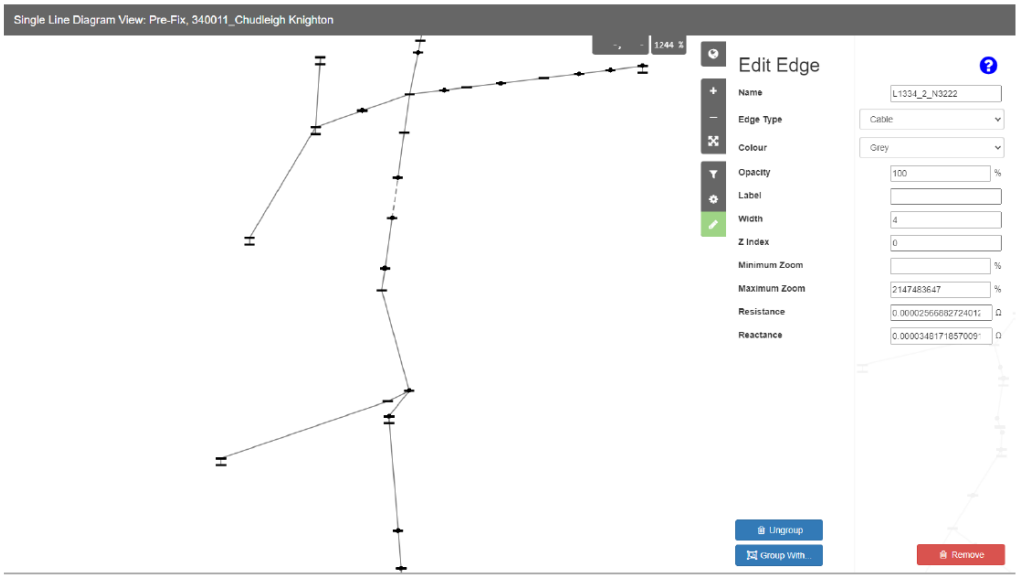

Figure 4.8.2 – Single Line Diagram Interactive Editor

This feature can be utilised to manually mark-up the single line diagrams with previous fault events, HV fuse operations and where there have been multiple auto-reclose events. Where there is pre-fault activity on a feeder, the locations of any previous faults or autoreclose events can be taken into account when determining the likely location and cause of any network anomaly.

Where escalation fits of devices on a feeder downstream of a Primary substation have been recommended, based on the pre-fault activity observed, the required location can be marked up on the single line diagram interactive editor to highlight to staff where these would need to be installed.

This is a feature that has not been utilised during the Pre-Fix trial but may be utilised by operational staff when using the system.

4.9. Automated FPI Search Zone

The fault location feature of C-DIP, based on automatically generated FPI search zones, is given in Figure 4.9. The amber line traces the flow of the fault from Primary to fault location. The red zone represents the most likely fault location based on the real-time status of FPI post-fault alarms. In the pre-fault domain, the amber traces the current flow to defect and the red zone represents the most likely defect location. This is a powerful feature as it embeds expert knowledge within C-DIP to give business users insight into the geographical location of pre- or post-faults within minutes of the network disturbance event occurrence.

Use of the search zone feature alone in the pre-fault domain has limited benefit as it will not give the user a precise location for the source of the disturbances. Depending on the topology of the network and the location of the FPIs, when combined with distance calculations for pre-fault, the search zone can aid in ruling out certain locations. This is especially helpful where there a number of branches within a circuit, meaning that distance to defect calculations that indicate a number of locations can be isolated to a certain branch of the circuit. This is dependent on the number and location of FPIs installed on a feeder.

The ability for an accurate and operationally useful search zone to be generated, is dependent on the FPI being functional and communicating correctly. It is also vital that the installation location and the orientation of the FPI is correct and recorded accurately. If there is any issue with installation then an incorrect search zone can be generated. If the communication of any FPI is not functional at the time of the fault, then a search zone will still be generated but will likely be larger than if the FPI had been functional.

Additionally, if available, protection devices such as autoreclosers could produce binaries and communicate these back into the C-DIP to further refine search zones. Any device would require the ability to generate binaries upon occurrence of a fault and communicate this to the C-DIP within 10 minutes of a fault event occurring.

To date, the FPI search zones have been used in limited cases to highlight issues to both field staff and helicopter patrols. Learning from these cases is discussed in more detail in sections 6 and 7 of the report.

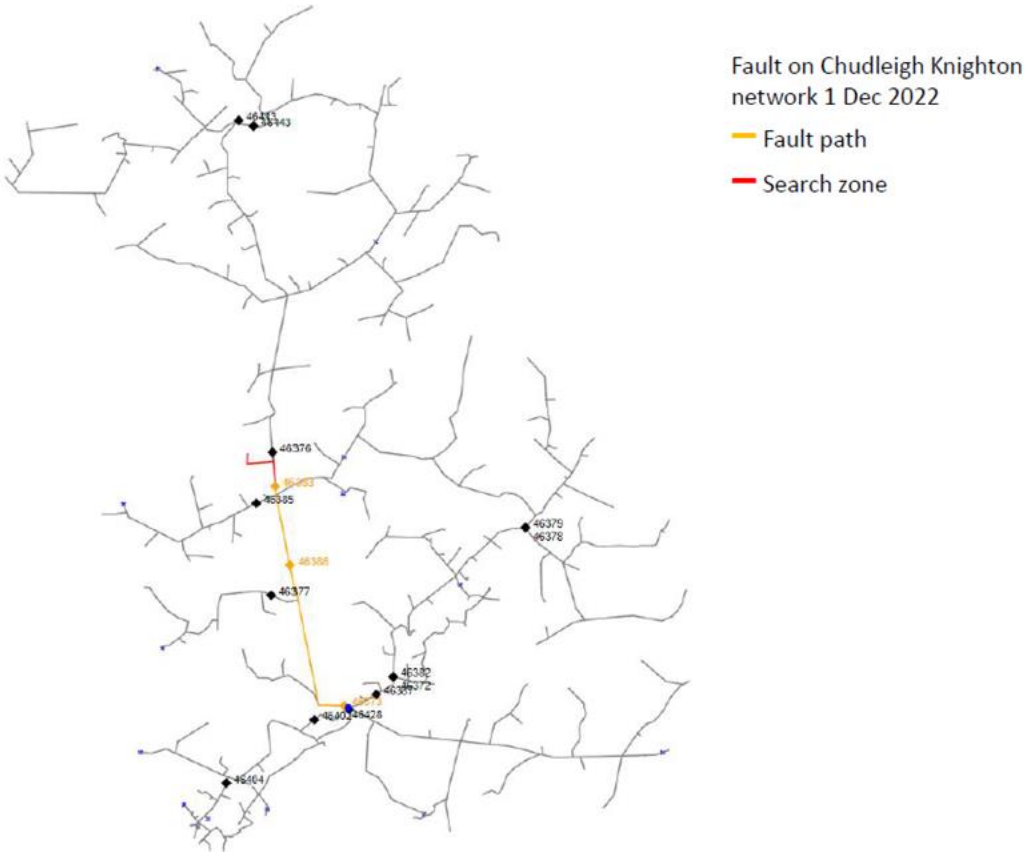

Figure 4.9 – Illustrative FPI search zone (reducing network search zone by 80%)

4.10. Manual and Automatic Distance-to-Fault/Defect Analysis

The Fault Location feature of the C-DIP, using impedance-based pre- and post-fault distance assessments, is given in Figure 4.10. The system (or, in manual mode, the user) automatically selects the point-on-wave to analyse the network disturbance and determine impedance-to-fault based on the number of parallel transformers in operation at the time of the disturbance.

This is an incredibly powerful feature as it embeds expert power systems analysis within the C-DIP to give business users insight into the fault type and impedance-to-fault for pre- or post-faults within minutes of the network disturbance event occurrence. This process is automatically completed by the system, controlling the point-on-wave selection and other input parameters. However, this process can still be completed manually where required. Manual analysis can still be used in cases where verification or recalculations are desired, or to use data from data sources that are currently unsupported by the automated methodology, such as PQube XML summary files. Due to the uncertainties within the impedance path of phase to earth faults, as discussed in section 7.2, the automatic distance to fault calculations are only currently in place for phase to phase and 3-phase faults.

Figure 4.10 – Impedance to Fault Calculation Engine

As shown within figure 4.10, the impedance to fault calculation engine will automatically select point on wave for the current and voltage waveform and from those values determine the impedance to fault/defect. This will then be automatically plotted onto the map viewer and single line diagram for user visualisation. The manual operation is very similar to the automated process, with the difference that the point on waves are manually selected and the calculated impedance value is copied into a recalculation option and then plotted onto the map viewer/SLD. User guides for the manual impedance to fault calculation method are available upon request.

During the early stages of design and development of the system, there were a number of different methods considered for distance to fault calculations. These included a phase-to-phase reactance method which used Fast Fourier Transform (FFT) on PQube waveforms, and three direct impedance methods plotted using impedance, reactance and resistance. Table 4.10 outlines these methods and their relevant strengths and weaknesses.

Table 4.10 – D2F Methods Comparison

D2F Method	Description	Strength	Weaknesses
FFT (Reactance)	Reactance-to-defect derived via FFT on PQube waveform	Good accuracy.	More complicated implementation and less computational efficiency than direct impedance methods without providing significant accuracy benefits. Only addresses phase-to-phase faults, not phase to earth faults.
Direct (Impedance)	Impedance calculated via Ohm's law and plotted using impedance method.	Ease of implementation.	Significantly less accuracy than both reactance-based methods.
Direct (Resistance)	Impedance calculated via Ohm's law and	Ease of implementation.	Significantly less accuracy than both reactance-based methods.

	plotted using resistance method.		
Direct (Reactance)	Impedance calculated via Ohm's law and plotted using reactance method.	Good accuracy AND ease of implementation.	Limited accuracy with phase to earth faults

Based on the early results from the system trial, the method chosen to proceed with was direct impedance calculation plotted using the reactance method. This was because it provided a highly efficient and scalable solution which also offered comparable accuracy to the FFT methodology for phase-to-phase faults.

4.11. Manual and Automatic Fault/Defect Location Plotting

In order to optimise business use of the system and pave the way for business-as-usual adoption, the geographical plotting of fault locations (underpinned by SINCAL model ingestion and conversion described in preceding sections) was integrated with NGED's GIS by way of GeoServer. As seen in Figure 4.11.1, this gives the business users the facility to access real-time updates of disturbance locations. This is completed automatically by the C-DIP and presented to the user. This plotting can also be performed manually when required which is especially useful in the instances when distance to fault calculations are not performed automatically. Currently this is the case when events are classed as indeterminate, as discussed in section 4.7. On these occasions the PQube may have triggered but due to a FPI device either not being installed on the faulted feeder or not communicating at the time of the fault. The PQube waveform can be used to run the manual impedance to fault calculation and plot the distance to fault locations onto the correct feeder. This issue can be overcome by either applying automatic distance to fault/pre-fault calculations on all waveform captures or to integrate C-DIP with other network systems that can provide information on when a feeder has experienced a fault.

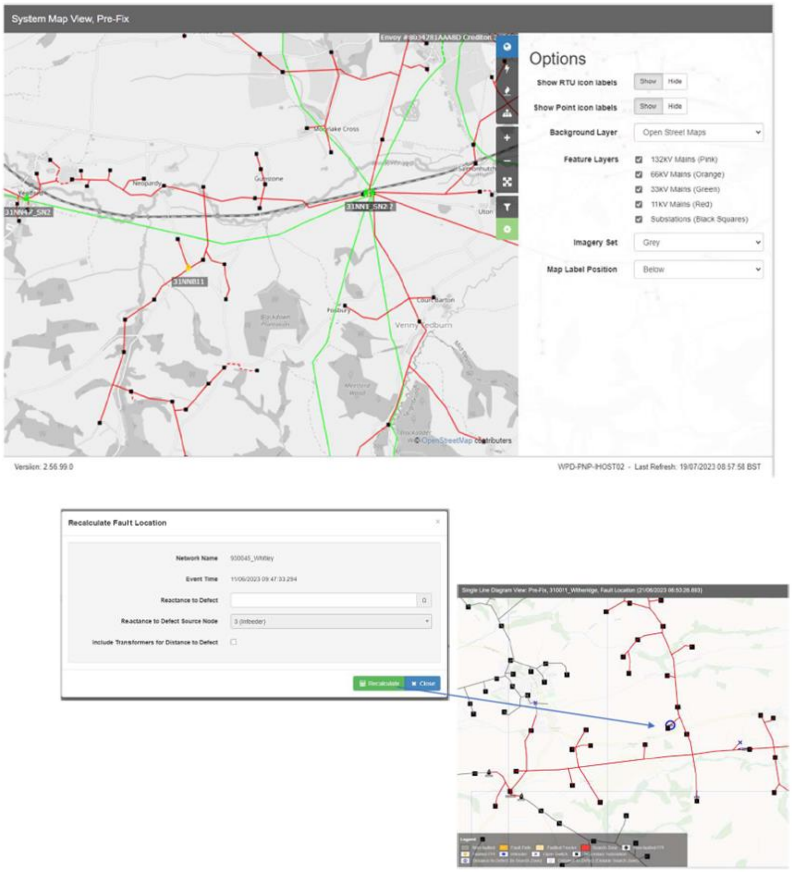

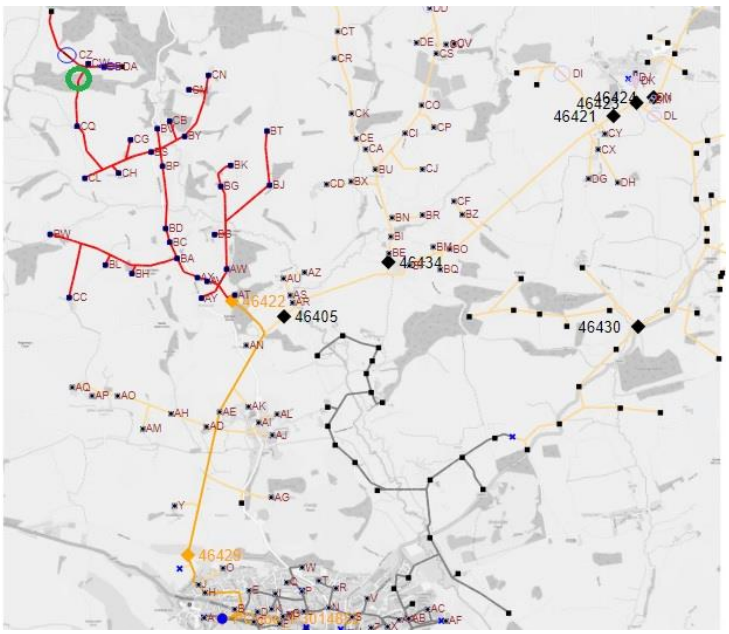

Figure 4.11.1 – Fault Location Geo-plotting

Figure 4.11.1 shows an example of fault location geo-plotting, where the faulted feeder is shown in light yellow, the fault path is shown in dark yellow and the fault search zone is shown in red. The predicted fault locations, both within the search zone and outside of the search zone, are shown by the blue circles. The actual fault location on this occasion, confirmed from site, is shown by the green circle.

One issue that remains with the fault location geo-plotting feature is that when the devices trigger on the faulted feeder under fault conditions, other feeder NX44 devices also observe the disturbance and record a pre-fault event. This can result in the other feeder, where the fault has not occurred, being highlighted with the fault path and a subsequent search zone. This is issue will exist on any system with devices are installed on multiple feeders and reporting back without real time processing to rule out certain feeders from fault events. Through integrating information from other network systems, where notification of the faulted feeder can be sent to the C-DIP, the feeders not affected by the fault can be discounted from the fault location plot. The other option is when a post-fault event is detected by a device, all other information from class II devices installed within other feeder breaker panels or downstream on other feeders is discounted. These options will be explored and developed are part of future C-DIP releases.

4.12. Real-time Transmission of Waveforms

For the purposes of Pre-Fix, the suite of features within C-DIP is completed by the automatic transmission of waveform data on event creation by the source devices. Within 10-minutes of a disturbance event, the source data is automatically analysed to determine fault type and location as well as classification. The decision to have a 10-minute delay was based on the latency in device communications, allowing all devices that had observed the event to transfer the data capture file into the C-DIP, which was essential to obtain all relevant information on any network event. At the time of deciding upon having a 10 minute delay, feedback was obtained from the control room as to whether this was quick enough to provide useful information to inform switching decisions. A balance is required to ensure that the delay is long enough to account for latency in device communications and short enough to provide useful operational information.

Near real time data transfer gives business users (in particular operational users) a much deeper insight into the geographical source of a network fault or disturbance and the most likely root cause. In the post-fault domain, this could allow operational staff to make better-informed switching decisions to restore supplies to customers more effectively and efficiently. In the pre-fault domain, this information could help to inform proactive fault mitigation decisions (for example, overlay of cable to circumvent suspected faulty joint locations).

As seen in Figure 4.12.1, new Envoy firmware allows the transmission of PQM waveforms to occur in real-time rather than waiting on a daily .tar file upload, which is essential to allow real time response to post-fault events. Note ‘Date Created’ and ‘Date Added’ columns showing the 1-minute difference. Figure 4.12.2 shows the transmission delay of 19 hours where the older Envoy firmware was used.

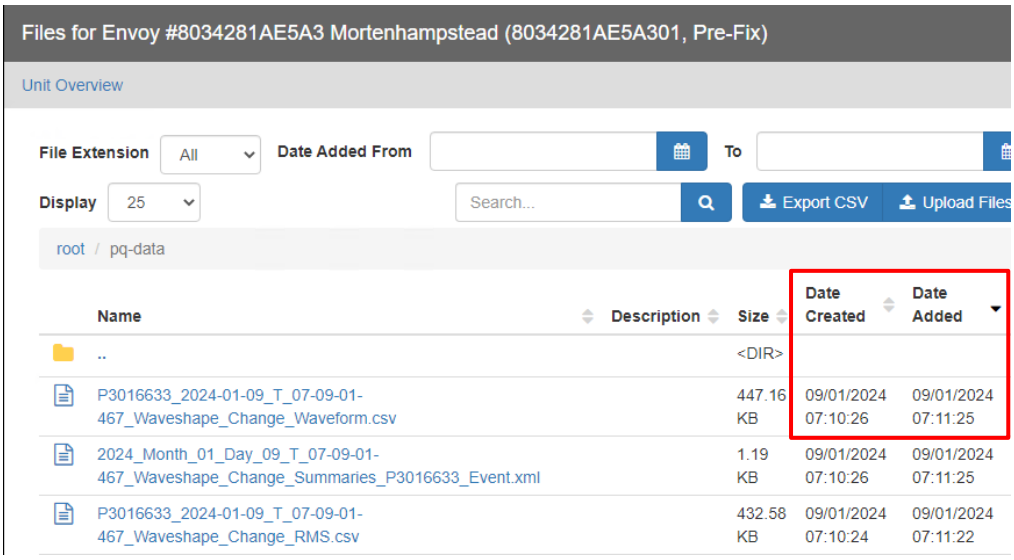

4.12.1 – Real-time transmission of waveforms using new Envoy firmware

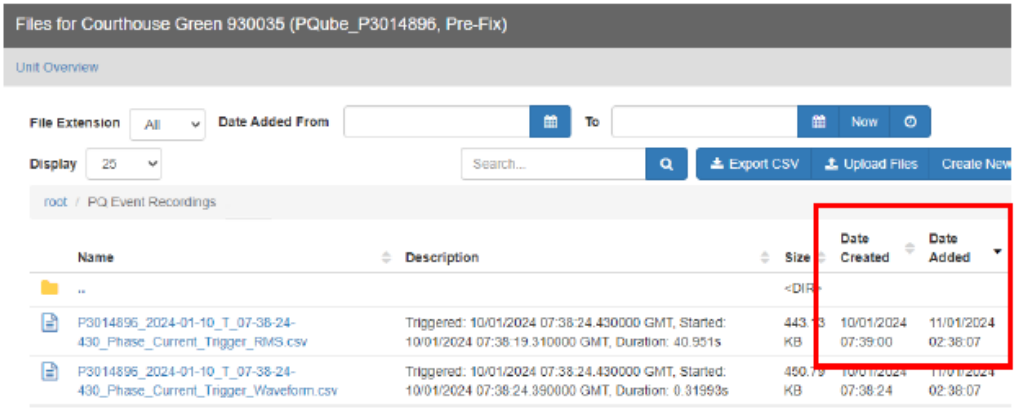

4.12.2 – Transmission of waveforms with old Envoy firmware (up to 24 hour delay)

4.13. Power Quality Monitor Cross-Triggering

Figures 4.13.1 and 4.13.2 demonstrate an NX44 cross-triggering a PQube in real-time in order to give simultaneous device waveform captures as discussed previously in section 3.4.2 (without having to make the trigger settings of the PQube3 more sensitive, which could result in unwanted additional waveform captures).

As seen in Figure 4.13.1, ‘Digital_1’ captures on the PQube are those which were cross-triggered by an NX44. This example shows a cross triggered phase-to-phase fault.

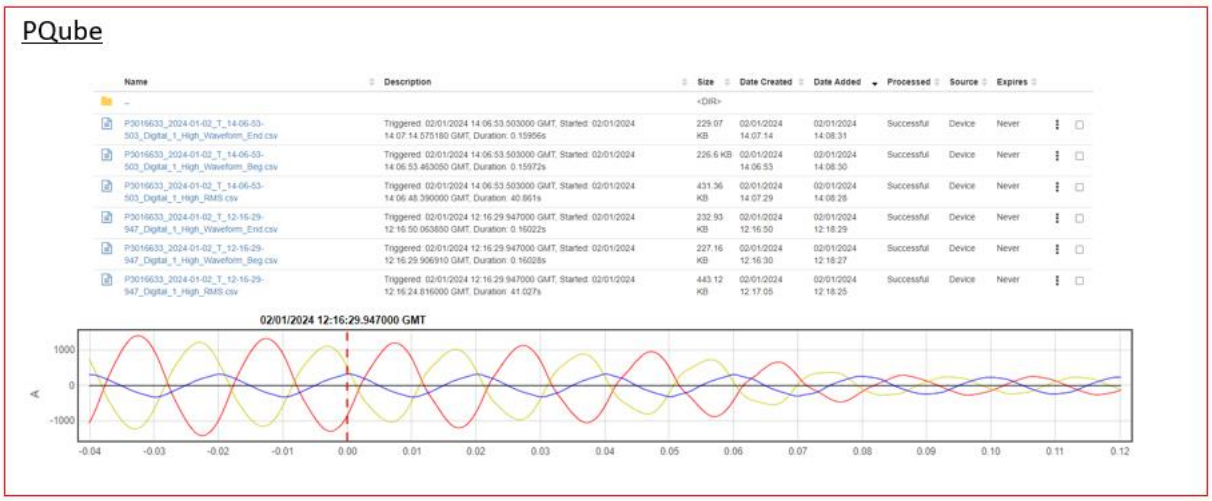

Figure 4.13.1 – Cross-triggering of PQube3 by NX44 to capture a Ph-Ph fault

A cross-trigger waveform capture is given in Figure 4.13.2 for a Phase-to-earth fault. Not only does this demonstrate that wiring the PQube into the substation UPS (running at 110V DC) avoids the issue of power interruption to the PQube during Ph-E faults (when LV AC supplies can be temporarily interrupted) but also gives the PQube the same reliability of triggering and capturing an event as a feeder FPI.

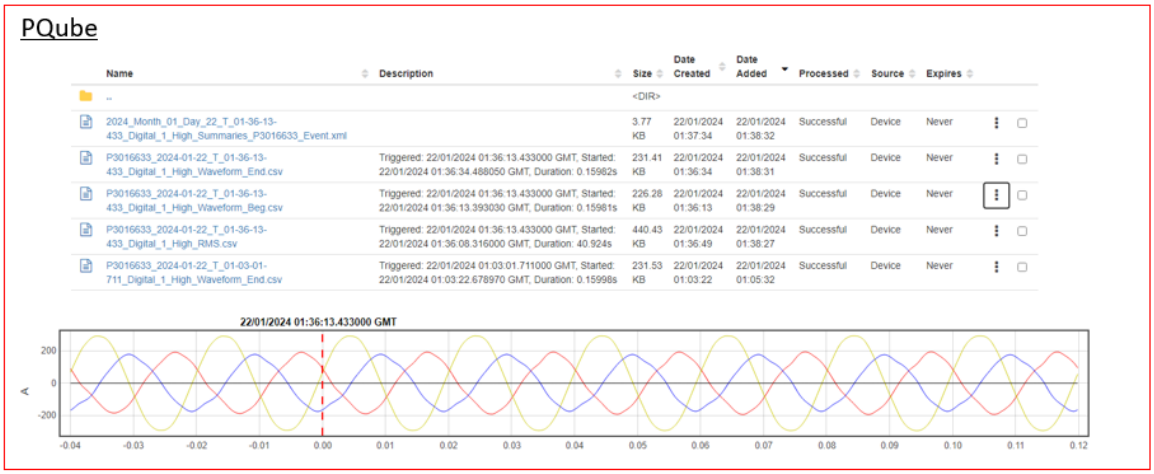

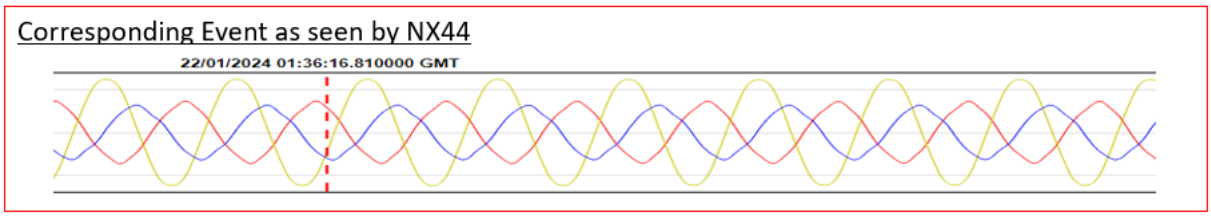

Figure 4.13.2 – Cross-triggering of PQube3 by NX44 to capture a Ph-E fault

4.14. Feeder Watch List Report

The iHost API can be queried for a report which lists all activity seen by Pre-Fix devices in a customisable Excel format. This report is currently run fortnightly to build up a watch list of HV feeders exhibiting pre-fault and post-fault activity.

The report includes various pre-fault metrics related to the magnitude and frequency of pre-fault activity, as well as the number of phases and cycles affected, allowing the user to analyse the feeder watchlist based on different metrics having different priorities.

An example "Feeder Watchlist" report output is given in Figure 4.14 in this case, ranking the activity of HV feeders according to the maximum I^2t (energy within a pre-fault event) divided by the peak current during the I^2t event. An explanation of I^2t can be found in section 6.4.

Of Interest?	YES			Relative I2T	I2T divided by base current loading
Pre/Post Fault	Pre-Fault			I2T/Peck Current	I2T divided by peck current
Row Labels	**Max of I2T**	**Max of I2T/Peck Current**	**Max of Relative I2T**	**No. of Pecks**	**Average of Peak Ph-Ph Delta (A)**
930047 - Walsgrave 8	8745.04	18.15	125.45	88	228.51
930031 - Cox Street 15	9030.84	15.66	5657.07	2	623.08
930040 - Sandy Lane 8	10887.9	15.19	607.53	276	119.77
930033 - Courthouse Green 4	4979.2	13.67	39.53	94	227.93
930045 - Whitley 11kV 6	2923.08	10.60	47.43	73	134.76
930041 - Spon Street 3	5634.67	10.44	28.92	88	117.19
930042 - Dillotford Avenue 3	4350.89	10.23	112.66	85	218.36
930045 - Whitley 11kV 10	5353.67	9.55	66.53	257	157.24
930040 - Sandy Lane 13	3091.25	9.31	47.34	125	171.45
930040 - Sandy Lane 15	2926.53	9.01	20.86	141	171.30
930038 - Holbrook Lane 5	2080.68	8.18	50.62	97	219.81
930033 - Courthouse Green 6	4077.63	8.04	107.35	210	165.10
930033 - Courthouse Green 5	8509.77	7.15	114.45	124	200.63
930041 - Spon Street 9	2840.39	6.83	50.74	30	199.92
930040 - Sandy Lane 4	1401.21	6.40	21.56	270	160.05
930047 - Walsgrave 18	2831.66	6.28	35.57	71	198.15
930047 - Walsgrave 10	2209.02	6.24	22.43	73	146.34
930048 - Claverdon 3	625.48	6.04	12.51	24	125.30
930040 - Sandy Lane 7	3098.69	5.81	37.13	236	170.74
930041 - Spon Street 8	2156.45	5.79	29.53	71	204.01
930048 - Claverdon 7	1521.81	5.64	19.39	112	197.17

Figure 4.14 – Example Feeder Watchlist

During the trial the feeder watchlist has developed as more data was obtained and the possible indicators to the presence and severity of anomalies were observed, analysed and refined. Ranking of feeders on the watchlist was experimented with, ranking them by frequency of pecks, maximum I^2t and relative maximum I^2t. Ranking by relative maximum I^2t seems to have the most effectiveness in highlighting a feeder anomaly as being likely to progress to failure. Where feeders had experienced a fault, these were highlighted in red and comparisons could be made with the confirmed fault location and pre-fault predictions. Feeders highlighted in yellow are ones that are new to the watchlist compared with a previous version and those in green are feeders that have been on previous issues of the watchlist. The use of this watchlist is discussed further in section 6.

4.15. Automated Waveform Classification

The classification methodology is given in Figure 4.15. The classification algorithm was set up on the basis of using a Convolutional Neural Network (CNN) pre-trained using datasets created to introduce permutations in signal-to-noise ratio (representing departure from ideal signal quality conditions and reflecting, more accurately, the signals received from field devices) and variations in the faulted phase for a wide range of common fault signatures.

Other methods were considered including 2 layer imaging, 3 layer imaging, multi-layer perceptron time-series analysis and hashed data time-series analysis. However, based on accuracy, loss, computational efficiency and training requirements the CNN approach was selected. More information on this can be found in the published CIRED paper on this topic.

An initial set of 21 electric fault signatures was used to train the CNN fault classifier based on the IEEE Power Engineering Society Technical Report 73: “Electric Signatures of Power Equipment Failures” [8]. This comprised overhead line, cable, transformer, capacitor and surge arrestor components, each of which has more than one common mode of failure.

The prototype CNN was created in python using the TensorFlow Keras module [9] with three layers of convolution, 64 filters and a kernel size of three. Pre-training the model allowed for a faster user experience when it came to classifying a particular waveform automatically.

A total dataset size of 2100 was used for the initial classification and this was expanded to 2200 in re-training (following the detection of new fault types).

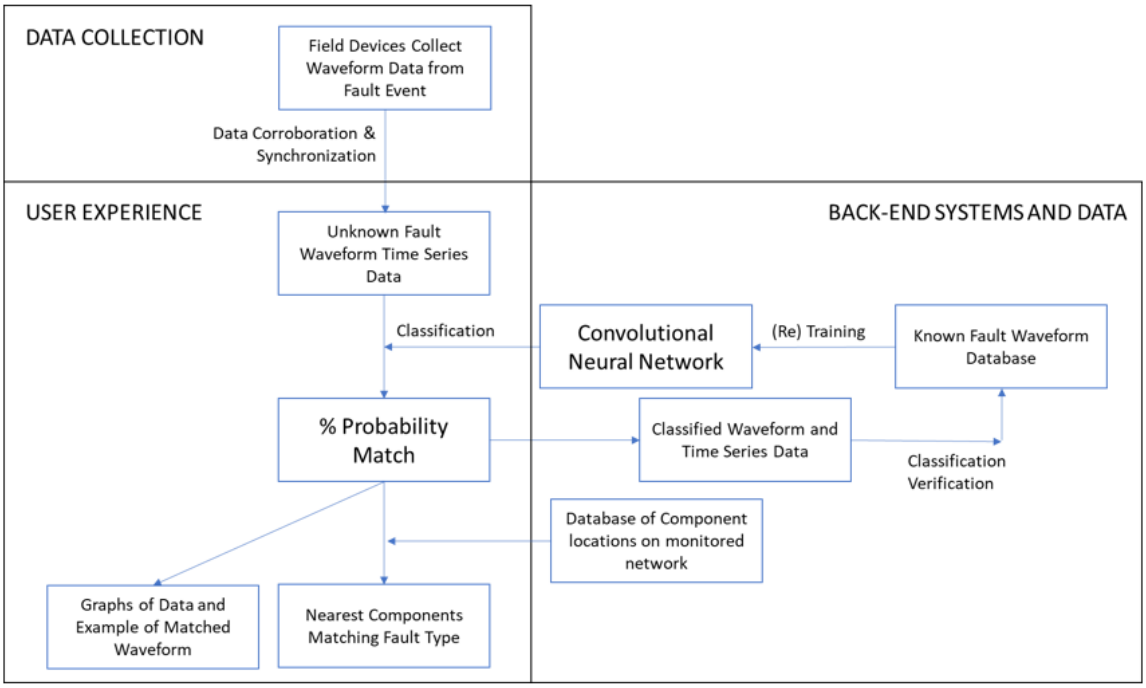

Figure 4.15: Classification of faulted components using electric failure signature templates

During the model training, the datasets were split at random into 80% for training and 20% for validation. Test data was separated from the training data prior to training then tested with the final

model. The training/validation split was selected to strike the balance between enough data for training and enough samples to validate classification effectiveness.

Outputs of the CNN give the user the closest match between the input fault signature data and a known fault signature type, along with a percentage certainty score.

In the C-DIP, the user has the option to view the input data and the matched waveform as graphs, to allow for manual verification before continuing. Clearly, on occasions it could be possible for no match to be found (or to be found with a confidence outside of configured tolerances). In this case, these classifications are displayed as “no classification match”, to allow for these exceptions.

A key novel feature of the classifier within the C-DIP is that the CNN classifier is capable of being retrained in order to add new fault/pre-fault categories as real-life fault data is captured. Users can manually update the waveform classification within the network faults browser, if the known fault cause is different than that classified within C-DIP. These manual updates allow the CNN classifier to be retrained. Examples of waveform classification can be found in sections 6.3 and 7.3, along with success rates of pre-fault and post-fault classifications.

5. C-DIP Pre-Requisites

5.1. System Requirements

For any DNOs looking to replicate the Common Distance Information Platform and its functionality, the integration of the following systems is needed (as a minimum):

- Tools for commissioning field equipment (ensuring the correct installation and commissioning of devices, correct application of device settings, correct recording of device installation locations and confirmation of remote communications integrity);
- A controlled HV network model giving topological connectivity of assets including accurate circuit impedance parameters, switch locations and switch states;
- Real-time switch status information from field devices (such as circuit breakers, auto reclosers, automated switches and isolators). This information should be fed into the controlled HV network model to adapt the network topology (defining which assets are in and out of service) in real time;
- A geographical information system defining the geographical layout of the network (for use in displaying the location of defects and post-fault event locations);
- The DNO asset database (to allow the classification of faulted or defective components to be matched to the nearest asset of that type in the locality of the fault or defect).
- Integration to system users, such as field staff tablets and the Control Room via the Network Management System (NMS).

In addition, data needs to be collected and transmitted from field devices (as described in Section 5.2) and it is recommended that this is automatically collected, transmitted and processed with maximum usage and efficiency benefits being obtained when the system is deployed on-premises.

5.2. Device Requirements

For any DNOs looking to replicate the Common Distance Information Platform and its functionality, the following device types are needed as a minimum:

1. Power quality monitors installed on the 11kV / 6.6kV (HV) side of Primary distribution transformers;

2. Communicating FPIs installed in feeder breaker panels at the head-end of HV feeders;
3. Communicating switches and/or communicating FPIs (wherever possible) at strategic locations along HV feeders.

5.3. Process Requirements

As well as having the policies and procedures in place for the installation, configuration, operation and maintenance of the C-DIP system and its devices, the following core functional processes are needed to deliver full operational benefits to DNOs (as described in more detail in Section 4):

- Post-transmission filtering of noise (to cater for devices that do not have the onboard functionality to discriminate defective component behaviour from noise);
- Grouping of device events (allowing for data transmission latency and device clock drift);
- Automated generation of search zones and distance-to-fault / distance-to-defect locations (including automated notification to field staff and other business users);
- Automated classification of events (including automated notification to field staff and other business users); and
- Time-to-Fail quantification assessments.

Part 2: Operational Learning

Part 2: Operational Learning covers the effectiveness of the system to determine fault/defect presence, fault/defect location and evolution of defects (pre-faults) to customer-interrupting faults (post-faults).

Learning has been identified by asking the following questions:

1. What worked well and should be repeated?
2. What did not work well and should be changed?
3. Learning from applying the C-DIP in both pre-fault and post-fault domains.

Wherever possible (within scope/time/budget constraints), changes were made during the course of the project as a result of the on-going learning process. However, where changes could not be made during the course of the project (due to scope/time/budget constraints), these have been captured as recommended changes for any follow-on projects by NGED or other GB DNOs.

The following areas are included within this section of the report:

1. Circuit Defect (Pre-Fault)
    a. Defect Detection
    b. Defect Location
    c. Defect Classification
    d. Time to Failure
    e. Pre-Fault Location C-DIP Performance
2. Post-Fault
    a. Post-Fault Detection
    b. Post-Fault Location
    c. Post-Fault Classification
    d. Post fault Location C-DIP Performance
3. Results Verification
4. Avenues for Further Research

System learning, relating to the development of C-DIP (including the required functionality of hardware and software components, and their inter-dependencies) during field trials is contained in Part 1 (System Learning). This section also identifies the pre-requisites (such as the carefully considered and judicious selection of device settings to detect and transmit HV defect waveforms), which are needed to deliver operational outputs and benefits.

The operational learning covers the findings from the trial period of the Pre-Fix project which began in June 2022 and concluded in March 2024. The trial covered a total of 17 Primary substations, 11 of which are located around Coventry in NGED's East Midlands licence area with the other 6 located around Dartmoor in NGED's South West licence area.

There were a total of 17 feeders monitored in the South West all of which were predominantly overhead line construction. There were a total of 102 feeders monitored in the East Midlands, with 21 of these being of mixed OHL/UG construction and the remaining 81 being predominantly underground cable construction.

6. Pre-Fault

Pre-Fault events are observable disturbances in the electrical signal of the network that are not extreme enough to trigger network protection equipment but are indicative of an event or defect. By analysing the rate, shape and magnitude of these events, it is possible to track feeders on the network that have these defects, and begin to correlate these metrics with the time it takes for the defect to evolve into a full fault.

6.1. Defect Detection

What worked well?

Current-based waveform distortion triggers that compare residual error between cycles have been effective at capturing pre-fault events.

What was or should be changed/improved?

Voltage-based triggers and current inrush triggers are sensitive to noise when settings are low enough to capture pre-fault events and therefore it is essential that current waveform distortion triggers are in place for pre-fault devices.

6.1.1. Waveform Triggering

Due to the nature of pre-fault events having a smaller fault current and voltage change than occurs during a post-fault, the triggers that are suitable for detecting them are significantly different. A comprehensive list of all of the triggers used and changes made during the project can be found in the Pre-Fix equipment settings philosophy documentation. During 2022 and early 2023, it was observed that pre-faults tend to have minimal effects on the voltage of the waveform, meaning that voltage-based triggers struggle to detect them. Limitations with current inrush-based triggers have also been observed, as both the current magnitude and duration of pre-fault events means that these triggers have to be extremely sensitive before they can detect pre-faults. However, making the settings sensitive enough to capture pre-fault events has caused issues with noisy triggering during peak loading times.

The most success at detecting pre-faults has been observed with a trigger based on current waveform distortion on both Class 1 and Class 2 devices. A waveform distortion trigger will compare each current waveform cycle with the previous one and trigger an event and a waveform capture when the residual error between the two cycles exceeds a certain value. An illustration of this process is shown in Figure 6.1.1. During Q4 of 2022, a current-based distortion trigger for the PQube3 was developed and has shown more success in detecting pre-fault conditions compared to other triggers built into the power quality monitor's functionality. As a result, we would recommend this type of trigger for the integration of further devices looking to capture pre-fault events on the network.

During the network trial, it was observed that on several occasions, fault events at higher voltage levels (132kV and 33kV) were observed by several Primary substations and recorded by the C-DIP as pre-fault events. It is therefore essential that the occurrence and timing of these events can be recorded and passed to the C-DIP so that any pre-fault events attributed to this time can be discounted. However, it is key that any waveform classifier is also trained to observe and classify these events to ensure that any true coincident pre-fault activity that occurs is not discounted.

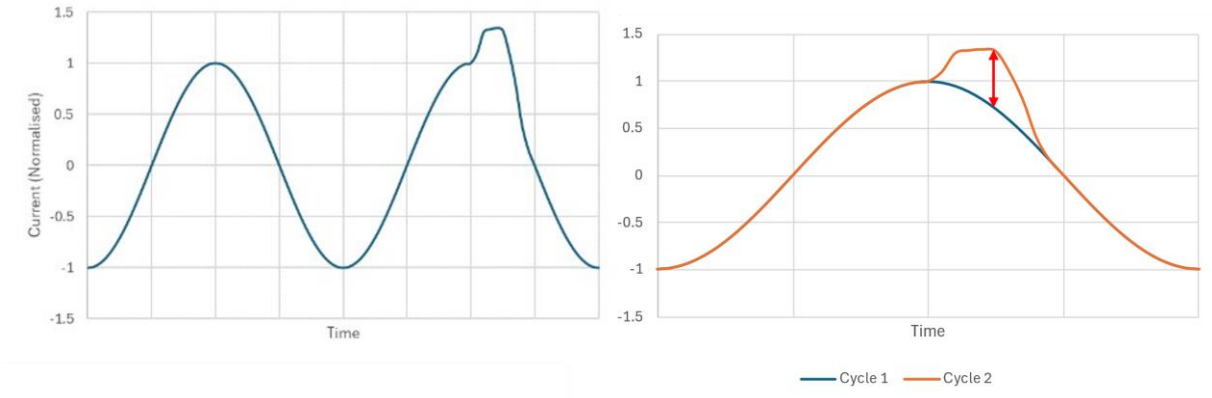

Figure 6.1.1: Waveform distortion trigger illustration

6.1.2. Device Settings

Based on pre-fault activity observed during the Pre-Fix project, the magnitude and duration of defects fall below the trigger settings of standard protection equipment on the network, meaning devices must be more sensitive to events than protection equipment. However, this needs to be balanced with not making the device so sensitive that it triggers consistently on minor waveform deviations during peak loading. This balance has been experimented with during the project to try to find a suitable trigger level, and a level of either 100A or ~5% of the Primary 1ph RMS break rating residual error for 10% of a cycle has been found to be a suitable level for class 1 devices. Initial trials using a 5A distortion for 25% of a cycle and using 25A inrush triggers to make the power quality monitor as sensitive as the feeder breaker class 2 devices were unsuccessful. In times of peak loading, the normal power fluctuations of the network were enough to trigger captures that had no (pre-)fault condition. These were so frequent that they would fill the memory banks of the power quality monitor and prevent further captures from being made, causing some fault events to be missed. We have reviewed the ability of some third-party devices to trigger on pre-fault activity based on their current functionality and have found similar results, with the inrush settings being somewhat limited when looking to detect pre-fault activity. See the Schneider electric T300 test report in the appendices for more details on this process.

The pre-fault detection settings of Class 2 devices can be even more sensitive than Class 1 devices, as Class 2 devices typically will be installed in locations with a lower load current where it is easier to discriminate between pre-fault activity and natural load changes on the network. In this case, a 20A residual error between samples at the same point on the cycle has been a suitable trigger condition.

The sampling rate of the devices used needed to be sufficient to observe short distortions in waveforms. It was found that a sampling rate of 32 samples per cycle was sufficient for Class 2 devices, and a sampling rate of 256 samples per cycle was sufficient for Class 1 devices. Sampling rates lower than these values were not tested.

6.2. Defect Location

What worked well?

A novel approach termed the 'driving point voltage methodology' (DP) has successfully predicted the location of pre-fault defects in 11/12 faulted cable networks and the principle of operation has also been demonstrated in overhead line networks. A direct impedance-to-defect approach for very large pre-faults (current magnitude exceeding 500 Amps) has also been successful, with 2/2 success cases on overhead line networks.

What was or should be changed/improved?

Based on field trial analysis, the dependency on accurate network model impedance and real time switching status information was highlighted.

Weighting predictions based on current magnitude have proved to be successful but do tend to favour defects located closer to the Primary substation. An alternative approach is to use a composite weighting which considers both frequency of defects and current magnitude. Plotting of raw impedance values can make the network schematic unclear and therefore weighted predictions are needed to plot pre-fault activity for decision making purposes.

Pre-fault location was demonstrated from Q3 2022 onwards in the form of FPI search zones which combined directional (pre-)fault passage indication and GIS network models to localise defect locations. Defect location was then further enhanced through development of impedance-based approaches. The C-DIP platform offers calculators which calculate impedance-to-defect for both phase-to-phase and phase-to-earth defects.

6.2.1. Impedance-to-Defect

The approach adopted by Pre-Fix for calculating impedance-to-defect required both current and voltage as input parameters for the automated algorithm. Using Class I devices (such as PSL PQube3s), the voltage during a network defect activity can be directly measured to feed into the distance-to-defect algorithm. The algorithm calculates a fault loop impedance using Ohm's law, where current is defined as the peak current magnitude and voltage is defined as the voltage point coincident in time with the peak current (line-to-ground for phase-to-earth defects and line-to-line for phase-to-phase defects). See section 4.10 for further details on the impedance-to-defect calculation (both manual and automated).

An impedance-to-defect, or forward line impedance is extracted from the overall fault loop impedance based on the nature of the fault i.e., whether phase-to-phase or phase-to-earth. The forward impedance path is overlaid on the HV network model to give potential defect locations and to quantify the metric distance-to-defect along the HV feeder(s) from the Primary substation. FPIs installed in feeder breaker panels (or at the head-end of a feeder) are used to isolate the faulted circuit from the rest of the network. As Class I devices were installed on the transformer incomer, they provide aggregate views of all the feeders. This meant the direct impedance-to-defect methodology required a very notable current spike (500A+ phase-to-phase) as to cause notable voltage depression and isolate the impedance-to-defect from any waveform contribution associated with base loading on other feeders. An example of such a waveform captured by a PQube3 is given in Figure 6.2.1 below, showing a phase-to-phase pre-fault defect on an underground cable network with significant depression in the corresponding line-to-line voltage. The direct trigger installation method developed during the project, ensures that there will be a waveform capture from a Class I device for any pre-fault event detected by a more sensitive Class

II device trigger. Therefore, whenever there is a voltage depression caused by a pre-fault event, the direct impedance to defect methodology can be used.

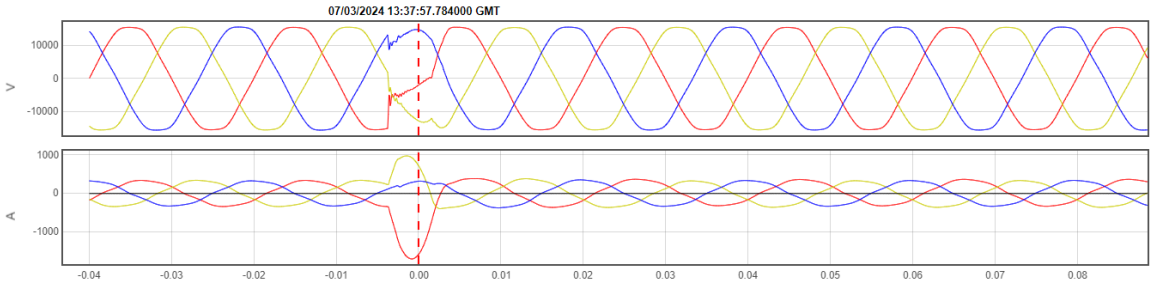

Figure 6.2.1, Current and voltage profile as recorded on a PQube3 for a large pre-fault defect on an underground cable network.

Very large pre-fault defects which caused voltage depression on the PQube3 waveform, as described above, were not seen frequently. This meant the direct impedance-to-defect approach was only applied a limited number of times – twice on overhead line network and once on an underground cable network. In these three instances, strong performance was achieved, with predictions landing in the correct spur or circuit section. However, an alternative approach clearly needed to be developed for wider applicability to the vast majority of pre-fault defects, which were much smaller in magnitude and were predominately detected by Class II devices.

6.2.2. Driving Point Voltage

Observations from the field trial in the pre-fault domain showed that the algorithm for calculating impedance-to-fault in the post-fault domain could not be always be directly transferred to the pre-fault domain due to insufficient current magnitude as to cause notable voltage depression in class I captures. Additionally, class II devices, which were configured with detection thresholds to be more sensitive to pre-fault defects, do not capture voltage in all circumstances (for example, in feeder breaker panels where there is no voltage signal present within the panel). This meant that the direct impedance-to-defect calculation could not always be applied. To overcome this, the Pre-Fix team pioneered an alternative, entirely novel, approach termed the ‘driving point voltage methodology’ (DP) which used historical pre-faults and their corresponding post-fault locations to derive a driving voltage. Pre-faults were matched to post-fault locations (i.e., a known impedance-to-defect) if the pre-fault disturbances ceased after the post-fault, and if waveform archetypes and the phases affected overlapped. These driving voltages were then used to calibrate a network for future pre-faults, where predictions would be made based on pre-fault current (from Class II device) and the driving point voltage previously derived. The methodology is demonstrated in Figure 6.2.2, using an example cable fault from June 2022.

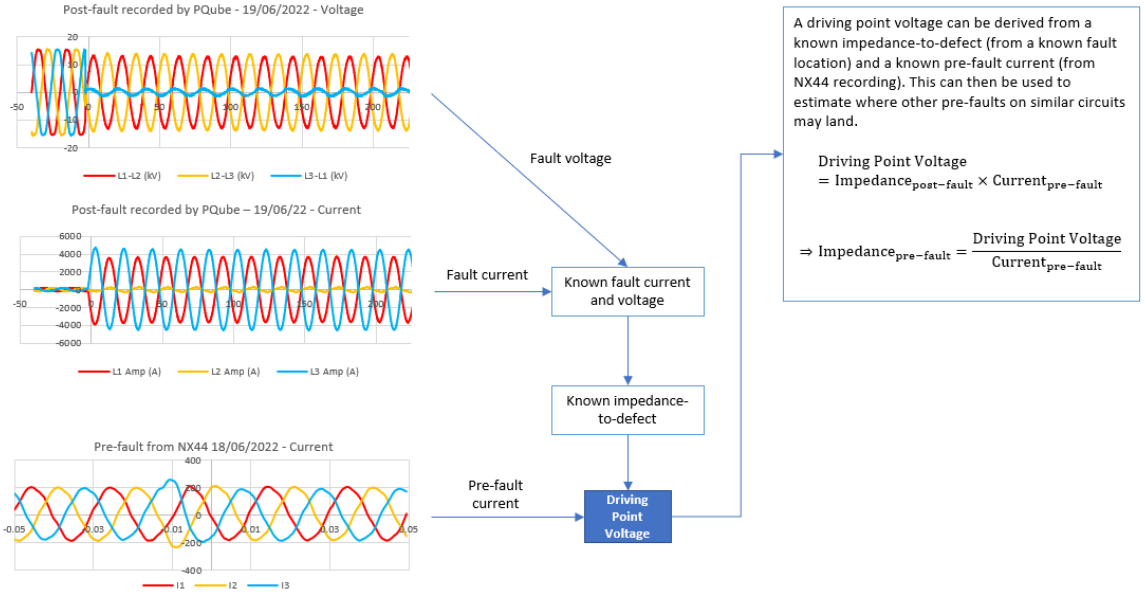

Figure 6.2.2 -Flowchart depicting the derivation of a driving point voltage for an underground cable fault.

As well as applicability to pre-faults of smaller magnitudes captured by Class II devices (which accounted for the majority of pre-fault activity), the main advantages of the driving point methodology was in eliminating requirement of coincident voltage measurement for pre-faults and in not requiring an explicit earthing model. Instead, the dependency would be in waiting for a circuit to fault in order for a network to be calibrated (note, 15 of the 17 total Primary substations monitored experienced at least one fault during the trial period) and forward predictions to be made of subsequent activity. However, case studies also showed that driving point voltages from calibrated sites could be adjusted and transferred to uncalibrated sites of similar network characteristic type (e.g., similar material construction and impedance per length values). This enables the roll-out of pre-fault devices on networks with similar characteristics without the need for calibrating each new site. In some examples, successful defect location was possible even when there was a 20% variation in material construction; however, for a trusted defect prediction it is recommended to transfer driving point voltages from a calibrated site with less than 5% variation in construction type.

Using the driving point methodology, defect location predictions were made on circuits with significant levels of pre-fault activity. During the course of trial, these predictions were able to be validated for ten distinct default locations, where the circuit ran to failure (which occurred seven times) or when independent validation equipment was deployed (in the form of partial discharge mapping, which occurred three times). Predictions were made using multiple event captures to produce a heatmap of plausible defect locations. Figure 6.2.3 gives an example of successful pre-fault location on an uncalibrated network. In this instance, the actual fault location aligned well with the prediction, with the faulted joint being 20 metres from the heat spot prediction (red).

For each individual pre-fault event on a feeder, the impedance to defect can be directly plotted on to a network diagram. However, for pre-fault events associated with a particular defect the pre-fault current magnitude has been observed to vary slightly. This can result in the pre-fault events associated with one network anomaly being plotted with a spread within a particular cable section. This can then lead to difficulties in interpretation of the visual representation of the pre-fault activity. To ensure easier interpretation of the results the use of weighting of pre-fault events and the use of heat maps for visual representation of pre-faults was developed.

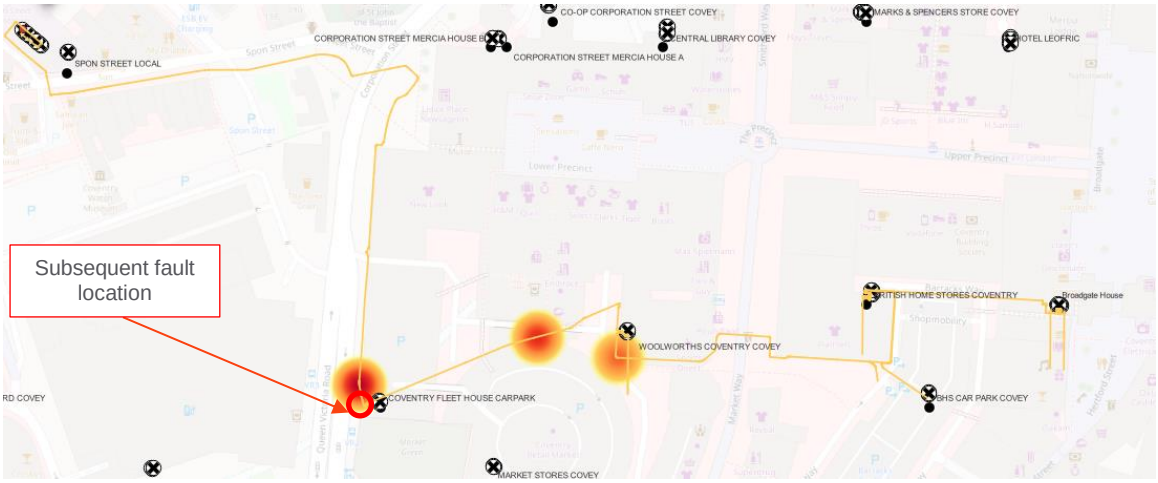

Figure 6.2.3: Pre-fault location prediction heatmap on underground cable network, weighted based on the current magnitude of defect.

6.2.3. Heatmaps and Weighting

Heatmaps were used for pre-fault location predictions as they allowed for the easiest visualisation of multiple pre-fault events which could be seen in the lead-up to post-faults. As pre-faults tended to disperse between circuit sections, a weighting approach was used to isolate the most likely section to fault based on density of the heat-spots. Density was originally weighted using frequency of pre-fault defects (i.e., the point of highest density would be the cable section where most pre-faults landed), however, learning from circuits which ran to failure suggested that weighting based on current magnitude may give better indication of actual fault location.

Additional validation of this method was provided by partial discharge mapping, where current magnitude performed best for heatmap weighting for three further sites. Alignment was also found where the frequency of defects was used for weighting, though results were not as conclusive. The team continues to consider both frequency and current magnitude, as well as a composite weighting that considers both together (defect frequency multiplied by current magnitude), as a larger sample size is required before conforming to a single weighting factor.

Peck frequency | Current Magnitude | Composite weighting – Peck Freq*Current Magnitude

Figure 6.2.4: Experimenting with heatmap weighting.

Furthermore, composite weighting also allows for better identification of cases where there are multiple defects on a circuit at different locations, as heat density will be more dispersed (whereas

a weighting based on current magnitude would favour the defect of lowest impedance, i.e., closest to the Primary). This has been notable in two instances where weighting using the composite factor described above (peck frequency multiplied by current magnitude) identified hotspot locations on the bottom half of circuits, which would otherwise have been weighted less if using current alone. In both these instances a defect was confirmed using partial discharge mapping on joints less than 20 metres from predictions, see examples in Fig. 6.2.5 and 6.2.6.

Figure 6.2.5: Prediction made using composite weighting gave a heat spot on lower half of the circuit, following which PD mapping was used to validate the presence of a defect.

Figure 6.2.6: Prediction made using composite weighting gave heat spot on lower half of the circuit, following which PD mapping was used to validate the presence of a defect.

Whilst defect location has been very successful when weighting predictions based on current magnitude, weightings based on the frequency of activity have been less conclusive. The disadvantage of a solely current weighting means a biasing of defects closer to the Primary. A potential workaround has been considered through use of a composite weighting (which considers both frequency and current). However, more instances of pre-fault location are required to validate this composite weighting and quantify the proportion which should be attributed to current magnitude, and the proportion attributed to frequency.

Whilst results have been successful so far, more confirmed pre-fault and post-fault locations are required to build confidence in the methodology. This could potentially include taking more proactive action, such as further partial discharge testing to confirm the presence of a defect without having to run to failure. The automation of distance to pre-fault and production of the heatmaps will be added in future releases of the C-DIP.

6.2.4. Overhead Line Driving Point Voltage Use Case

The driving point methodology is more mature on cable networks, having been developed using Class II devices installed on the underground cable network (NX44s). Despite this, the methodology has been successfully transferred to overhead line network using overhead line FPIs (Smart Navigator 2.0s). The case study below gives one such example.

Pre-faults were detected by Smart Navigators at 17:52 on 05/01/2023, as shown below. The disturbances caused a spike in current of approximately 100 amps, but were not large enough to cause supply interruption or trip any network protection devices.

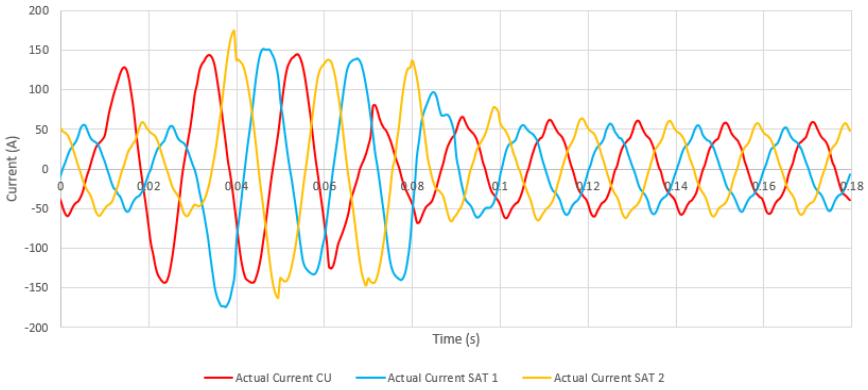

Figure 6.2.7: Pre-fault detected by Smart Navigator 2.0s on 05/01/2023, later attributed to tree encroachment after helicopter patrol.

The driving point methodology was used to predict three equal-impedance locations (on three different spurs). Predictions were used to inform a routine helicopter patrol on 19/01/2023, where two instances of tree growth encroaching on the overhead line safety clearance were observed in close proximity (within 90m) of one of the predictions. A comparison between the predicted (red circles) and actual locations of tree infringement (marked) is shown in Figure 6.2.8.

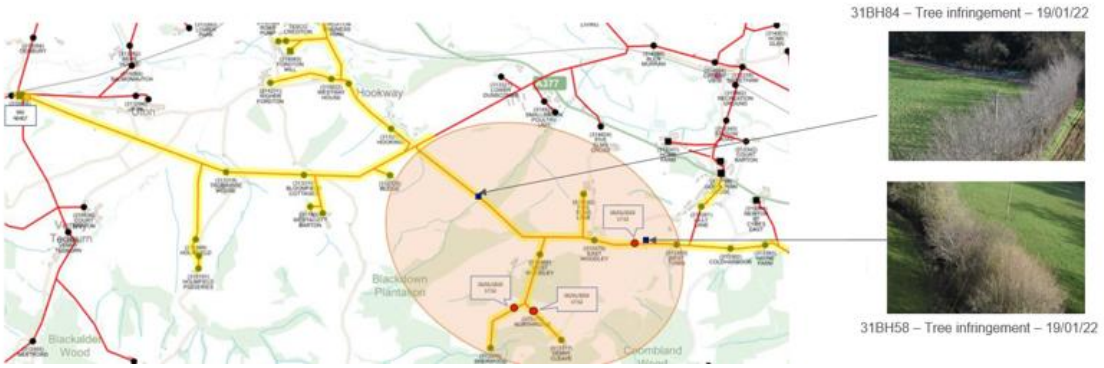

Figure 6.2.8: Distance-to-Defect illustration on rural HV overhead line network comparing predictions (red dots) and subsequent instances of tree encroachment (black squares marked).

In this example, remedial work was immediately scheduled to remove the tree growth and prevent an unplanned HV outage. Pre-fault activity ceased once this work was completed, giving confirmation that the defects observed were directly linked to the locations of tree infringement.

This case study demonstrates more cases of confirmed OHL pre-fault locations are required to gauge the efficacy of the driving point methodology on overhead line networks and compare accuracy in relation to underground cable networks.

6.3. Defect Classification

What worked well?

Pre-Faults (such as incipient cable joint faults) were able to be identified by a convolutional neural network matching those published in the IEEE report PES-TR73.

What was or should be changed/improved?

Since the convolutional neural network needs confirmed root causes to aid performance validation, more data would continue to be required to build confidence in the veracity of existing classifications as well as providing evidence for training new archetypes.

6.3.1. Waveform Classification

Based on the IEEE report PES-TR73, it is known that waveform distortions will differ in shape and magnitude based on the type of component that failed, and how it failed. Using the report as a baseline, a convolutional neural network (CNN) was trained using the waveforms in the report and applied to waveforms captured in the field. In doing so, it has been confirmed that different pre-fault defects will also result in different waveforms, which has allowed for the prediction of which component on a network has a defect present before it has failed and caused a fault condition. Different CNN models have been developed for different devices, as the difference in location, data captured, and sampling rate has led to significant differences in the observed waveforms for the same event between different device types.

An example of where the findings from Pre-Fix match those of the IEEE report is most easily found with incipient cable joint pre-faults, which can be seen below in Figures 6.3.1 and 6.3.2. Variants of these pre-faults which show multiple pecks in close succession have also been observed, as well as pecks that have evolved into multi-cycle phenomena, also below in Figures 6.3.3 and 6.3.4. Throughout the project trial, no obvious differences in pre-fault waveform were observed between varying cable joint types or cable types. This is another avenue for potential research to understand differing behaviours of various joints and cables as pre-fault anomalies progress towards failure.

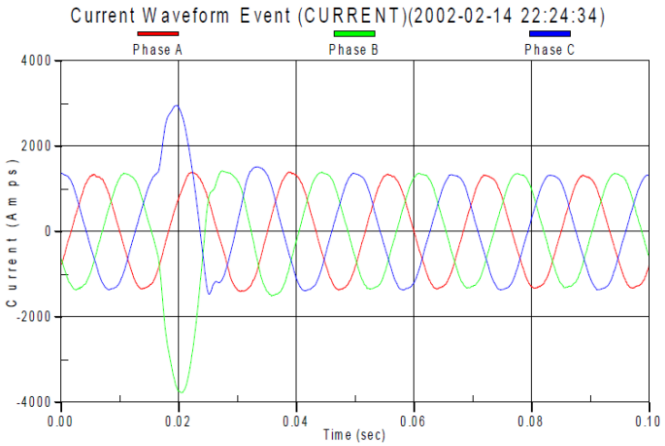

Figure 6.3.1: IEEE Report example of an incipient cable joint pre-fault

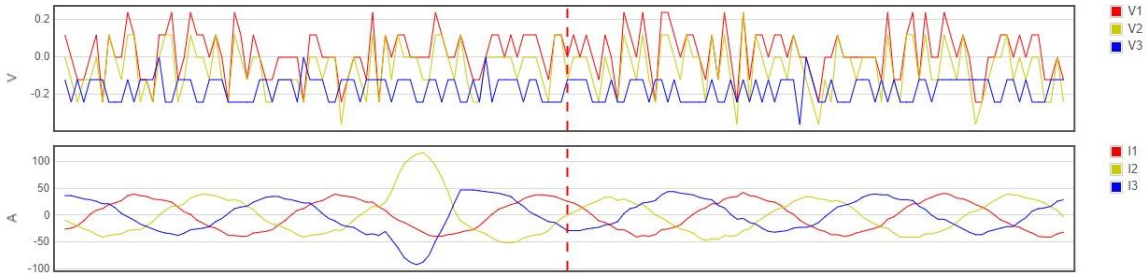

Figure 6.3.2: Incipient cable joint pre-fault captured by a class 2 device at Courthouse Green Primary feeder 6, matching the shape of the IEEE example

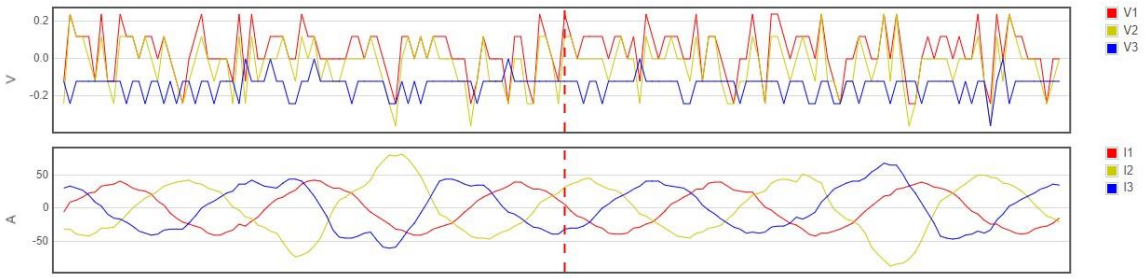

Figure 6.3.3: Incipient cable joint pre-fault captured by a class 2 device at Courthouse Green Primary feeder 6, with multiple incipient cable joint pecks within the same capture

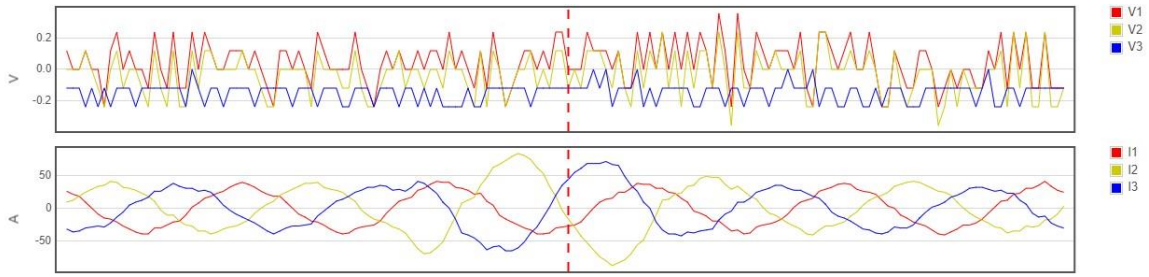

Figure 6.3.4: Incipient cable joint pre-fault captured by a class 2 device at Courthouse Green Primary feeder 6, lasting more than one cycle

Using waveform classification to predict all faults is not always possible, as not all faults have a build-up of pre-faults and some faults can be caused by human error affecting a healthy cable, such as building works severing a cable. Another limitation is the lack of a complete database of every pre-fault waveform, as the IEEE report specifies two pre-faults that are relevant to underground cable networks, but not pre-faults relevant to overhead line networks.

Since the beginning of the project, the number of pre-fault classifications that have been trained into the model has increased by using NGED fault reports and the root causes of them found by field teams on site and comparing this to any pre-fault waveforms that lead up to the fault, and that also stopped immediately after the fault had cleared and/or repairs had been made. An example of this is a potential overhead line disc insulator pre-fault in Figure 6.3.5.

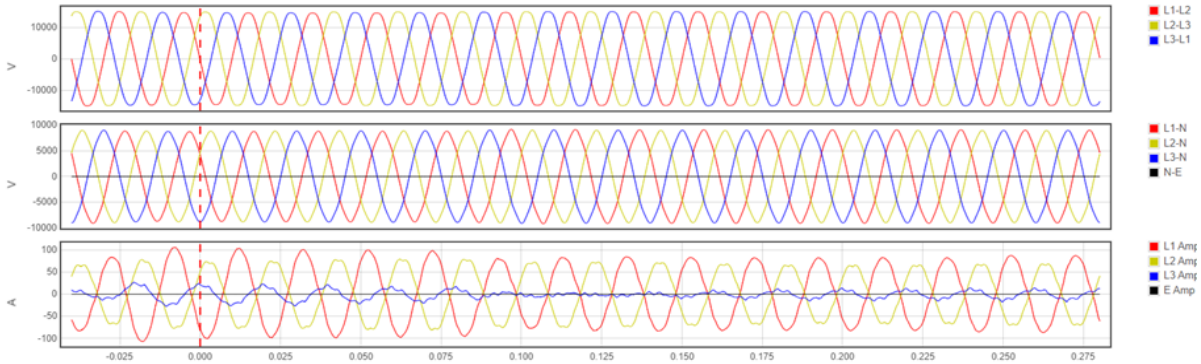

Figure 6.3.5: Potential overhead line disc insulator pre-fault captured by a class 1 device at Chudleigh Knighton Primary in the lead up to a disc insulator fault

This method allows a hypothesis to be formed that these pre-faults are tied to a specific asset, allows the training of an updated model, and the application of that model to other cases where these unconfirmed pre-faults are seen. It is difficult to definitively tie a pre-fault to a post-fault based only on this post-fault build up analysis, so this retraining and reapplying to see if the situation repeats itself is necessary to build confidence that the pre-fault and post-fault are connected. When working with pre-faults, a particular focus has been placed on waveforms from Class 2 devices when analysing pre-fault activity, as they tend to see much lower peak loading and can therefore be configured to be more sensitive without the introduction of excessive noisy captures.

To determine the accuracy of the CNN model at predicting the post-fault asset affected, the build-up to 18 faults across 12 feeders that faulted during the project and had had the fault cause confirmed on site was analysed, with a view to confirming whether common pre-fault classifications (>10% of results) matched the findings of the field teams. Pre-faults that could have locations plotted were used in order to tie them to the approximate location of the fault, and pre-fault captures were monitored for 2 weeks or more after the event to investigate whether the fault and repair had stopped their occurrence in the area in which the fault occurred. The classification

result of the I^2T (the energy within a pre-fault peck, explained in detail in section 6.4) Peak event that occurred before each post-fault was also compared against the field team findings to confirm if that provided a better indication of the post-fault event than the pre-faults surrounding it. A full breakdown of the results from this exercise can be found in the D&A faulted watchlist feeders waveform analysis presentation, with a summary shown in Tables 6.3.6 and 6.3.7 below. During this analysis, a number of the OHL based faults did not have a known pre-fault event associated with them, so would not have been able to predict that asset type (though the post-faults were trained, see the equivalent table in section 7.3). The classification method in this case would pick the next closest fault type when predicting what the fault was.

Table 6.3.6: Results from the analysis of the most common pre-fault waveform classification in the build up to a fault against known fault causes

Faulted Asset	Number of Events	Most Common Classifier Asset Prediction
Cable Joint	3	Cable Joint x3
Cable	2	Cable Joint x2
Cable or Cable Joint (Unconfirmed)	5	Cable x1, Cable Joint x4
HV Fuse Operation	1	Cable Joint x1
OHL Foreign Contact	2	Cable x1, Unknown Asset (3ph Swell) x1
Pole Termination	2	Cable x1, Cable Joint x1
Disc Insulator	3	Disc Insulator x1, Cable Joint x1, Unknown Asset (3ph Swell) x1

Table 6.3.7: Results from the analysis of the I^2T event pre-fault waveform classification in the build up to a fault against known fault causes

Faulted Asset	Number of Events	I2T Event Classifier Asset Prediction
Cable Joint	3	Cable Joint x3
Cable	2	Cable Joint x2
Cable or Cable Joint (Unconfirmed)	5	Uncaptured (CT Saturated) x1, Cable Joint x3, Cable x1
HV Fuse Operation	1	HV Fuse Operation x1
OHL Foreign Contact	2	Cable x1, OHL Foreign Contact x1
Pole Termination	2	Disc Insulator x1, Cable Joint x1

Disc Insulator	3	Disc Insulator x2, OHL Foreign Contact x1

An important note in the investigation of new waveform types is to investigate the events surrounding waveform captures before attributing them to a certain post-fault type. Examples of waveforms that happened in very close proximity to a disc insulator fault, and did not repeat after the fault have been seen at Claverdon, one of which is shown in Figure 6.3.8. This led to an initial investigation into whether this would be a suitable pre-fault marker for disc insulator faults. However, further investigation found that this was part of a Primary-wide event, as shown in Figure 6.3.9, and therefore could not be tied to disc insulator events as a whole.

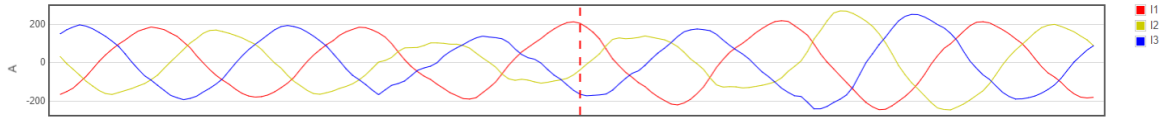

Figure 6.3.8: Pre-fault captured at Claverdon 5 days before disc insulator fault on feeder 6

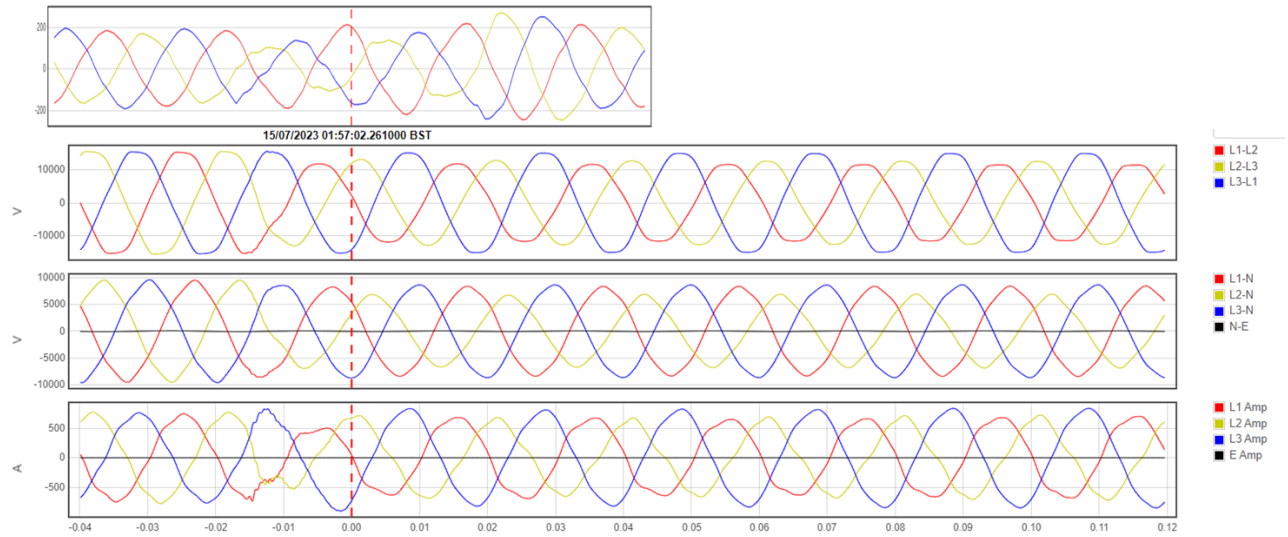

Figure 6.3.9: Claverdon coincident class 1 and class 2 device captures showing a Primary-wide event was occurring rather than a feeder specific one

7 new potential pre-fault waveform categories have been identified during the project, as well as a category that denotes no fault has occurred that is used to help filter out noise. This is up from the initial 3 pre-faults in the IEEE report. The new pre-faults found within the project are three-phase swells (shown in Figure 6.3.10), which does not currently have an obvious asset associated with the waveform and is something that is being investigated, and three potential disc insulator waveforms, covered in the case study in section 7.3.

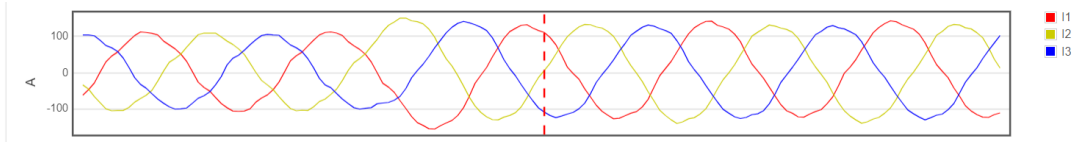

Figure 6.3.10: 3-phase swell capture captured by a class 2 device

6.3.2. Cable Joint vs Cable Pre-Fault

The IEEE report PES-TR73 has separate pre-fault waveforms mentioned for cable joints and underground cables. These pre-faults are somewhat similar in form, though can be distinguished, and are shown below in Figures 6.3.11 and 6.3.12. Both pre-faults show predominantly phase-phase activity, though can also affect all three phases. However, while both show a peck in the main phase affected, the cable fault shows a depression in one of the two phases, while the cable joint fault shows a smaller peck instead.

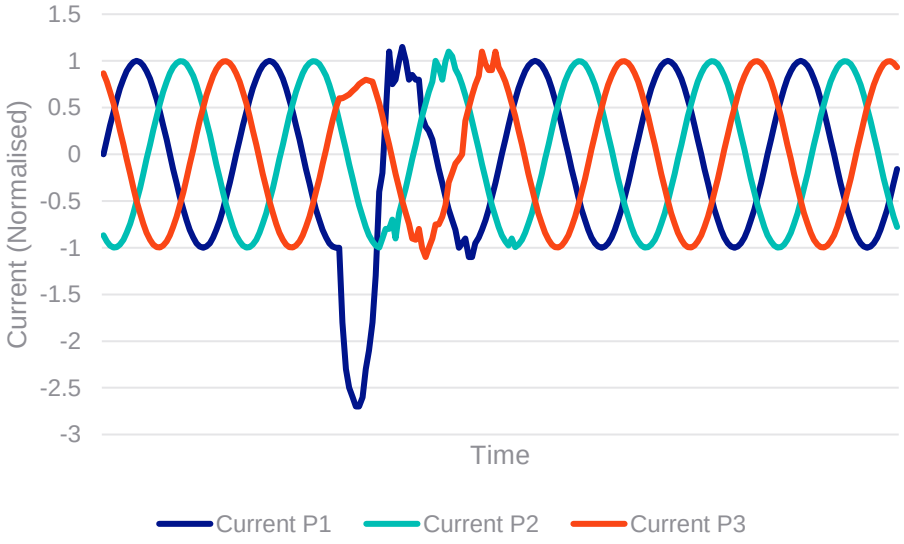

Figure 6.3.11: Incipient cable pre-fault

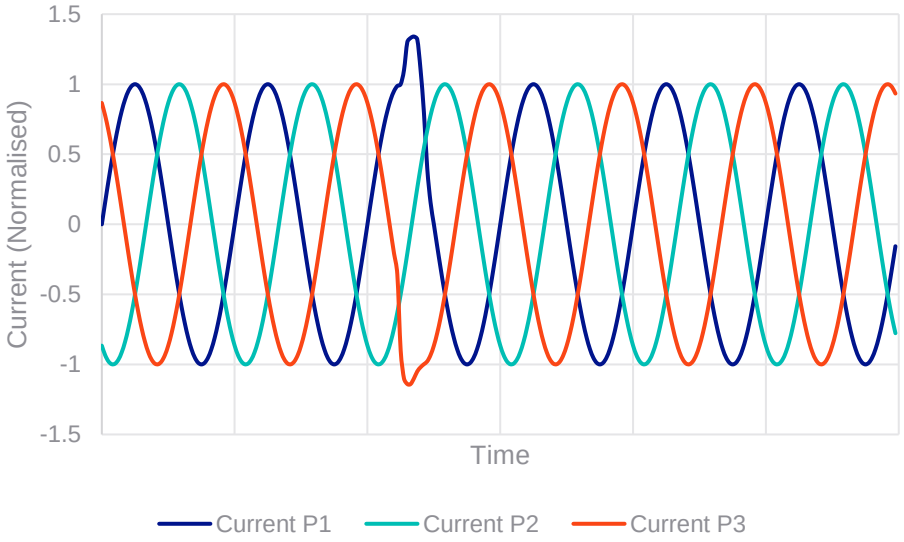

Figure 6.3.12: Incipient cable joint fault

During the project, it has been observed that the incipient cable joint fault was significantly more common than the incipient cable fault waveform, and contrary to the findings in the IEEE report however, waveforms that match the incipient cable joint pattern have been observed in the lead up

to faults on the cable itself. During the analysis of the 18 faults shown in the previous section, this occurred in 5 cases when looking at the I^2T event, and 6 cases when looking at the most common pre-fault prediction in the lead up to the event. This has led to the question as to whether there should be a combined category for these two fault types, and opens the question as to whether the type of underground cable in use is relevant to the resulting defect waveform as a potential future avenue for research.

One site which allowed for a more detailed analysis of this phenomenon was Whitley Primary substation feeder 11. This feeder had a cable joint fault on the 14th July 2023, followed by a cable fault a few metres away from the repaired joint on the 22nd August 2023. In the lead up to the cable joint fault on the 14th July, examples of the IEEE defined incipient cable joint pre-fault peck were observed affecting the red and yellow phase, one example of which is shown in Figure 6.3.13.

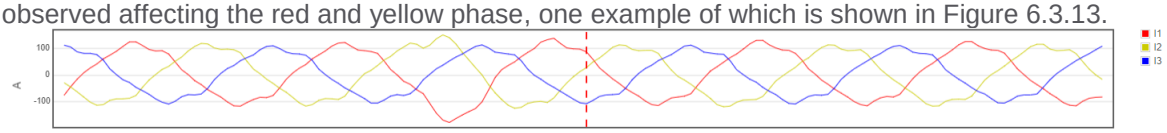

Figure 6.3.13: Pre-fault captured by class 2 device 1 day before cable joint fault on Whitley Primary feeder 11

After the repair work to the joint, there were no further pre-faults for around 2 weeks, after which pre-faults similar to the cable joint pre-faults were observed also on red and yellow phase, one of which is shown in Figure 6.3.14. Plotting the location of these pre-faults led to a similar location to the cable joint pre-faults associated with the cable joint fault on the 14th July.

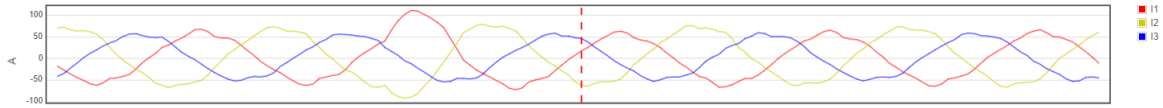

Figure 6.3.14: Pre-fault captured by class 2 device 2 weeks after cable joint fault, 4 weeks before cable fault at Whitley Primary feeder 11

The pre-faults continued until 5 days before the cable fault on the 22nd August, with the final pre-fault captured, shown in Figure 6.3.15 also affecting red and yellow phase, but lasting longer than previously observed pecks. It should be noted that there was no observed spike in I^2t, however the pre-faults in both instances (for cable fault and cable joint fault) were similar in shape and current magnitude.

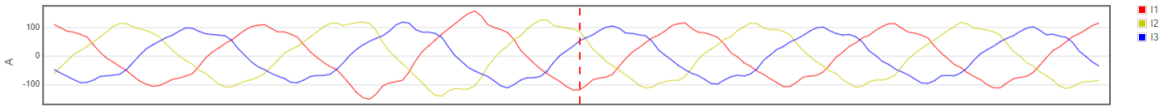

Figure 6.3.15: Pre-fault waveform captured by class 2 device 5 days before cable fault on Whitley Primary feeder 11

Pre-faults which could be located to the same area as the cable joint and cable that faulted halted after the fault, adding credence to these pre-faults being related to the faults observed. Analysing this site with both a known cable joint and cable fault in the same location showed that there can be significant overlap between the pre-faults observed in the build up to cable and cable joint faults.

6.3.3. Defect evolution of waveforms

For pre-faults, the evolution from two-phase to three-phase activity in the lead-up to a fault has been observed, as well as duration and frequency changes over time. Examples of waveforms from feeder 6 at the Courthouse Green Primary substation that have evolved from a standard incipient cable joint peck to displaying multiple pecks per capture, and/or multi-cycle pecks have been shown previously in Figures 6.3.2, 6.3.3 and 6.3.4. The feeder mentioned has yet to fault during the trial, but partial discharge mapping on that feeder has detected the presence of a defect

in the same circuit section as the pre-faults captured were calculated to have originated from. More information on this methodology can be found in section 8.1. Other examples of pre-fault pecks evolving in duration were seen at Whitley and shown above in Figures 6.3.14 and 6.3.15. Similar behaviour in pre-fault waveforms has been observed at the Spon Street Primary substation on feeder 6, which did have a cable fault in November 2023. This can be seen in Figures 6.3.16 and 6.3.17.

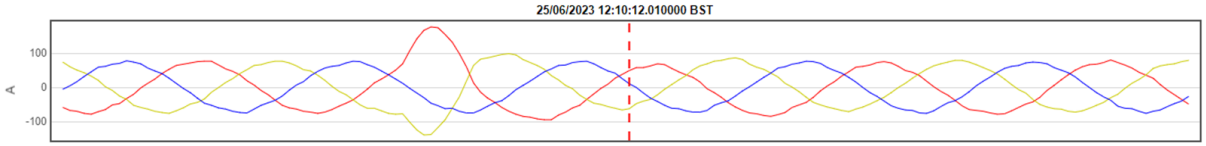

Figure 6.3.16: Incipient cable joint peck lasting less than half a cycle

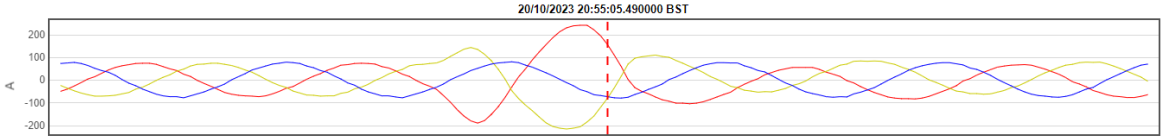

Figure 6.3.17: Incipient cable peck lasting a full cycle

The evolution of pre-fault pecks from two-phase to three phase was seen in a large number of the monitored feeders that went on to fault in the trial, while the duration of the peck seemed to have less correlation. The full investigation into waveform analysis and factors that could contribute to the time-to-failure is covered in section 6.4.

6.4. Time to Failure

What worked well?

Based on observations within the field trial to date, a spike in I^2t (heat energy dissipated in a pre-fault defect) combined with the evolution of the number of phases affected is a good leading indicator of cable failure, with observations ranging from four days to three months between peak I^2t spike and failure.

What was or should be changed/improved?

Ranking proximity-to-failure using absolute values, such as total pre-fault current and I^2t can bias the results towards circuits of higher loading. Using composite factors that baseline these values (e.g., by dividing through by nominal current) helps to reduce this bias while still giving high relative rankings to faulted circuits.

6.4.1. Methodology

To investigate time-to-failure the Pre-Fix team observed leading indicators in the pre-fault lead-up to post-fault events. As part of this, a reporting function (termed a wireframe report) was developed to extract events captured from all devices along with associated waveform metadata such as current magnitude and I^2t (heat energy dissipated in a pre-fault defect). One of the main uses of the wireframe report was in informing and building a watchlist of active underground cable feeders with the goal of ranking by likelihood of, and proximity to, failure. Underground cable feeders were chosen initially due to higher prevalence of pre-faults (however, the introduction of NX44-PQube3 direct trigger has allowed for better visibility of overhead line pre-faults later in the project). Factors (termed 'leading indicators') are summarised in Table 6.4.1 which includes a list of post-faults, a matrix of several leading indicators and time-to-fault in each instance.

Type of Fault	I^2T Spike?	Three Phases Active (Pre-Fault)?	Pre-fault Current Magnitude Spike?	Previous Fault on Same Circuit or Adjacent Feeder? (Last 3M)	Time-to-fault after Largest I^2T Spike
Cable fault	Yes	No	Yes	No	13 days
Cable fault	Yes	Yes	Yes	No	7 days
Cable damage	Yes	Yes	Yes	Yes	3 months
Cable fault	Yes	Yes	Yes	Yes (same circuit)	6 days
Cable damage	Yes	Yes	Yes	No	14 days
Faulted joint	Yes	No	Yes	No	5 days
Cable fault	Yes	Yes	Yes	No	4 days
Cable fault	Yes	Yes	Yes	Yes (same circuit)	9 days

Table 6.4.1: Table of post-faults with matrix of leading indicator factors.

Due to high noise-to-signal ratio at some Coventry sites, the report was developed to be able to filter out background noise from legitimate pre-fault activity. The scale of filtering was such that individual devices on very noisy circuits could experience a reduction from 3000 total captures to less than 50 distinct, non-spurious captures. This demonstrated the necessity of having a robust noise-filtering algorithm in place before attempting to analyse large waveform datasets. Some later case studies, however, demonstrated the need for revisiting the raw data. This was relevant in instances where noise filtering was too sensitive and legitimate activity was overlooked. Moving forwards, the team retained and analysed the unfiltered data for analysis to feed additional insights into the feeder watch list which had been filtered out. During the course of the Pre-Fix project, some behaviour was observed such as repetitive three-phase swells on HV feeders, which appeared as small increases in current for a few cycles occurring in regular intervals throughout the day. These observations have been passed across to NGED's wider business for further investigation as there is still uncertainty regarding if the three phase swells are background network activity or pre-fault events. One key recommendation here, is to ensure that any network activity is accounted for in waveform filtering and that this may be required to be updated once monitoring of a circuit has begun.

Number of Phases Affected

Number of phases affected refers to the number of current channels which are distorted or exhibit pre-fault activity as a result of a defect. Pre-fault activity on underground networks was predominately phase-to-phase, even in instances where the subsequent post-fault was phase-to-earth. Notable, however, was the transition from two phases affected to three phases affected in the lead-up to a fault. The time-series plot in Figure 6.4.2 gives an example of the evolution of

phase activity over time in the lead-up from pre-fault to post-fault. See also Fig. 6.4.3 and 6.4.4 giving examples of the evolution from two-phase to three-phase pre-fault activity on an underground cable circuit.

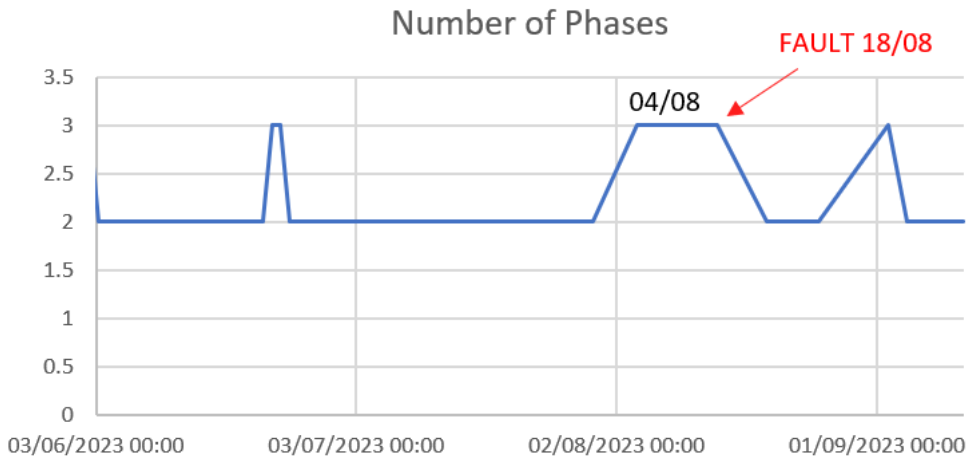

Figure 6.4.2: Time-series plot of the change in phases affected during pre-fault activity leading up to a post-fault event.

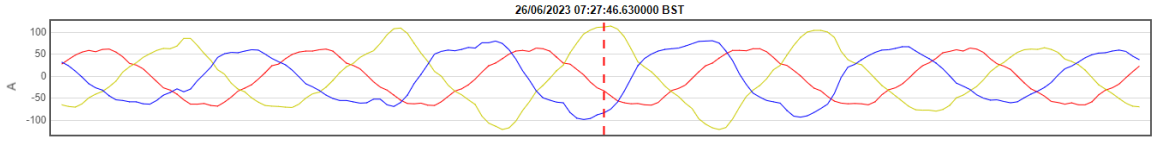

Figure 6.4.3: Current profile from NX44 showing an example of a two-phase pre-fault event.

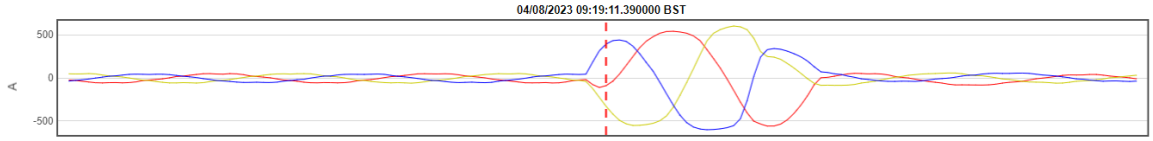

Figure 6.4.4: Current profile from NX44 showing an example of a three-phase pre-fault event.

An evolution from phase-to-phase to three-phase was experienced in almost all cases were a circuit ran to failure, and was a more notable failure indicator than a persistent three-phase defect (i.e., a defect which begins and remains three-phase). It was also observed that an evolution of phase-to-phase to three-phase activity was more notable when coinciding with a spike in another leading indicator (such as an I^2t spike or an increase in pre-fault current magnitude) as demonstrated in Table 6.4.1. Three-phase activity by itself, for example second spike after fault in Figure 6.4.2, was not as strong an indicator in comparison.

One consideration when observing the evolution from two phases affected to three phases affected was to confirm that the disturbance was a legitimate pre-fault defect, and not attributable

to some other network phenomenon, such as three-phase swells or switching activity. Swelling was filtered out using waveform classification, whereas switching and fault activity on adjacent feeders was filtered using corroborative sources of information, such as NGED fault reports.

Number of Cycles Affected

During the course of the project, a working hypothesis was tested to understand if the number of cycles affected by the pre-fault defect would increase in the lead-up to post-fault. Whilst this was seen in several examples, correlations were not as strong as with the number of phases active. However, it should be noted that the trial timescales are relatively short when compared with the entire life of the cable.

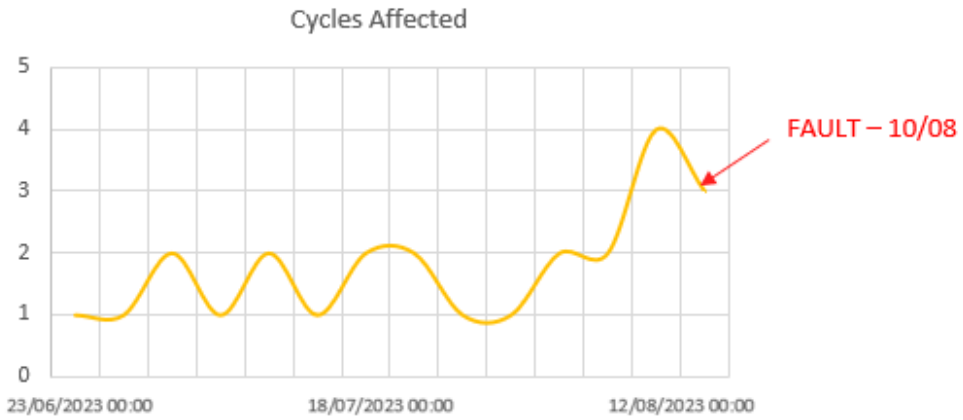

Figure 6.4.5: Time-series plot of the evolution of cycles affected during pre-fault activity leading up to a post-fault event.

Some minor correlations were picked up between number of cycles affected and the weather e.g., rainy weather resulting in a large number of multicycle captures in the subsequent days. Weather patterns were not investigated in depth or at scale, but could be a potential future research avenue.

Energy within disturbance - I^2t measurement

I^2t refers to the relative heat energy dissipated in a pre-fault defect (measured in ampere squared seconds), quantified by projecting the nominal (pre-disturbance) waveform and calculating the difference when overlaying the pre-fault waveform, see Figure 6.4.6.

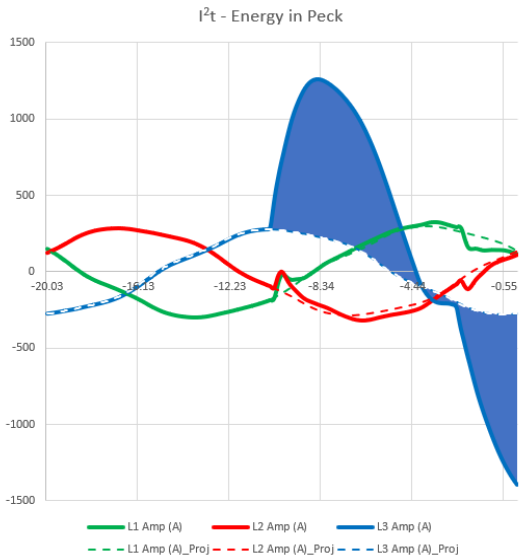

Figure 6.4.6: Graphical representation of the I^2t metric, shaded in blue.

In all cases of post-fault on underground cable networks, a spike in I^2t was experienced in the lead-up to the operation of protection. The spike could be due to either an increased current magnitude, or an increase in defect duration, but usually both. I^2t spikes were generally within the range of 1000-5000 A^2s, though in one example reached almost 10,000 A^2s. In comparison, baseline pre-fault activity ranged from 200-500A^2s, depending on circuit loading. A comparison between baseline pre-fault activity and an I^2t spike is given in Fig. 6.4.7 and 6.4.8, below.

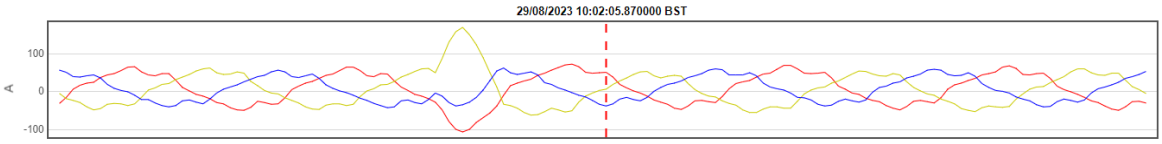

Figure 6.4.7: Current profile recorded by NX44 showing 'baseline pre-fault activity'.

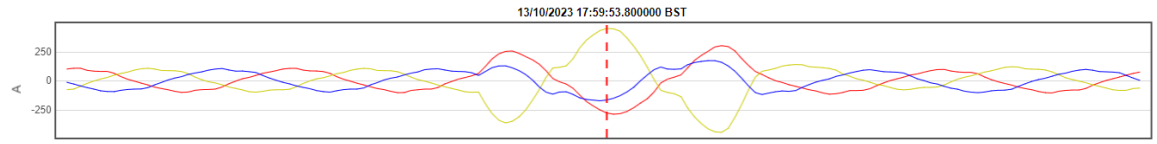

Figure 6.4.8: Current profile recorded by NX44 showing an I^2t spike of approx. 2000A^2s.

A key learning point was that it was necessary to confirm direct linkage between the I^2t observations and the post-fault, and eliminating contributions from external factors such as switching or fault activity on adjacent circuits. For example, in one case study a very large I^2t of 20,000 A^2s was observed on an underground network, flagging the circuit as under high risk of failure. However, analysis of fault reports showed it was coincident with switching activity. A key recommendation is to ensure that any network switching activity can be accounted for within the C-DIP. There are plans in future to integrate switching activity within the NGED network into the C-DIP so that any coincident pre-fault activity can be discounted. To help build confidence that an I^2t spike was directly linked to a subsequent post-fault the Pre-Fix team explored three avenues: confirming no concurrent activity on adjacent or parallel feeders via fault reports, confirming no I^2t

spike observed after the post-fault, and confirming that the actual fault location coincided with the predicted location of the I^2t spike.

I^2t spikes were identified from up to three months prior, to only four days prior to the fault. In some cases, multiple I^2t spikes were experienced, with the second being in very close proximity to the fault. See example in Figure 6.4.9, below.

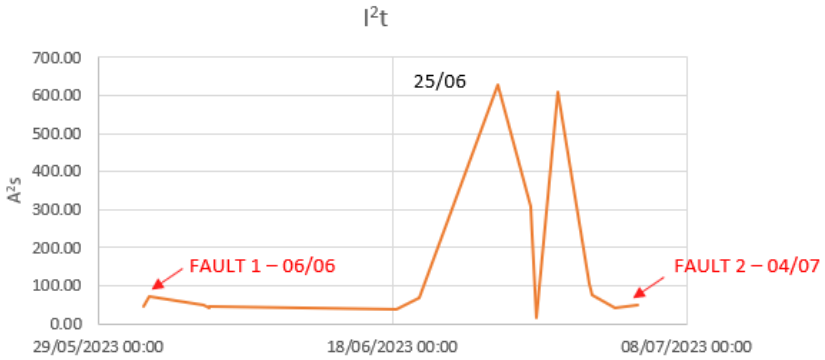

Figure 6.4.9: Time-series plot of the change in I^2t (A^2s) showing two large spikes in the pre-fault activity leading up to a post-fault event (FAULT 2).

Later iterations of the wireframe report added a composite metric (I^2t divided by the baseline current) as it was found to be less biased towards circuits of higher loading. With higher baseline loading, any pre-fault event will have a higher current magnitude and therefore a higher I2t. This would result in feeders with higher loading and higher I2t pre-fault events being higher up the wireframe watchlist report and highlighted as being more likely to experience a fault earlier. Dividing the maximum I2t value by the baseline current and giving a relative maximum I2t value removes this effect.

Results so far have shown that ranking by I^2t gives the best indication of proximity of failure as circuits which subsequently (or historically) faulted rank higher on average as compared to other metrics. Research is still ongoing to quantify time-to-failure after experiencing an I^2t spike and whether the magnitude of I^2t can be used to inform network intervention or escalation measures, such as when and where to conduct partial discharge mapping. Additionally, a future avenue exists in comparing the relative importance of I^2t current magnitude against duration of an I^2t spike.

Peak Current Magnitude

Peak current magnitude refers to the largest current point (in absolute terms) experienced during a pre-fault defect (single-phase for phase-to-earth defects or peak-to-peak for phase-to-phase defects). As with I^2t, spikes in current magnitude were experienced in the build-up to almost all post-faults. Ranking using peak current magnitude did not prove effective, as it tended to bias circuits of higher loading due to not accounting for a higher current baseline on these circuits. The focus was instead moved to the delta in pre-fault current, see below.

Peak Current Delta

Peak current delta refers to the largest deviation from the baseline load current and can be the maximum change in each phase or the maximum change across two phases, depending on the type of defect. See Figure 6.4.10, showing an example of the evolution in pre-fault current leading up to a post-fault. Ranking by peak current delta performed better than ranking by absolute current magnitude due to being less biased towards high-load circuits.

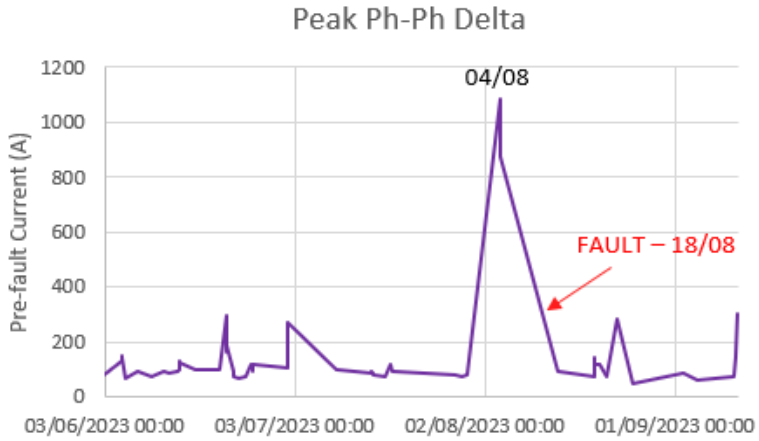

Figure 6.4.10: Time-series plot of the delta change in Ph-Ph current (A) peaks in the lead-up to fault.

Previous Earth Fault on Same or Adjacent Circuit

The underlying theory for this factor was that earth faults on the same, or an adjacent circuit, may produce electrical stress on assets and exacerbate existing defects. For example, due to a rise in earth potential caused by HV protection operation on an adjacent feeder. Circuit sections which have withstood recent fault passage may also be at higher risk of failure, as in one example, an underground cable circuit failed twice in the same circuit section within a month.

6.4.2. Findings & Future Research Avenues

Current learning suggests I^2t is a potential failure indicator. Of 78 feeders in the watch list (out of 126 feeders in total), all 10 that failed (or had a confirmed defect) experienced an I^2t spike and were in the top 30 feeders in terms of I^2t magnitude. Furthermore, three faulted feeders were placed in the top 10, including position #1 and #3. However, it is important to note that a further thirteen sites on the watch list experienced I^2t spikes but are yet to fail. More research is required to quantify time-to-failure after experiencing an I^2t spike. Potential relationships could also be investigated with regards to the magnitude of I^2t, as well as with cumulative variants (such as cumulative I^2t), composite factors (such as I^2t divided by baseline current), and other opportunities such as investigating the angle of inception in the pre-fault defect.

One challenge for quantifying time-to-failure was the difficulty in assessing whether post-faults were actually predictable via pre-fault observation. Initial indications were possible via waveform classification (i.e., if a pre-fault and subsequent post-fault had the same asset signature), and from alignment of pre-fault location predictions with actual reported locations of post-faults. Another challenge was confusion created on the feeder watch list due to post-fault switching events, which could resemble I^2t spikes. These were manually filtered, but could be automatically filtered once real-time integration of switching is in place.

For scale-up of this analysis, a larger data pool of linked pre- and post-faults is required, potentially through monitoring over a larger area, or for a longer period of time. Furthermore, more data is required via verified post-fault locations with verified root causes to enhance the capability of connecting a pre-fault directly to a post-fault and to build confidence in the leading indicator metrics.

Additionally, future research avenues are suggested for leading indicator metrics that were not investigated, especially with regards to overhead line networks. These are listed below:

- Angle of inception in the pre-fault defect.

- Comparing peck magnitude against local node fault level.
- Insulation stress on assets caused by earth faults on adjacent circuits.
- Investigating relationship between cable type/line construction and time-to-fail.
- Investigating relationship between cable joint construction and time-to-fail.
- Weather and heat.
- Harmonic content of the waveform.

6.5. Pre-Fault Location C-DIP Performance

What worked well?

During the course of the Pre-Fix project, 78 potential defective HV feeders have been identified from the total of 126 feeders monitored. Of these 78 feeders, defect location predictions have been made on 30, of which 17 have either exhibited a post-fault event or been independently analysed with partial discharge mapping. Pre-fault location estimations have been successful, with 16/17 predictions validated to be in the same circuit section as the post-fault.

What was or should be changed/improved?

The transient nature of some faults on overhead line networks has limited the number of validated pre-fault locations compared to underground cable networks. However, successful pre-fault location has been achieved through analysis of very large pre-faults (in excess of 500A) and the application of the impedance-to-post-fault methodology. Insight has been gained into more persistent defects (such as evolving cracked insulators), however a longitudinal study would build further confidence.

6.5.1. Results and Discussion

Performance for pre-fault location was best achieved on underground cable networks, where predictions were made using the driving point methodology and later validated by running to failure or partial discharge mapping. Correct identification of an overhead line pre-fault anomaly occurred at least four times, where the post-fault location could be validated. This occurred due to one instance of helicopter patrol of the line (see case study in section 6.2), and three other instances where notable pre-fault activity, predicted in a similar location to a post-fault, ceased once the post-fault had cleared (see examples in Fig. 6.5.2 and 6.5.4). Additional predictions were made but their exact location could not be validated (due to the common transient nature of faults on overhead line networks leading to successful recloses). Following on from Pre-Fix, helicopter patrols have been initiated to validate more pre-fault and transient fault locations on overhead line networks.

Table 6.5.1 provides an overview of performance metrics in terms of pre-fault localisation validation using post-fault locational information for both underground cable and overhead line networks. In addition, partial discharge (PD) mapping was used to validate defect locations on underground cable networks ahead of supply interruption. The metrics below encompass the 21-month trial period 1st June 2022 to 31st March 2024.

Pre-fault location predictions were deemed successful if they were in the same circuit section as the post-fault or the point of highest partial discharge. Whilst pinpoint distance accuracy was not targeted or expected, accuracies ranging from 10m to 350m were achieved. Notably, in all three cases of PD mapping, accuracies of within 30m were achieved with regards to the points of

highest confidence (i.e., the heat spot). This could allow fault location teams to identify the defective joint within the circuit section. No correlations have yet been found regarding pre-fault current magnitude (Amps) and magnitude of PD (pC) observed.

Table 6.5.1 – Summary of confirmed pre-fault defect locations for the period 1st June 2022 to 31st March 2024

Network Topology	Confirmed via Post-Fault	Confirmed via PD Mapping	Average Accuracy (m)
Underground Cable	7/9	3/3	200
Mixed OHL/UGC Topology	1/1	-	450
Overhead line	4/4	-	900
Total	**12/14**	**3/3**	

The above results were confirmed via post-fault location based on genuine post-faults (excluding manual maloperations and vandalism) as well as sites where a pre-fault defect was confirmed via partial discharge mapping. Of 15 pre-faults which ran to failure, 8 were used to calibrate the networks and determine a driving point voltage, and the other 7 fault locations were predicted using the driving point voltage methodology and confirmed to be correct following subsequent location of the post-fault. Partial discharge mapping was used to confirm the correct location of a pre-fault defect at three additional sites which had experienced large I^2t spikes, as discussed further in section 8 of this report.

The two underground cable incidents which were missed were not automatically processed due to noise filtering by the C-DIP, as these sites had a very high noise-to-signal ratio due to excessive three phase swells. Useable signal was found within the noise at one of these sites, and predictions landed in the correct circuit section when retrospectively extracted and analysed. Based on this, the team decided to retain all filtered data to ensure that it was easily accessible for analysis where necessary. No useable pre-fault signal was found at the other site, potentially because the NX44 on the circuit was persistently filling its daily quota with noise captures (attributed to three-phase swells). Consequently, a prediction was not able to be made. Following on from this, the team are using portable power quality monitors to investigate the potential source of noise on this circuit.

6.5.2. Driving Point Voltage vs Impedance-to-Defect for Pre-Fault Location

Whilst the driving point methodology has been successfully applied to overhead line networks (see case study presented in section 6.2), in the initial stages of the trial there was less opportunity to gauge performance as the testing of defect predictions is more difficult (i.e., PD mapping is not applicable and many defects are transient). In the latter part of the trial, there has also been the opportunity to explore OHL defects via helicopter patrols due to the increase in confidence in the results. Despite this, a notable observation is the presence of very large pre-faults which have been experienced on some overhead line networks which have allowed for the direct impedance-to-defect approach using class I waveforms.

Large OHL pre-faults have been attributed to current spikes of greater than 500 Amps, sufficient magnitude to trigger waveform captures on PQube3s with distinct voltage depression, though still considered pre-faults as they do not trigger any protection operation or loss of supply. Successful reclose events are also an avenue of analysis in OHL networks. Since current and voltage profiles are present in both these instances, the direct impedance-to-defect methodology can be applied and a forward line impedance plotted. This has given good performance in two scenarios, but there is currently insufficient data to estimate an overall accuracy comparison against the driving point voltage methodology. Further analysis is required to compare the results from the driving point voltage methodology and the capture of larger pre-fault events using the PQube devices. It is recommended that where voltage and current waveforms have been captured by the PQube devices and there is a notable voltage depression, that the direct impedance distance to fault methodology is used. See Figure 6.5.2, detailing a timeline of predictions from pre-fault to post-fault (all predicted using the direct impedance-to-defect methodology applied to class I waveforms).

Figure 6.5.2: Timeline of defect location on OHL network using the direct impedance-to-defect methodology on PQube3 waveform (followed by post-fault location and comparison to later confirmed location).

Note, that the search zone provided in Figure 6.6.2 for the pre-fault event is larger than for the post-fault (auto-reclose) as it includes an error bounding of 10% to account for the lower confidence in the application of impedance-to-defect to pre-fault than to post-fault waveforms. Despite this, larger search zones can feed into routine overhead line patrols by helicopter teams (since these inherently allow for patrolling of larger areas).

Furthermore, large PQube3 pre-faults provide a potential indication of proximity to failure, as in both instances so far, the subsequent post-fault followed very shortly after the pre-fault disturbance (6-7 days), see Figure 6.6.3 giving a comparison between the pre-fault time and the post-fault time. Figure 6.6.4 gives a comparison between the location predictions for pre-fault and post-fault in this instance. In both instances, pre-fault activity ceased once the post-fault cleared.

Current profile for large pre-fault captured on 20/05/2023 at 23:13.

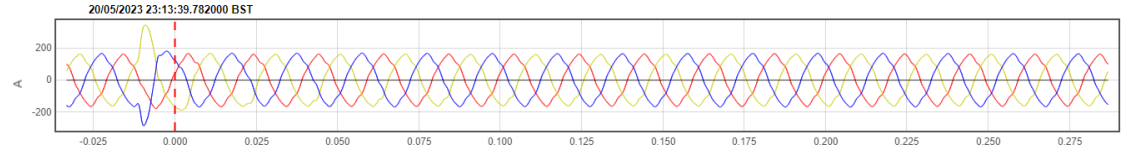

Current profile for post-fault which occurred on 27/05/2023 at 17:05, only one week later.

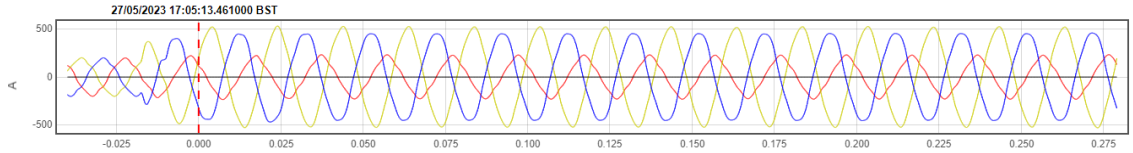

Figure 6.5.3: Comparison between pre-fault capture and post-fault capture time as well as location predictions.

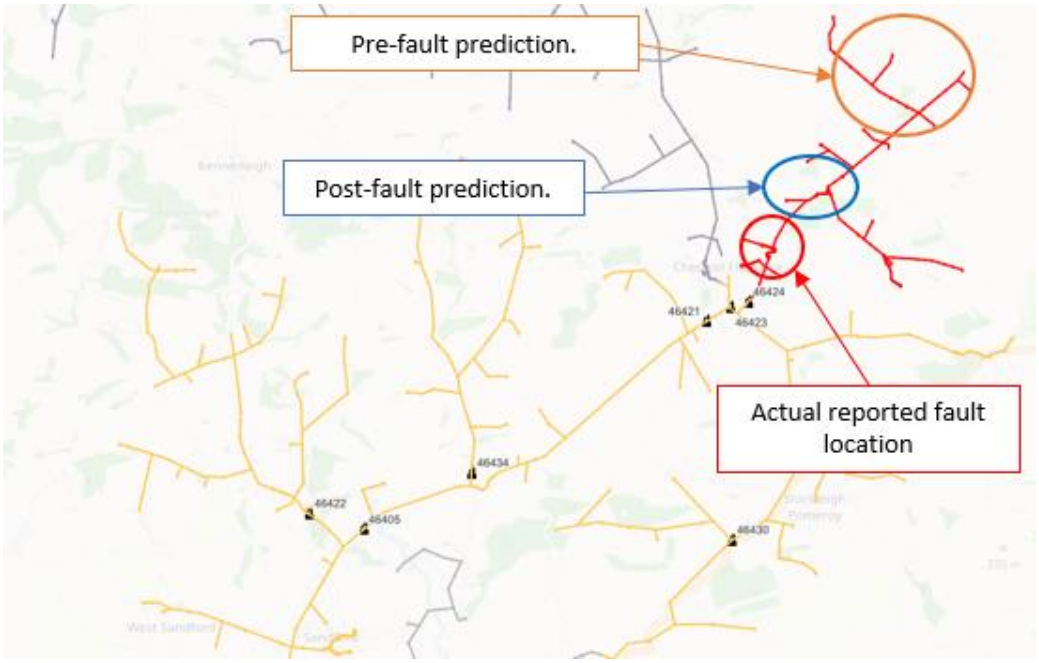

Figure 6.5.4: Comparison between pre-fault predictions (20/05/2023) based on impedance-to-defect from the PQube3, post-fault prediction (27/05/2023) and subsequent confirmed actual fault location (later attributed to blown fuses).

In figure 6.5.4 the pre-fault prediction, represented by the orange oval, is bounded by a 10% error bounding, whereas post-fault prediction, represented by the blue oval, is arbitrarily sized for visibility.

Comparisons of accuracy between the driving point voltage methodology and the direct impedance-to-defect methodology are difficult due to a low sample size of cases where the impedance-to-defect approach was applicable (i.e., very large pre-faults recorded by Class I devices). Both methodologies have suggested potential for good accuracy, with 3/3 successful location efforts using the impedance-to-defect methodology, and 11/12 successful locations using

the driving point methodology. It is recommended that the more analytic impedance-to-defect methodology is applied to class I waveforms where possible (where pre-fault current magnitude exceeds 500 Amps), and the driving point methodology is applied using Class II waveforms for the remaining majority of pre-fault activity.

7. Post-Fault

Post-fault events, or events where network protection is triggered, were targeted as a potential cost saver from the Pre-Fix project, as the algorithms involved are capable of estimating both the location and the cause of these events. Throughout most of the Pre-Fix project, this has been a retrospective exercise, but the functionality to analyse faults as they occur has been developed in such a way that location predictions can be provided within 10-15 minutes of an event.

7.1. Post-Fault Detection

What worked well?

Waveform distortion-based triggers performed well at capturing post-fault events on Class 1 and 2 devices.

Class 1 devices had success with capturing post-fault events with voltage-based triggers.

Using Class 2 devices to cross-trigger waveform captures on Class 1 devices allows captures to be triggered with the same sensitivity of Class 2 devices.

What was or should be changed/improved?

Current inrush triggers are ineffective at capturing smaller post-fault events without also capturing noise, but if given higher thresholds are capable of capturing large post fault events without the risk of noise.

7.1.1. Waveform triggering

As with pre-fault captures, success with a trigger based on waveform distortion on both Class 1 and Class 2 devices has been observed in post-fault scenarios. In these cases, the devices will compare each waveform cycle with the previous one and trigger an event and a waveform capture when the residual error between the two cycles exceeds a certain value. Reasonably early in the project, a current-based distortion trigger for the power quality monitors was developed and this trigger was also more successful in post-fault conditions as it was in pre-fault conditions than previously attempted triggers.

Unlike pre-faults, post-faults do show obvious effects on the voltage of the waveform, meaning that voltage-based triggers are useful to detect them. Current inrush-based triggers had poor performance picking up post-faults at the beginning of the project, and again these triggers have shown a propensity for noise in peak loading conditions so are not recommended. The current inrush-based triggers were ultimately phased out of the project quite early on due to this.

There has also been some success with using Class 2 devices to trigger Class 1 devices (as described in section 3.1). As Class 2 devices can typically be configured to be more sensitive than Class 1 devices without capturing as much of the excessive noise previously described, this allows for some waveform captures that wouldn't otherwise be possible, as shown in Figure 7.1.1, where a cross-trigger allows the capturing of a single-phase event which causes a current increase of just under 100A for the PQube, meaning it would not have triggered based on current settings.

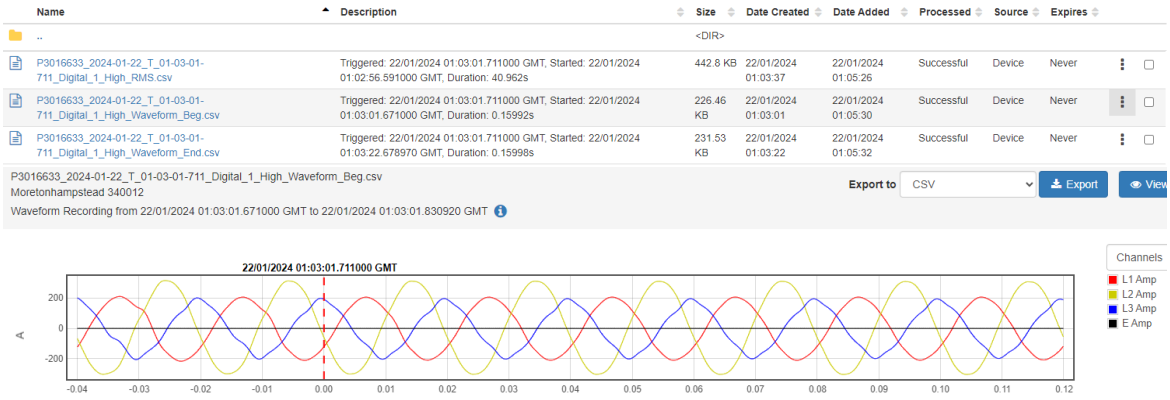

Figure 7.1.1: Waveform capture from a Class 1 device that was triggered by a Class 2 device.

7.1.2. Device Settings

As with pre-faults, device settings need to balance ability to detect faults with not making the device so sensitive that it triggers consistently on minor waveform deviations during peak loading. This balance has been experimented with during the project to try to find a suitable trigger level, and a level of either 100A or ~5% of the Primary 1ph RMS break rating residual error for 10% of a cycle has been found to be a suitable level for class 1 devices. Class 1 devices also had success with voltage-based triggers that triggered on a swell/sag of 10% of normal phase-phase or phase-earth readings, as well as rapid voltage changes of 3% for either phase-phase or phase-earth readings. Between June 2023 and mid-January 2024, there were 173 reported fault events, and with these triggers enabled, 111 events were captured. Of the 62 events not captured, 41 of these were due to power supply disruptions to the unit as described in the next section. The remaining 21 events not captured were due to a mixture of reasons, including the class 1 device filling its event capture buffer, as well as communication issues at the time of the event. Ultimately, these have been grouped together as a combined category of “event not captured” due to device performance. A breakdown of the event results can be seen in Figures 7.1.2 and 7.1.3 below.

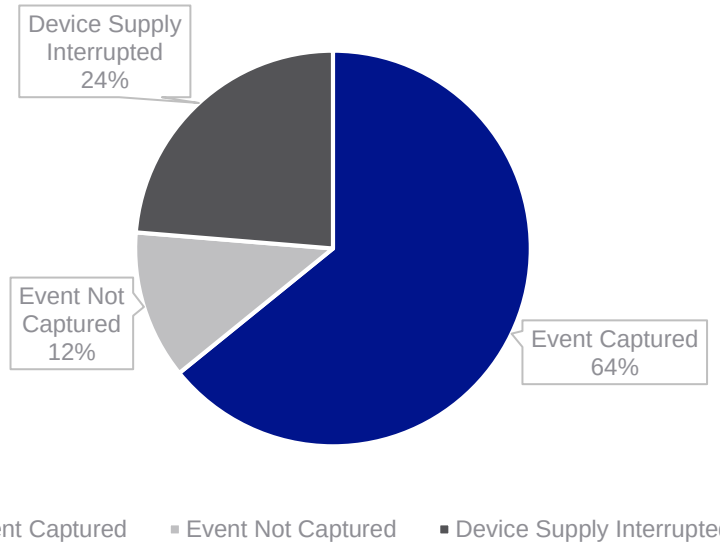

Figure 7.1.2: Breakdown of Class 1 device performance for faults reported between June 2023 and mid-January 2024

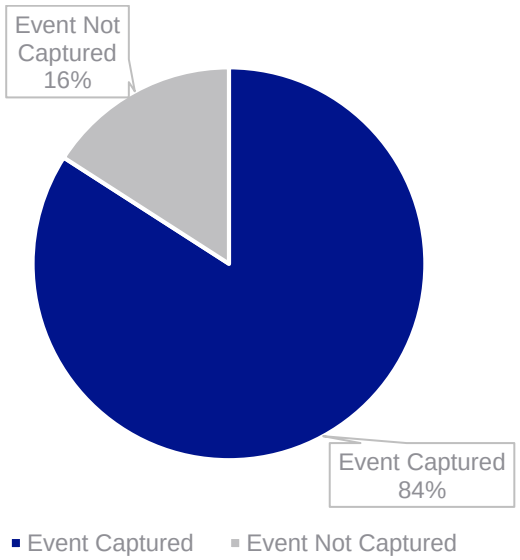

Figure 7.1.3: Breakdown of Class 1 device performance for faults reported between June 2023 and mid-January 2024 excluding events where the Class 1 devices power supply was interrupted.

As discussed before, Class 2 devices can afford to be more sensitive with residual error triggers, as they typically will be installed in locations with a lower load than Class 1 devices. In this case, a 20A residual error between samples at the same point on the cycle has been a suitable trigger condition.

7.1.3. Device Installation

It has been observed that installation of Class 1 devices using the 110V DC tripping batteries in the Primary substation is preferable to installing using the normal 230V AC supply where possible. This is due to some faults causing an interruption to the 230V AC supply in the substation itself,

which causes the Class 1 device and the communication hub to lose power and restart which means fault waveforms are not captured. The method of connecting devices straight to the 230V AC supply was selected as a rapid install method in order to collect data during the trial. In any future installs the recommendation is to use a 110V DC supply where possible, and in scenarios where this isn't available then the devices powered from the 230V AC supply should have a back-up battery/UPS. This issue has been most prevalent in phase-earth fault conditions, though has been observed once in phase-phase fault conditions, so is not solely a phase-earth fault phenomenon. As can be seen from Figure 7.1.1, this has the potential to affect ~25% of event captures, making it a priority when considering future installs. The loading of the Class 1 devices and communication hub used in this project was bench-tested before any installs, and showed that in almost all cases, less than 100mA was required to keep the devices powered on a 110V DC supply, shown in table 7.1.4, though this would need to be repeated for other Class 1 devices in order to safeguard the batteries in the case of an actual event.

Table 7.1.4: Class 1 device and communication hub loading on a 110V DC power supply

Situation Observed	Reading	PQube & Envoy Loading (mA)	PQube Only Loading (mA)	Envoy Only Loading (mA)
Device Power-Up	Max at Spike	274.58	287.09	115.33
	Max After Spike	98.08	67.35	29.72
	Average After Spike	77.09	50.12	20.77
Device Baseline	Max	88.22	63.03	29.37
	Average	70.94	48.13	20.40
Event Capture and/or API Upload	Max	95.02	70.73	30.39
	Average	72.55	49.02	19.03

For the sake of the various algorithms involved in the system, it was assumed that parallel transformers were equally loaded at all times, and using this assumption had provided promising results though has not conclusively proven this to be the case. In future, installations of multiple Class 1 devices at a single substation could be utilised to prove or disprove this hypothesis.

Screening cables and CTs was found to improve the ratio of signal to noise captures, though the most major contributor to this, particularly on class 2 devices, was to install the device with a CT that matched the CT on site. For example, if the CT ratio on site was 500/1, a 1A:0.333V CT was recommended over a 5A:0.333V CT. Using the wrong CTs led to a significantly higher level of noise captures, to the extent that it often filled the memory banks of the Class 2 device and reduced the chance of capturing actual events.

7.2. Post-Fault Location

What worked well?

Post-fault location for phase-to-phase and three-phase faults has been highly successful, with 23/24 successful fault locations (ranging from accuracies of 7m to 600m) across all types of network topologies. Case studies during storm conditions have also proven capability of successful fault location, with backup analysis methods even in rare instances where devices have filled their waveform capture quotas, through analysis of summary files. Location efforts for phase-to-earth faults have been made possible on underground cable networks via pre-fault location aimed at the phase-to-phase pre-faults which precede them.

What was or should be changed/improved?

The accuracy of phase-to-earth fault location is not as effective as phase to phase fault location in saving operational time during fault location. Analysis of the fault loop impedance path has shown that the impedance loop is heavily dominated by the neutral (or liquid) earthing resistor, introducing additional uncertainty. Additionally, a lack of known locations for phase-to-earth faults (as most are of transient nature) has made it difficult to numerically estimate fault return paths for different topologies of network. Work is ongoing to further develop the process, but in future, would be improved by more confirmed fault locations.

For the purpose of post-fault location, electrical faults can be classified into the number of phases affected and whether there is any earth return component.

The relative proportion of faults classified as phase-to-earth, phase-to-phase or three-phase are represented in the pie chart below which is based on 160 detected post-faults (including transient faults and successful recloses).

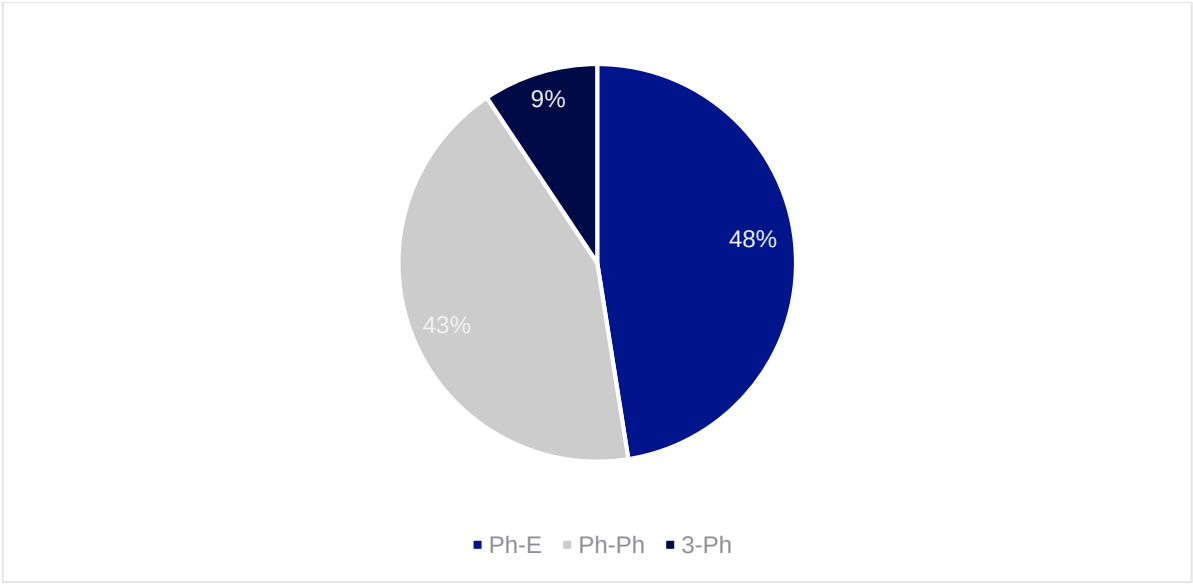

Figure 7.2.1: Pie chart breakdown of detected post-faults (160 in total), classified phase-to-earth (Ph-E), phase-to-phase (Ph-Ph), or three-phase (3-Ph), for the trial period June 2022 to December 2023.

A high confidence FPI search zone can be deployed on C-DIP and provided to field staff almost immediately for all fault types. This is because FPI search zones only consider the direction of fault passage and no information about the phases affected, or the return path. The only dependency of the FPI search zone is correct installation of FPIs in the correct locations and reliability of device communications.

The following sections will discuss learnings with regards to fault location on different fault types. This is then followed by several case studies detailing post-fault location on various network topologies.

7.2.1. Phase-to-Phase Faults

Post-fault location on both phase-to-phase and three-phase faults has been highly successful with 23/24 successful fault locations across all types of network topology (see section 7.4 for full table of performance). The success of the results was attributed to the certainty in the phase-to-phase fault loop. This is because the forward and return paths of the fault loop travel through the electrical conductors and their impedance is known with a high degree of certainty.

Three-phase faults (which accounted for 14 out of 160 faults captured) can be analysed using the phase-to-phase methodology, whether balanced or unbalanced, by selecting the point-on-wave where the third phase current travels through the zero-crossing and, thus, the contribution at that particular point in time can be assumed to be negligible.

Evolving faults (e.g., phase-to-earth evolving to phase-to-phase to three-phase) can be analysed by focusing on the phase-to-phase portions of the waveform. Similarly, whilst unbalanced three-phase-to-earth faults carry uncertainty in the quantifying the earth return impedance, this can be overcome by analysing the phase-to-earth or phase-to-phase portions of the waveforms during fault evolution (see example in Figure 7.1.7).

7.2.2. Phase-to-Earth Faults

Pre-fault disturbances on underground cable networks were observed to be predominately phase-to-phase, even in the instances where the subsequent fault was phase-to-earth (pre-fault anomalies were linked to phase-to-earth post-faults if predicted pre-fault locations aligned with actual reported locations, and if pre-fault activity dropped off after the post-fault). This allowed the phase-to-phase analysis methodology to be applied with adjustments for the voltage in the pre-fault domain. Performance has been successful in predicting phase to earth fault locations through locating phase to phase pre-faults, with six of six phase-to-earth cable faults landing in the same switching section as the confirmed post-fault location via pre-fault analysis.

The main challenge in post-fault location was locating earth faults on overhead line networks. Detailed analysis has been performed on the fault loop impedance path of phase-to-earth faults on HV feeders of three different Primary substations within the Pre-Fix trial area. In all cases, the fault loop impedance path was found to be heavily dominated by the Neutral (or Liquid Neutral) Earthing Resistor (NER/LNER) with this impedance element alone representing 97% - 99.5% of the entire fault loop impedance. When combined with uncertainties in the earth return path (due to, for example, changes in soil resistivity), the errors in quantification could lead to significant variation in determining the fault location based on the predicted versus actual fault location. It is clear that a small error in assumed NER/LNER impedance and earth resistivity can lead to a significant difference in the overall impedance path (ultimately leading to inaccuracies in the location of earth faults). A recommendation has been taken forwards by NGED's business to assess LNER impedance characteristics more frequently (to update for evaporation etc) to provide accurate up-to-date impedance data for fault location purposes. Based on empirical observations, Pre-Fix identified uncertainties in LNER impedances but the methodology was not modified to

account for this in calculating earth resistivity (as the systematic quantification of errors was outside of project scope). However, accounting for the uncertainty in LNER impedance in the methodology for calculating earth fault resistivity will be a focus on follow-on work.

Learning was captured with regard to the fact that the distance to fault functionality will need to be sensitive to inaccuracies in network data, varying quantities of earth return impedance and non-linear arc behaviour.

Each LNER will most likely lose liquid over the six years between maintenance activities, but this has many factors, such as:

- How many faults have occurred
- The duration and magnitude of the faults
- Load Unbalance

The neutral is connected to the star point of the winding and/or load unbalance will shift the neutral point, this causes a high base current flowing through the LNER to compensate for the neutral point shift. This will cause more liquid to evaporate.

There is no way of quantifying which sites are worst affected until the maintenance/routine inspection is carried out and, at present, the impedance of the LNER prior to maintenance is not recorded. Therefore, it is recommended that existing policies are updated to provide the requirement and guidance for recording the measurement of the resistance pre-maintenance (as well as post-maintenance).

At time of writing, 12 out of 75 phase-to-earth post-faults (55 of which were transient) experienced during the trial have confirmed locations and coincident PQube3 captures. More confirmed fault locations are required to extrapolate earth return paths and calibrate ohm/distance values for different topologies of network. For faults with known locations, the earth return path has been quantified in Table 7.2.2, giving some insight into the plausible range of the earth return impedance per network topology (0.6-2.1Ω/km for OHL networks; 0.4-1.0Ω/km for mixed topology networks; 0.08-7.2 Ω/km for UGC networks), but insufficient to make accurate estimates.

Table 7.2.2: The variability of the earth return path impedance/km for phase-to-earth faults of confirmed location. Note: Events on 04/07/2023 and 08/05/2023 occurred on same circuit.

Date	Time	Region	OH/U	Z_{lumped_fault} Ω/k
09/09/2023	07:08	South West	OH	**0.643**
25/03/2023	19:53	South West	OH	**2.108**
29/11/2022	05:20	South West	OH	**0.607**
02/12/2023	15:41	East Midlands	OH/UG	**0.459**
04/07/2023	18:43	East Midlands	OH/UG	**0.977**
08/05/2023	13:15	East Midlands	OH/UG	**0.501**
14/09/2023	23:45	East Midland	UG	**0.623**
18/08/2023	10:19	East Midlands	UG	**0.683**
10/08/2023	06:19	East Midlands	UG	**4.871**
24/02/2023	13:21	East Midlands	UG	**0.081**
24/02/2023	13:21	East Midlands	UG	**0.72**
19/06/2022	19:28	East Midlands	UG	**7.197**

The current plausible range of range of impedance/km values for the earth return creates an overall error in search zone size of approximately 3000 metres as demonstrated by the geographical visualisation in Figure 7.2.3, below. Figure 7.2.3 shows the 3km accuracy range depicted by the purple circle, within a 7km portion of one feeder. This does not currently provide sufficient accuracy as to deploy resource to a specific area but search zones can still be provided and D2F locations may still give staff some insight into what switching locations to target to reduce Customer Minutes Lost (CMLs).

In the later stages of the trial, an alternative approach to calculating phase to earth post-fault locations was explored and showed some promise in improving the accuracy of D2F calculations to below 1000m. This alternative method is still being trialled and will be further refined as more phase to earth faults occur on the monitored circuits. There are plans to integrate this method into the C-DIP and the automated distance to fault functionality.

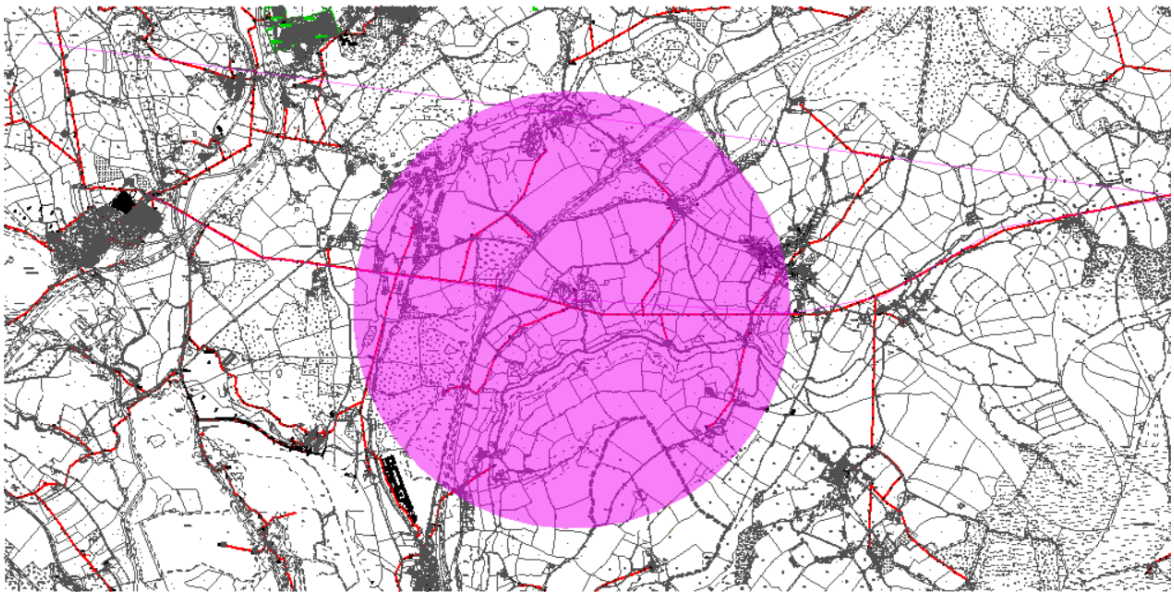

Figure 7.2.3 Phase to Earth Fault D2F accuracy plot.

Case Study: Overhead Line Fault

A fault occurred on an OHL network at 20:46 on 4th September 2023. Both the FPIs (Smart Navigator 2.0s) and the PQube3 detected the fault. A correct search zone was indicated by the FPIs, and the PQube3 was used to determine an impedance to fault and plot a fault location. Figure 7.2.4 shows the fault current observed during the fault, which caused HV fuse operation. Figure 7.2.5 shows the indicated FPI search zone, the DTF location and the actual location of the fault.

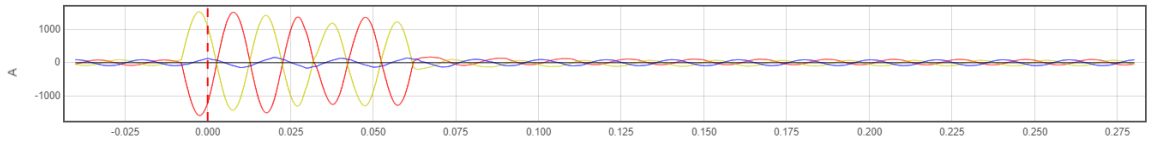

Figure 7.2.4: Fault current as observed from PQube3 during the OHL fault on 04/09/2023.

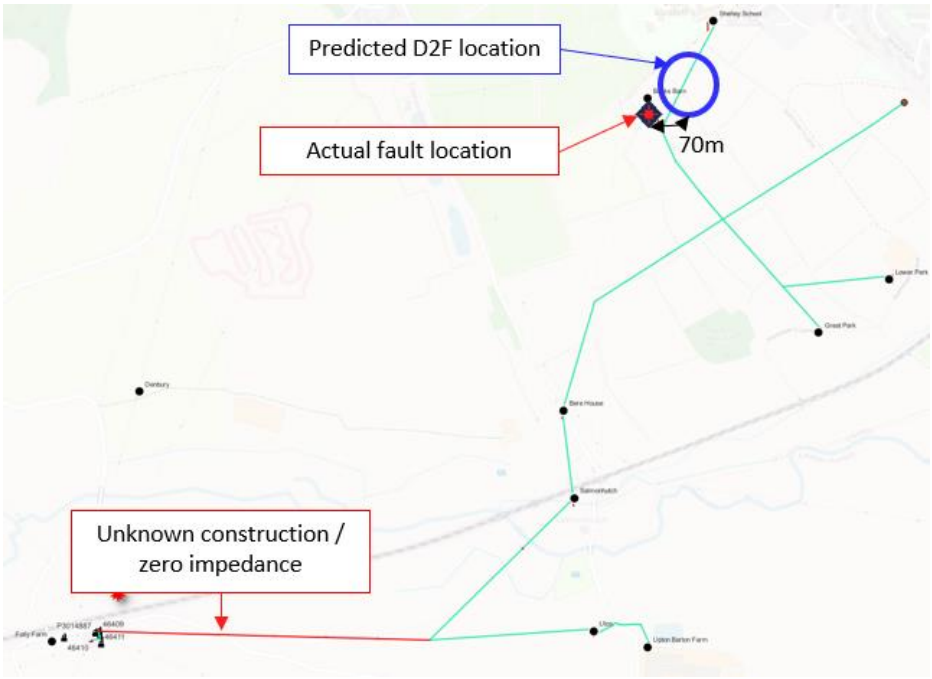

Figure 7.2.5: Fault prediction (DTF) and actual fault location for OHL fault on 04/09/2023.

In this case, the prediction was within 70m of the actual fault location, despite a section of unknown construction (red) which was assigned an estimated impedance/length, based on assuming same proportion as the rest of the network. This would have facilitated line patrols responding to the fault to be sent to actual fault location immediately, significantly reducing fault response times and associated CMLs.

Case Study: Underground Cable Fault

A fault occurred on an underground cable network at 05:07 on 14th July 2023. The fault was detected by both the FPI (feeder breaker NX44) and PQube3. The fault was observed as an evolving phase-to-phase (to unbalanced three-phase) fault which was later attributed to a faulty breach joint, see Figure 7.2.6 showing the current profile at the start of the fault. The NX44 was used to make pre-fault predictions using the driving point (DP) methodology which landed in the same circuit section as the subsequent post-fault. The distance-to-fault methodology was applied on the post-fault waveform and also landed in the correct circuit section, in proximity of the actual fault location (which was reported at later time). See Figure 7.2.7 for geographical representation of the results.

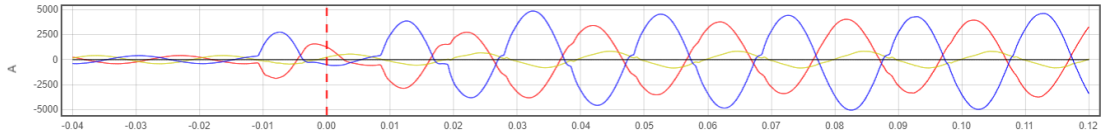

Figure 7.2.6: Fault current as observed from PQube3 during UGC fault on 14/07/2023.

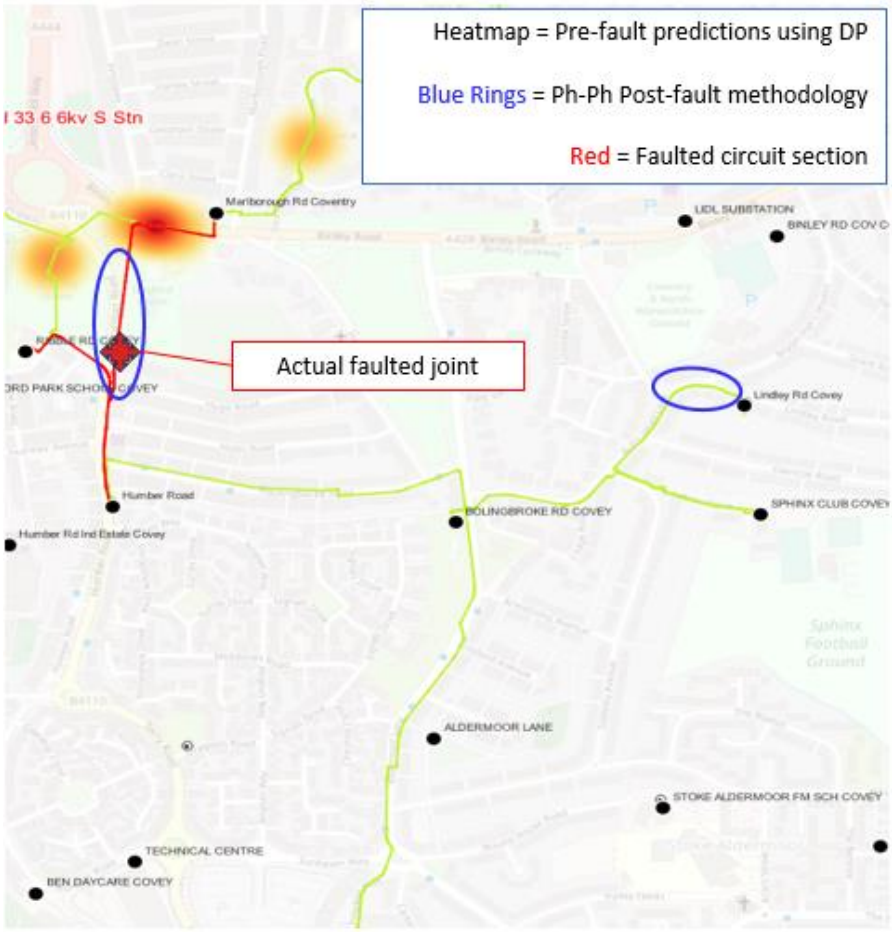

Figure 7.2.7: Fault prediction (blue ring) and actual faulted joint (red indicator) for fault on 14/07/2023. Heat spots show pre-fault predictions with a weighting based on current magnitude.

In this instance, the pre-fault predictions landed in the same circuit section as the post-fault predictions. The pre-fault heatmap would have informed staff of a potential issue within the circuit section and the post-fault D2F would have enabled quicker circuit section isolation and subsequent repair works following post-fault.

Case Study: Mixed OHL/UGC Topology Network Fault

A fault occurred on a mixed topology network at 04:15 on 10th December 2023. Both the feeder breaker FPI (NX44) and the PQube3 detected the fault. The fault in this instance was observed to be a balanced three-phase fault, see Figure 7.2.8, and was later attributed to a faulted joint. A correct search zone was indicated by the FPIs, and the PQube3 was used to determine an impedance to fault and plot a fault location (blue ring - showing predicted cable sections) in which the actual faulted joint was within, see Figure 7.2.9.

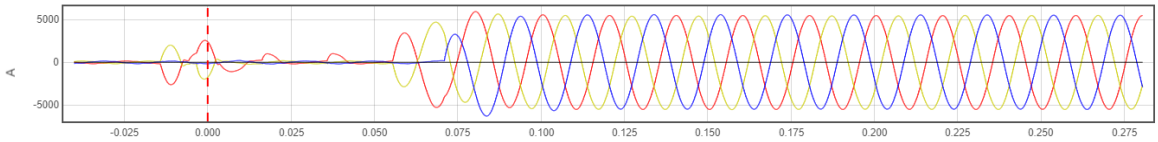

Figure 7.2.8: Fault current as observed from PQube3 during the network fault on 10/12/2023 showing a three-phase disturbance.

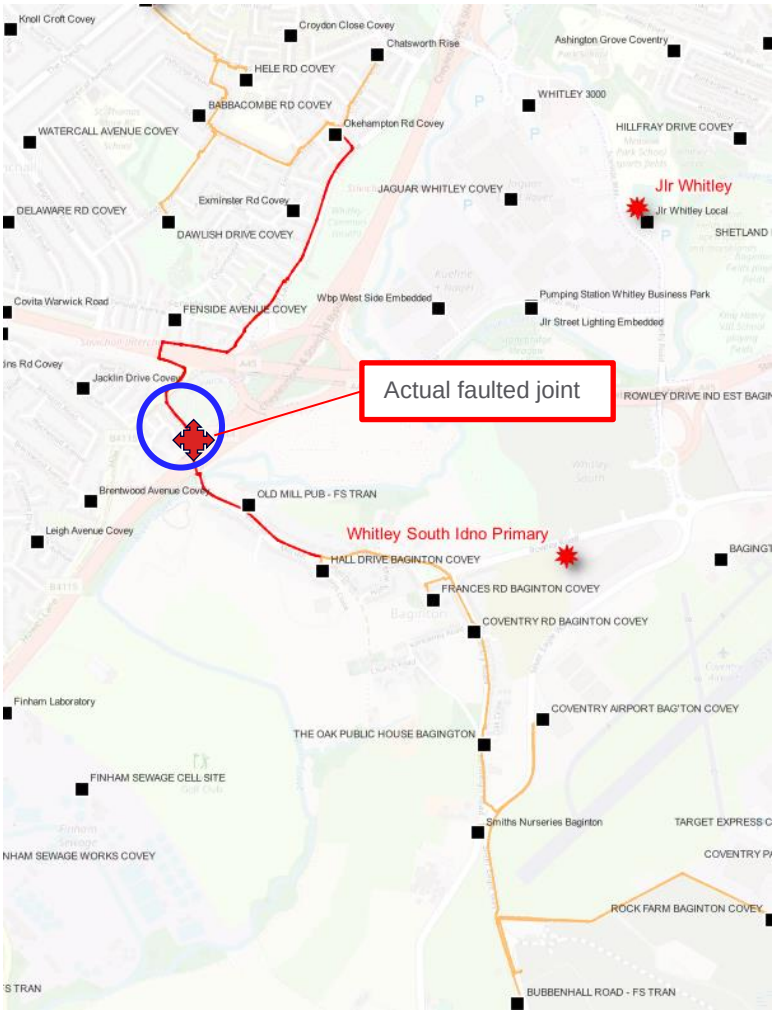

Figure 7.2.9: Fault prediction (blue ring) and actual faulted joint (red indicator) for fault on 10/12/2023.

A successful prediction would enable response teams to quickly identify and isolate the faulted circuit section in preparation for repair and replacement efforts.

Case Study: Storm Conditions

Storm activity in January 2024 led to a significant amount of fault activity on the overhead line networks in the South West trial area. This resulted in significantly increased device trigger rate and provided an opportunity to test the performance of the Pre-Fix system under stress conditions (i.e., where the system is flooded with a large volume of data in a short period of time). The following case study demonstrates an example of successful post-fault location under storm conditions.

An overhead line network, particularly prone to post-faults, was instrumented with PQube3s and NX44s on the feeder breakers (with cross-triggered PQube3 captures). These devices have daily and hourly quotas for waveform captures but are able to summarise events (in the form of XML summaries and binary logs) beyond their quota limits. This proved useful on 02/01/2024 when, despite reaching its daily quota due to abnormal stormy conditions, the PQube3 was able to provide a summary file with current and voltage metrics which were used to successfully predict the location of a fault to within 600m, see Figure 7.2.10. This case was also notable, as at the time of fault, an adjacent feeder from another substation was back-feeding the faulted feeder, giving a total feeder length of approximately 110km. This demonstrated good performance was possible even under abnormal network running arrangement.

Figure 7.2.10: Fault prediction (blue rings) compared to actual fault location (red ring) based on PQube3 summary file captured under stormy conditions.

Such a prediction would facilitate a much faster response to the fault from line patrol (potentially reducing time to locate the fault by several hours through sectionalising the line to the smallest impacted section therefore restoring supplies to more customers in less time). In this case, caused by conductors down – easily observable from a distance of even 600m. Further test cases are required to test the performance of post-fault location using PQube3 summary files and to build confidence in the storm response. A recommendation moving forward is that PQube3 summary files are ingested into C-DIP and analysed in real time (rather than post-event) as in this case.

Case Study: Pro-Active Switching from Real-time Fault Location

The C-DIP platform was tested in real time operations by generation of FPI search zones within 10 minutes of an FPI or PQube3 alarming (note, a 10-minute lag was configured intentionally to allow time for devices in low signal areas to call in). In one example, a transient phase-to-earth fault (see Figure 7.2.11) was detected on an overhead line network. The PQube3 and Smart Navigators both picked up the fault and a search zone was automatically generated as seen in Figure 7.2.12.

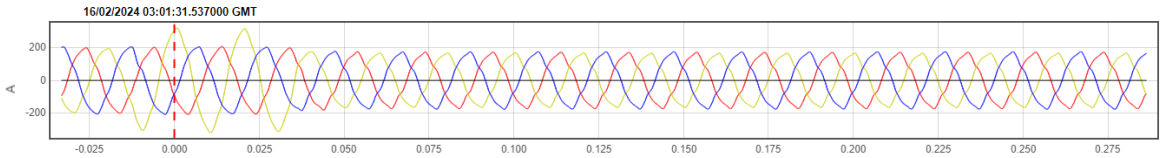

Figure 7.2.11: Fault current observed from PQube3 for transient phase-to-earth fault on overhead line network on 16/02/2024.

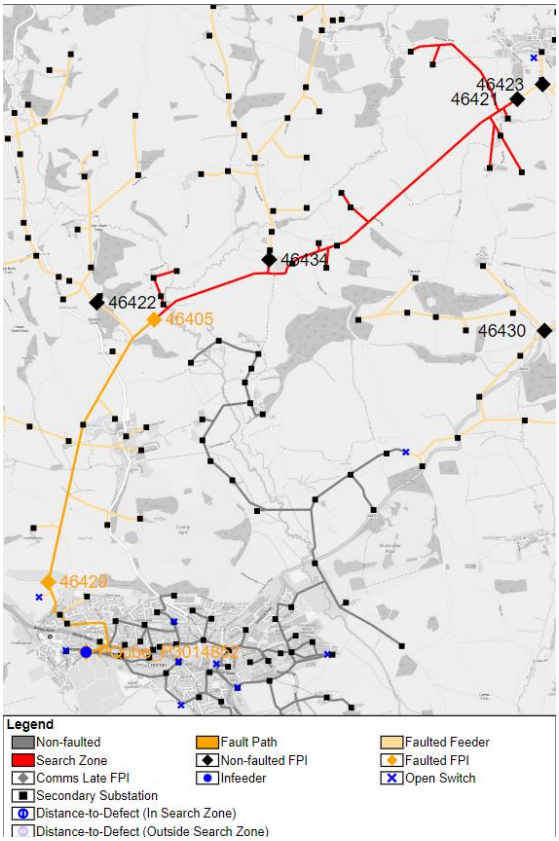

Figure 7.2.12: FPI search zone generated for transient phase-to-earth fault on overhead line network on 16/02/2024.

Based on the search zone generated by C-DIP, an operational switching decision was made to switch customers on the bottom half of the circuit (i.e., beyond the FPI search zone) onto an adjacent Primary. This meant that in the case of a repeat transient fewer customers would be interrupted and fewer customer-minutes-lost would be incurred (more notable for customers who have experienced repeat interruptions to their supply). Following on from this, an Air Break Isolator

(ABI) faulted on 21/02/2024. In this instance, the number of customers interrupted was reduced from approximately 1000 in the prior event to only 200 based on an operational switching decision informed by C-DIP.

Case Study: Potential Conductor Slap

A fault occurred on an OHL network at 01:05 on 10th September 2023. Both the FPIs (Smart Navigator 2.0s) and the PQube3 detected the fault, however the standard methodology for Ph-Ph post-faults resulted in a location approximately 1.5km away from the reported location of down conductors. Additionally, the FPI search zone did not align as expected, being upstream of the fault location. Manual inspection of the waveform identified a smaller current spike (implying further from Primary) at the start of the fault waveform, as highlighted in Figure 7.2.13.

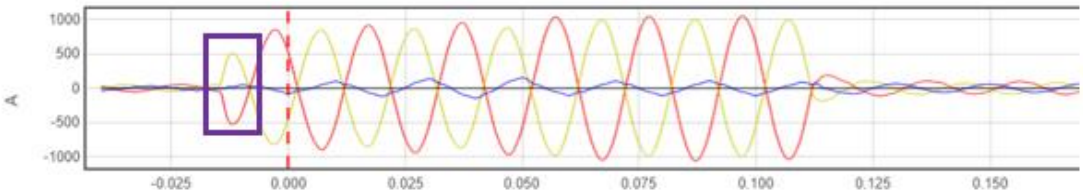

Figure 7.2.13: Fault current as observed from PQube3 during the OHL fault on 10/09/2023, showing potential conductor slap.

It was proposed that this may have been an example of conductor slap, where fault current from down conductors towards the end of a feeder induced clashing of conductors upstream and consequently another fault (represented by a larger spike in current which signifies a defect closer to the Primary). This would also explain why the location of the downed conductors was beyond the FPI search zone, as the FPI search zone would have instead been for the induced upstream fault caused by the conductor slap. Furthermore, Figure 7.2.14 shows that ranging the smaller current spike at the start of the fault gives a prediction much closer to the actual fault location of the downed conductors (within 250m).

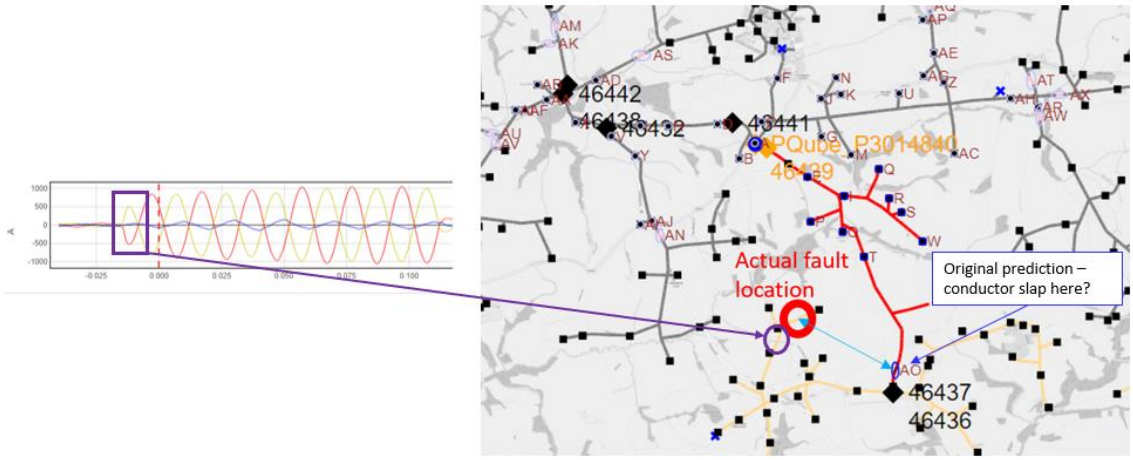

Figure 7.2.14: Comparison between original distance-to-fault prediction (blue rings), the actual location of down conductors (red ring), and manual analysis of the smaller spike at the start of the waveform (purple ring) for OHL fault on 10/09/2023.

This example demonstrated the potential for refining what seems to be an initially negative outcome through manual analysis. No other similar examples were observed during the course of the project.

Further illustrative post-fault location case studies can be found in Appendix B.

7.3. Post-Fault Classification

What worked well?

Faults were able to be identified by a convolutional neural network matching those seen in the IEEE report PES-TR73.

13 new categories of fault have been identified during the project based on confirmed fault causes reported by field teams

What was or should be changed/improved?

Multiple CNN models are required due to the differences in device sampling rates, inputs, and positions on the network.

Some categories have to be consolidated into more general categories that may not specify an asset due to similarities causing false positive results.

Unlike the mostly Class-2 based analysis of pre-fault waveforms, post-faults have been captured with a mix of Class 1 and Class 2 devices. As with pre-faults, the initial training of CNN models was based on the IEEE PES-TR73 report, and field data was later used to retrain CNN models. It is easier to verify whether certain waveforms belong to certain faults than it is for pre-faults, as post-faults are regularly investigated, and the root cause confirmed, meaning that the retraining of the CNN model for new categories is a much simpler process. This also makes it easier to verify the predictions made by the model in future when using the data from the field.

Based on the findings from the classification method so far, the minimum specification for device waveform captures to be usable in post-fault methodology matches those of the lowest sampling rate so far (32 samples per cycle), though a higher sampling rate to capture the waveform distortions in more detail is preferable. As well as this, having both current and voltage readings provides significantly greater accuracy when distinguishing between otherwise similar post-fault waveforms, and it is recommended that any device that was looking to have a trained model developed during integration to C-DIP would be able to record both metrics.

To determine the accuracy of the CNN model at predicting the post-fault asset affected, 28 faults with reported causes and locations across 12 feeders that faulted during the project and had had the fault cause confirmed on site were analysed, and whether the post-fault waveform classifications matched the findings of the field teams has been summarised in table 7.3.1. These faults include both the 18 faults referenced in the pre-fault section that had a pre-fault build up analysed, as well as 10 fault events from the South West area Primary trial substations, which are composed of primarily OHL rather than underground cable.

Table 7.3.1: Results from the analysis of post-fault waveform classification against known fault causes

Faulted Asset	Number of Events	Classifier Asset Prediction
Cable Joint	3	Cable Joint x3

Cable	3	Cable x2, Cable Joint x1
Cable or Cable Joint (Unconfirmed)	5	Cable x5
HV Fuse Operation	6	HV Fuse Operation x6
OHL Foreign Contact	2	OHL Foreign Contact x2
Pole Termination	2	Pole Termination x2
Disc Insulator	5	Disc Insulator x3, Not Captured x2
ABI failure	1	ABI failure x1
OHL Conductors down	1	OHL Conductors down x1

Confidence in the results of the classification method requires three points; a large sample size of events classified to allow for consistency to show, a high degree of accuracy when looking at the events classified for a particular asset, and a lack of false positive results when looking at the results from other assets. Based on this and the results in Table 7.3.1, the result with the most confidence would likely be predictions of HV Fuse Operations, while there would be less confidence in the ABI or OHL Conductors results due to a lower number of predictions.

7.3.1. IEEE Waveforms

As with the pre-fault classification, the basis of the post-fault classification model was the IEEE PES-TR73 report, and a convolutional neural network was trained based on the waveforms shown in this report. As the IEEE report contained more post-fault waveforms than pre-fault waveforms, there were more opportunities to see where field data findings match or do not match IEEE examples. A good example of this is overhead line tree contact faults, where observed events that were confirmed by field teams (Figure 7.3.3) had very similar waveforms on the affected phase to the IEEE reported waveform (Figure 7.3.2). Findings from the field data do show significantly more variation in the length of event, though as the IEEE report only captures a few examples of each fault type this is to be expected.

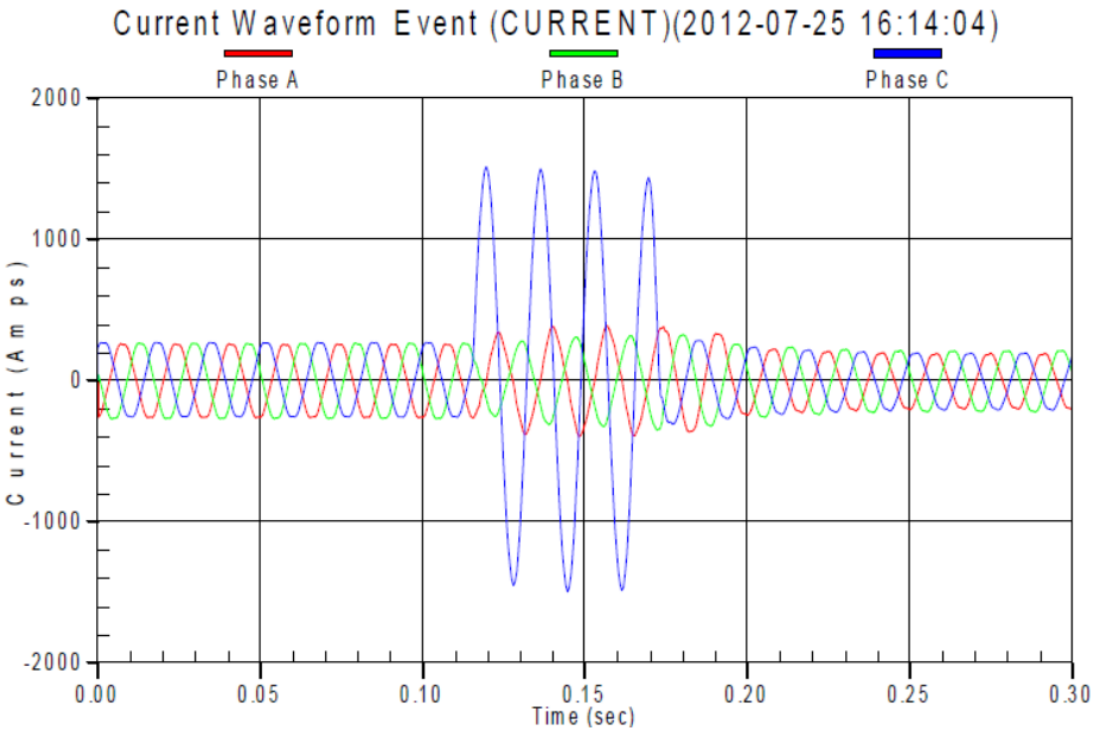

Figure 7.3.2: OHL Tree Contact fault from the IEEE report PES-TR73

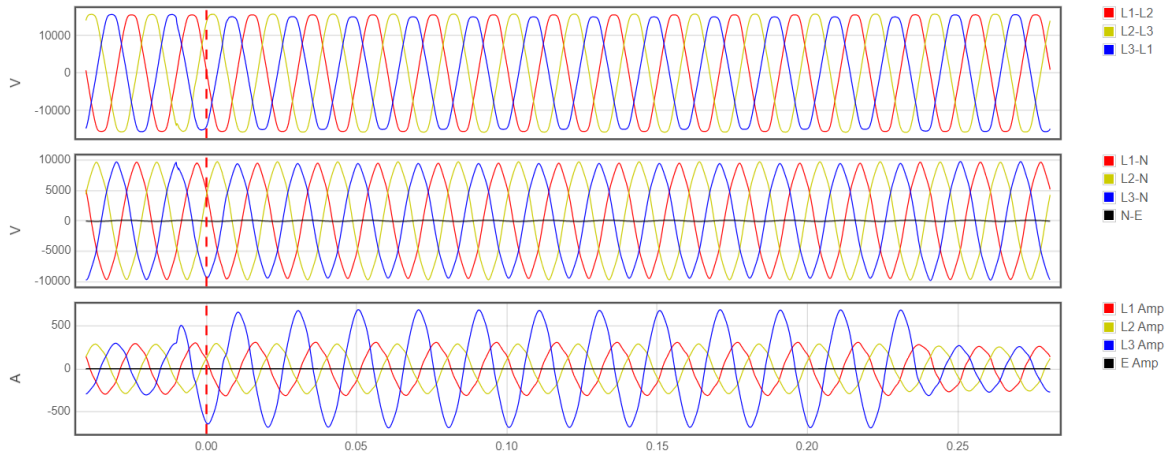

Figure 7.3.3: OHL Foreign Contact fault captured by a class 1 device during the Pre-fix project

7.3.2. New Waveforms

During the project, waveforms for various faults that are not covered in the IEEE report have been captured and analysed. As the root causes of these faults is confirmed by the field team, there is sufficient confidence to retrain the CNN model to recognise these faults as belonging to a particular asset. New fault types from both the Coventry trial area, which is predominantly underground cable, and the South West area, which is predominantly overhead line have been observed, as well as a number of waveforms that are shared between the two areas. Some examples of waveforms captured are shown below in Figures 7.3.4, 7.3.5 and 7.3.6.

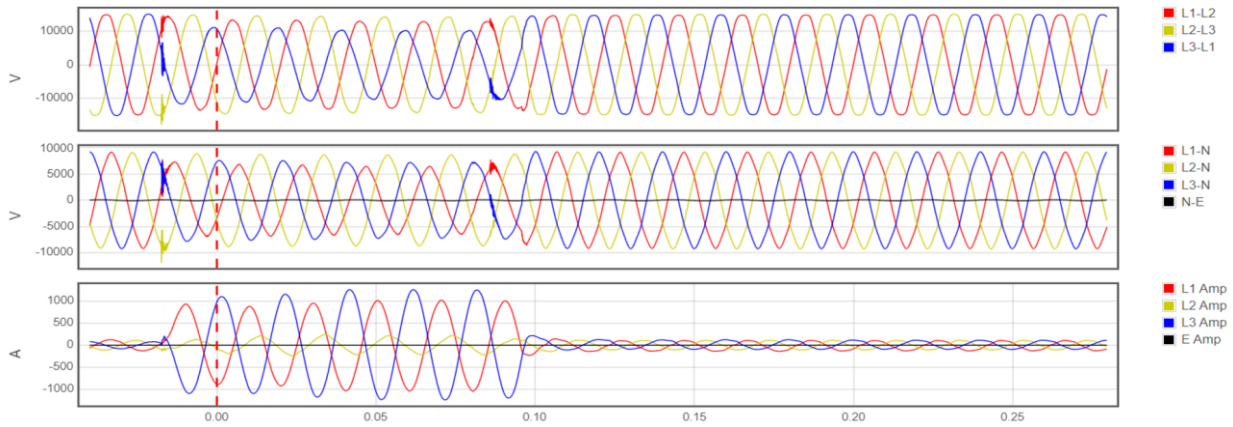

Figure 7.3.4: Pole Termination fault captured by a class 1 device

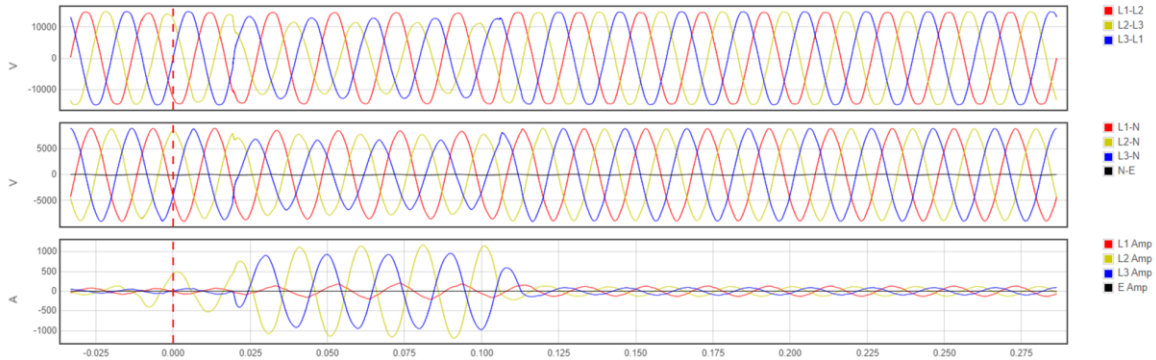

Figure 7.3.5: HV Fuse Operation captured by a class 1 device

An example HV fuse operation waveform is shown in Figure 7.3.5. During the Pre-Fix trial period there was a total of 12 HV fuse operation events where no subsequent network damage was found and the HV fuses were successful replaced. For 9 of these events, there was a PQube fully functional and reporting back into the C-DIP. Out of these 9 HV fuse operation events, the C-DIP captured waveforms and reported the event on 5 occasions. The HV fuse operation was reported by the C-DIP before any customer call-ins and the HV fuses found to be operated on all 5 occasions. The time that the C-DIP reported the HV fuse operation before they were found ranged from 6 minutes to 22 minutes. This time difference would allow the mobilisation of field staff before any customer call-ins and therefore reduce CMLs. The D2F locations provided would also aid field staff in finding the cause of the HV fuse operation as well as quicker customer restoration through replacement of the HV fuses.

On the 4 occasions, where the HV fuse operation was not captured by the PQube at the Primary, the average number of customers downstream of the fuses were significantly lower than the occasions where the event was captured. For the HV fuse operation events captured the average customer numbers downstream was 68, whereas for the 4 events that were not captured this was 9. This suggests that the number of customers downstream of the HV fuses and therefore load may impact on the ability for the PQube at the Primary to pick up on the current disturbance.

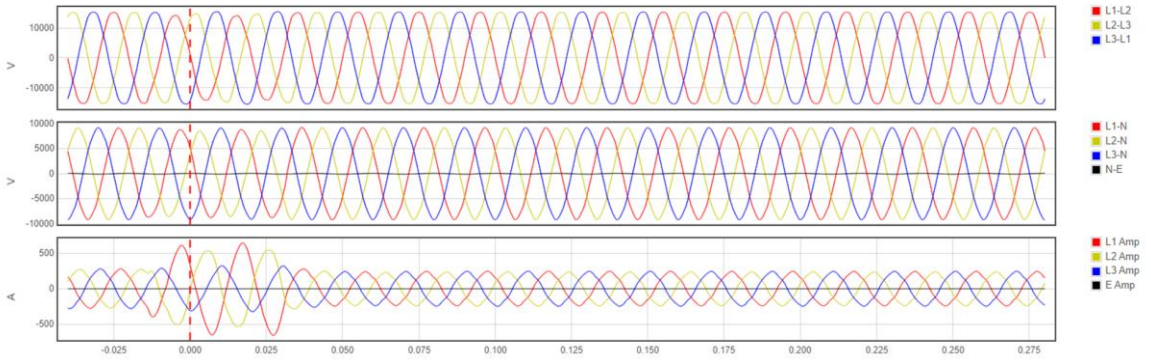

Figure 7.3.6: Conductors down fault captured by a class 1 device

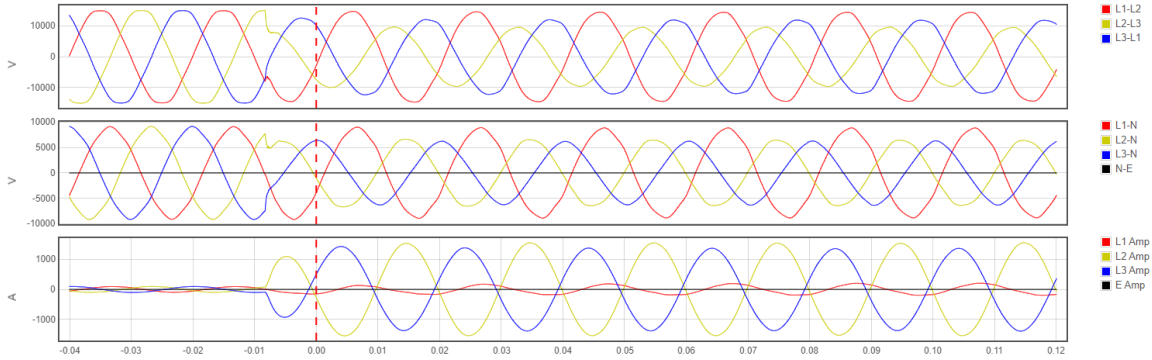

Figure 7.3.7: OHL fault caused by vehicle collision with OHL pole bringing transformer, LV conductors, and HV fuses down captured by a class 1 device

During the project, there have been a number of extremely similar waveforms that have shown the need to consolidate some of the classification categories into a more general category to avoid false positives from the CNN due to extreme similarity. An example of this is with the single-phase OHL foreign contact shown in Figure 7.3.3, and a single-phase ABI failure fault that was observed later in the trial shown in Figure 7.3.8.

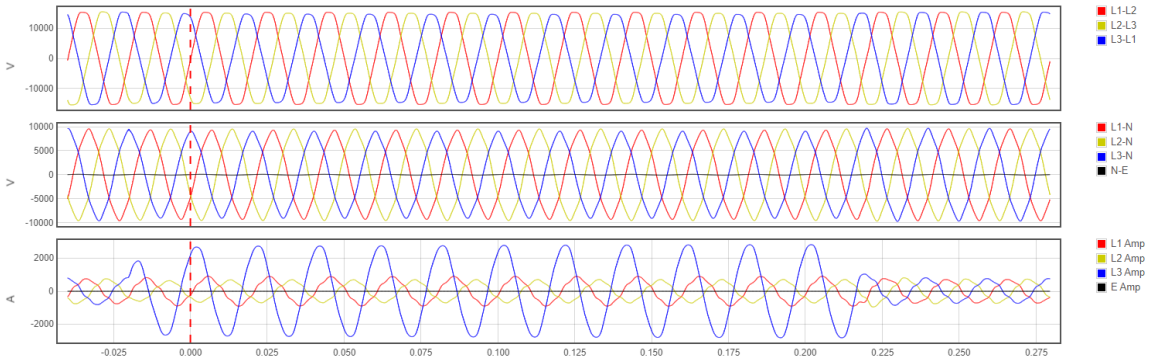

Figure 7.3.8: OHL ABI fault captured by a class 1 device

As both of these waveforms are similar in form, the CNN model has issues predicting one category over the other, and therefore these two categories were consolidated into a single phase-earth category with an undefined asset type.

Another avenue explored in relation to post-faults was whether the type of cable joint present had an effect on the resulting waveform during fault conditions. Several faults on Lovink type cable

joints were analysed, some examples of which are shown in Figures 7.3.9 and 7.3.10, but a common failure signature could not be established.

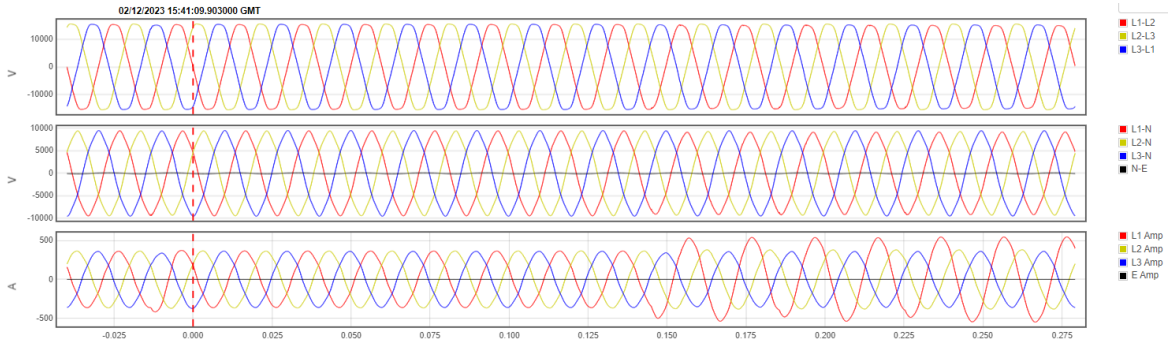

Figure 7.3.9: Lovink cable joint failure at Claverdon Primary captured by a class 1 device

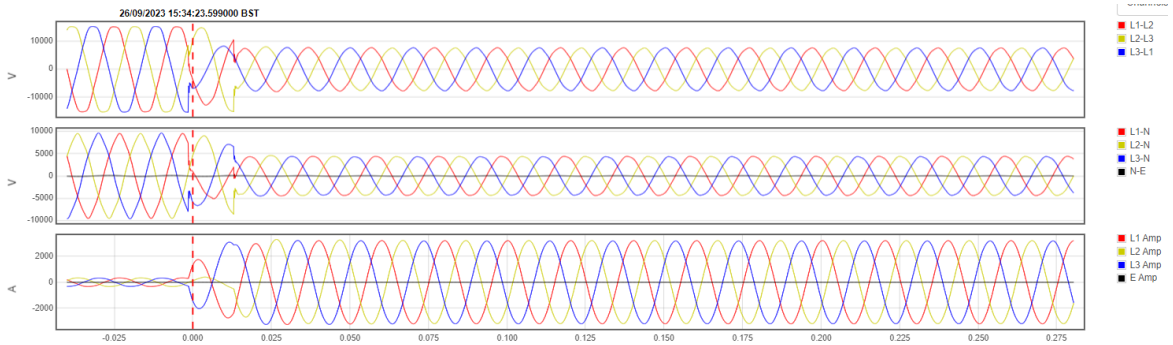

Figure 7.3.10: Lovink cable joint failure at Courthouse Green Primary captured by a class 1 device

As of this point in the project, after consolidating the categories that have required it, 30 potential post-fault waveform categories have been identified, as well as a category that denotes no fault has occurred that is used to help filter out noise. This is up from the initial 16 categories identified from the IEEE report. The additional 14 categories seen are pole termination failures, auto-reclose activity, switching incidents, disc/ABI failures, unplanned manual interruptions, oil fuse switch operation, broken fuse units, conductors down, faulty/cracked insulator, protection maloperation, HV fuse operation, Automatic Power Restoration System (APRS) operation, earth faults, and OHL pole destruction. Examples of the waveforms observed in these categories can be seen in the Waveform Archetypes presentation in Appendix C.

Case Study: Disc Insulator Failure

A particular case study of how the pre-fault and post-fault classification investigation has been conducted is with disc insulator failures, a photo of which is shown in Figure 7.3.11. This is a category that did not exist in the IEEE report, and it was theorised that these faults should have pre-fault events that occur as the insulator breaks down and approaches the failure that causes a fault condition. An investigation into the resulting waveforms from both class 1 and class 2 devices was performed, and a number of common conditions surrounding these failure events were captured, which included both events tied to the insulator itself, and a number of common situations such as Primary-wide events in close proximity to a disc insulator fault. Figure 7.3.11 shows a disc insulator failure waveform that was confirmed on site by a field team at Chudleigh Knighton. The features distinguishing disc insulator failures from some other single-phase archetypes is the significant voltage distortion in multiple phases, even where the current is mostly affected on one phase (blue phase in this case).

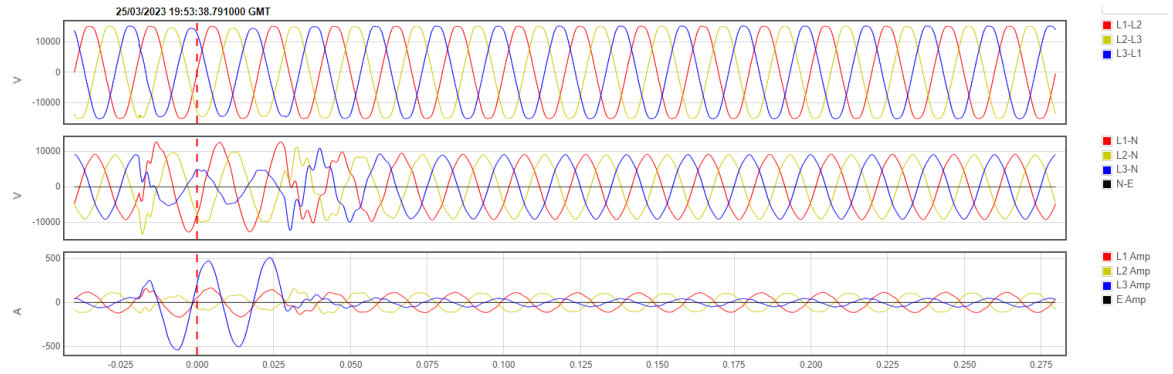

Figure 7.3.11: OHL Disc Insulator fault captured by a class 1 device at Chudleigh Knighton

These faults have shown a build-up of a number of pre-fault and transient fault events in the days before it occurred. Notably, a common feature with these faults is that there is often a transient fault with reclose event that clears the fault in the week leading up to the failure. In this example with Chudleigh Knighton, there was an auto-reclose event the day before the insulator failed permanently, see Figure 7.3.12 for the trip and Figure 7.3.13 for the reclose event. This auto-reclose activity was also observed on two other feeders. As with the post-fault waveform, while the blue phase is the phase that shows significant current distortion, there is significant voltage distortion on other phases throughout the fault.

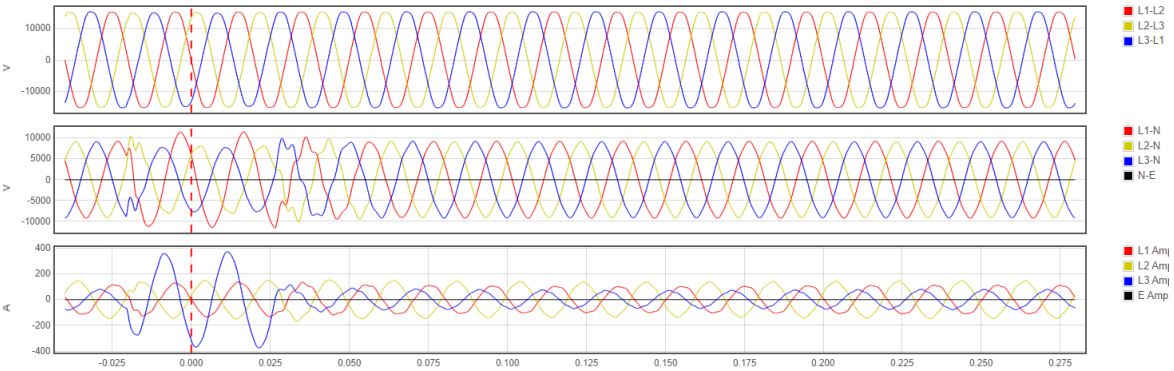

Figure 7.3.12: Class 1 device capture of Chudleigh Knighton transient fault (potential disc insulator "pre-fault" type 1), an event that caused an auto-reclose 1 day before the actual disc insulator fault event

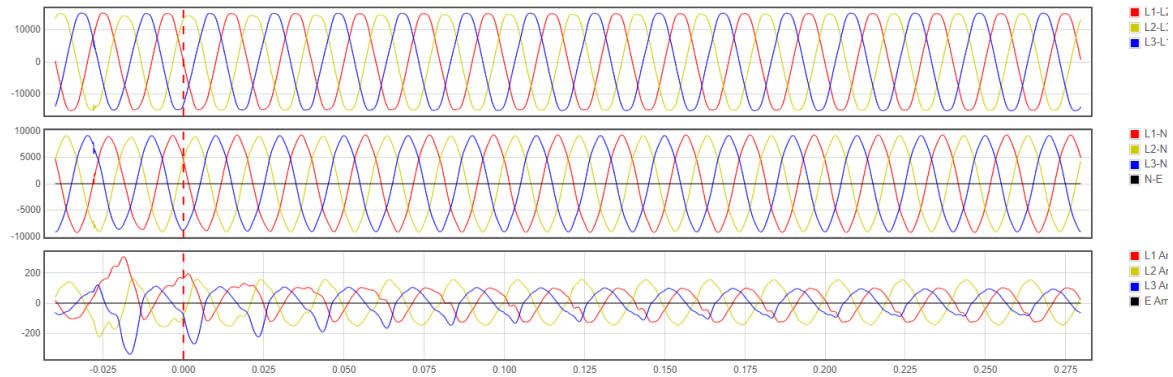

Figure 7.3.13: Class 1 device capture of Chudleigh Knighton auto-reclose event happening ~10 seconds after the previous event

The second type of event shown in Figure 7.3.14, and the first potential pre-fault observed at Chudleigh Knighton occurred 5 days before the fault. Note that the normal phase 3 current at this substation is significantly lower than phase 1 and 2 during normal operations, so the swell in this phase is of the most interest, rather than the other two phases.

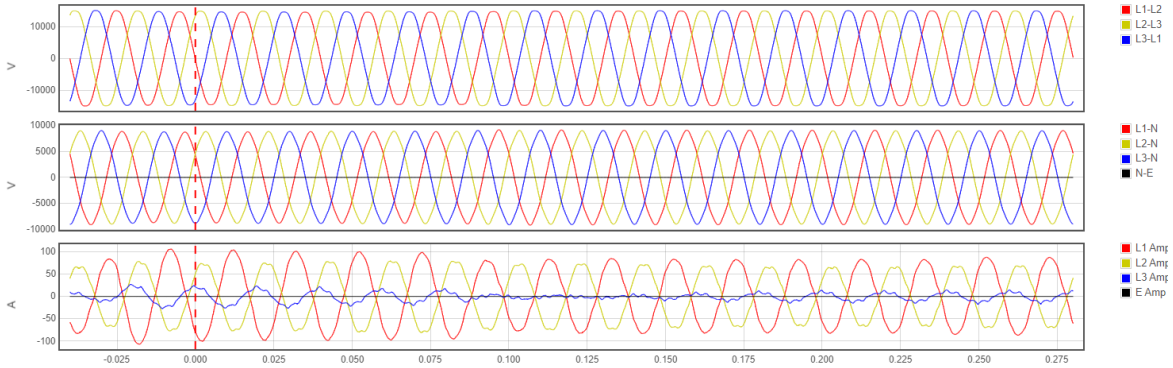

Figure 7.3.14: Class 1 device capture of potential disc insulator pre-fault type 2, a swell in the phase most heavily affected during the fault, captured at Chudleigh Knighton 5 days before the actual fault event.

Other Primary substations which have observed disc insulator failures include Claverdon, which has a number of Class 2 devices installed in the feeder breaker panel. These devices have seen a very different set of pre-fault waveforms in close proximity to a disc insulator event, and not following the disc failure itself.

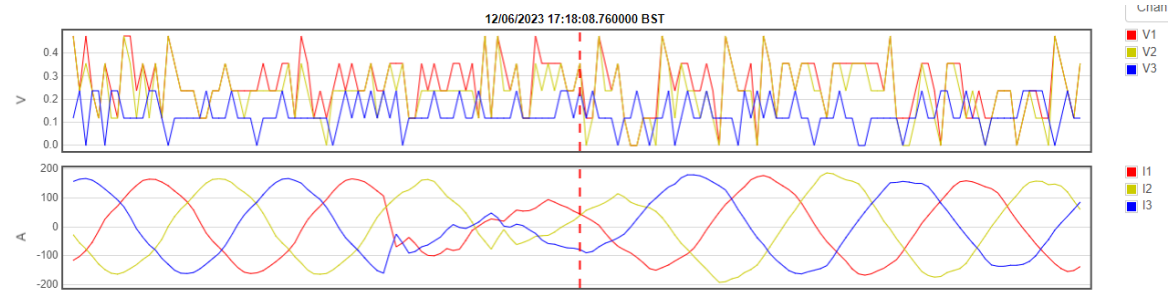

Figure 7.3.15: Class 2 device capture of potential insulator pre-fault type 3, captured at Claverdon ~7 days before fault on feeder 8

The general progression of events has shown that the isolated pre-faults (type 1 and 2, shown in Figures 7.3.14 and 7.3.15) are likely to begin to occur the earliest, with observations of these events happening at least 20 days before the fault event. These events have been observed earlier than this, but the prevalence of faults on the OHL networks during the project meant that other post-fault events occurred earlier than this, making it difficult to attribute these older pre-fault events to being disc insulator related. However, one point in favour of suggesting the events were tied to the eventual disc failure for these older events is that the events continued after other post-faults were reported, but not after the disc failure event. The transient events cleared by reclose activity with waveforms similar to those of the eventual disc insulator fault, show in Figures 7.3.12 and 7.3.13 have been seen as near as 2 hours before, to roughly a day before. It should be noted that at this stage this has only been observed and analysed on one occasion and is a hypothesis at the moment. More data and disc failure events will need to be observed to increase the confidence that the pre-fault events shown here do in fact always precede eventual disc/insulator failure.

The full suite of existing and newly classified waveforms can be found in Appendix C

7.4. Post-Fault Location C-DIP Performance

7.4.1. Performance Metrics

Post-fault location analysis, using impedance based distance calculations has been successful in providing an accurate indication of fault location which could be utilised to deploy field staff more efficiently. The Pre-Fix method successfully located 23 out of 24 phase-to-phase and three-phase faults with confirmed locations as shown in Table 7.4.1. Distance-to-fault (D2F) calculations were deemed acceptable if predictions landed in the same circuit switching section as the post-fault. These predicted locations have been compared to actual fault and incident reports for validation. Predictions have been able to successfully locate all underground cable faults within the correct circuit section, and 14 out of 15 overhead line faults to within 7m to 600m from the actual fault location. The single outlier (highlighted in red) was an overhead line fault experienced on 10/09/2023, which gave a prediction 1500m out of the actual fault location - although this has been suggested as a potential example of conductor slap, see case study in section 7.2.

As discussed in previous sections, the approach has been successful for phase-to-phase faults. Currently, the D2F calculations for phase-to-earth faults are not accurate enough and could not be used to deploy field staff more efficiently.

Table 7.4.1: Ph-Ph and 3-Ph Location Accuracy Assessment

Date	Time	Network Type	Fault Type (Based on Pre-Fix Waveform)	Distance from Confirmed Fault Location
26/02/2024	11:35	Mixed Topology	Ph-Ph/3-Ph	500m
02/01/2024	12:20	Overhead line	Ph-Ph	600m*
28/12/2023	05:08	Overhead line	Ph-Ph	Within FPI search zone**
26/12/2023	15:07	Overhead line	Ph-Ph	200 metres
12/12/2023	20:02	Mixed Topology	3-Ph	Within circuit section
10/12/2023	04:15	Mixed Topology	3-Ph	Within circuit section
26/09/2023	15:34	Underground cable	3-Ph	Within circuit section
10/09/2023	01:05	Overhead line	Ph-Ph	1500 metres
04/09/2023	20:46	Overhead line	Ph-Ph	130 metres
04/09/2023	14:51	Overhead line	Ph-Ph	300 metres
29/08/2023	15:25	Overhead line	Ph-Ph	500 metres
02/08/2023	08:52	Overhead line	Ph-Ph	100 metres
17/07/2023	07:42	Overhead line	Ph-Ph	280 metres
14/07/2023	05:07	Underground cable	Ph-Ph/3-Ph***	Within circuit section
12/07/2023	10:33	Overhead line	Ph-Ph	100 metres
27/05/2023	17:05	Overhead line	Ph-Ph	450 metres
09/05/2023	21:22	Mixed Topology	Ph-Ph	300 metres

23/04/2023	15:57	Overhead line	Ph-Ph	7 metres
12/04/2023	17:56	Overhead line	Ph-Ph	24 metres
19/03/2023	21:47	Underground cable	Ph-Ph	20 metres
10/03/2023	07:28	Mixed Topology	Ph-Ph	300 metres
28/12/2022	14:18	Overhead line	Ph-Ph	160 metres
10/12/2022	09:38	Overhead line	Ph-Ph	240 metres
19/06/2022	19:58	Underground cable	Ph-Ph/3-Ph	20 metres

*Fault occurred during stormy weather conditions and abnormal network running arrangement.

**Actual fault location unknown but from FPI search zone max distance must be less than 600m.

***Fault evolved from Ph-Ph to 3-Ph.

For the sake of comparison, a total of twelve permanent phase-to-earth faults with confirmed location were captured during the trial period. Manually analysing these faults using the current phase-to-earth fault loop model would give accuracies in the range of 1500-3000m. Performance with regards to permanent faults (with confirmed locations) is summarised in Figure 7.4.2. A new method for locating phase to earth faults was initially trialled towards the end of the project and showed improved accuracies, with average phase to earth fault location predictions of 900m. This new method will be further trialled in future and integrated into the C-DIP.

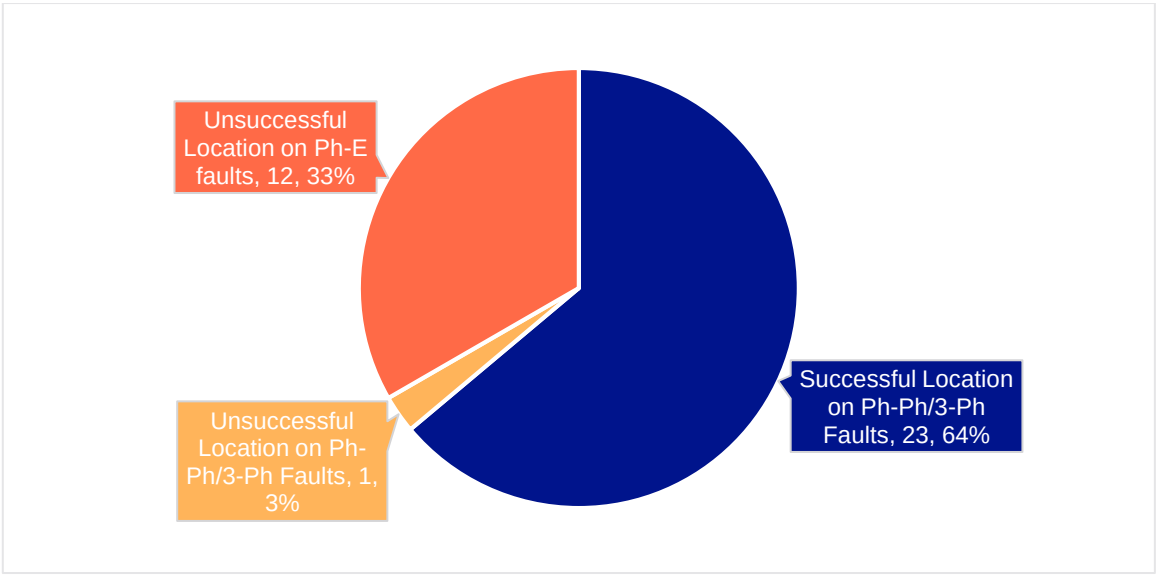

Figure 7.4.2: Pie chart of performance metrics, summarising 36 permanent faults with known locations and coincident class 1 capture during the Pre-Fix trial period.

8. Results Verification

8.1. Pre-Fault Result Verification

There were a number of methods for verifying and analysing Pre-Fix results in the pre-fault domain. Some of these were tested during the project and some are suggestions at this point but will likely be considered for testing in future.

Verification methods that were tested during the project include:

- Running to failure
- Partial Discharge Mapping
- Utilising Helicopter Surveys (including infrared, corona sensors as well as HD cameras)

The other verification methods that will be explored further in future include:

- Cable Overlay
- Proactive Switching (to isolate potential faulty section as a mitigation before cable overlay)

8.1.1. Running to Failure

Throughout the trial period of the project, several circuits experienced a network fault. Although this is not desired when aiming to detect and intervene on pre-faults before they evolve into faults, it has allowed significant learning, development and testing of the pre-fix system and algorithms. By having insight into location and severity of pre-fault defects, quicker network restoration and repair is facilitated when pre-fault predictions and post-fault analysis are combined. During the project, no information was used to facilitate network restoration due to development and testing of the system. Accuracy of the system in predicting pre-fault and fault locations have been detailed in the preceding sections.

8.1.2. Partial Discharge Mapping

Partial discharge (PD) mapping is a proven method for determining the health of underground cables. Circuit sections are isolated from the network and connected to test equipment, energised and tested at various voltage levels. The response of the cable to these testing signals is recorded and subsequently defects in the cable insulation can be determined and located.

The intention of utilising PD mapping in Pre-Fix was to determine if the predictions made regarding location and severity of defects would correlate with the results from PD mapping. The aim of this being to explore if PD mapping could be used as a follow-up to Pre-fix predictions which could then inform overall cable asset health scores and cable overlay schemes.

A total of 8 circuit sections, with pre-fault defects identified, were tested using PD mapping. The circuit sections were selected for defects based on maximum I^2t and highest frequency of pre-fault activity. A further 3 circuit sections with little pre-fault activity present was also tested as part of a control group.

There was very strong correlation between partial discharge activity and predicted locations for pre-fault activity. In all cases where pre-faults were predicted, partial discharge activity was detected with differences in distances within the circuit section of 2-10m. It should be noted that in some instances there was partial discharge activity detected where no pre-fault activity had been seen by the Pre-Fix system. In about 70% of cases where partial discharge was detected, pre-fault activity had been detected. Figure 8.1.1 shows one particular instance where pre-fault activity was detected on a cable joint alongside the location where partial discharge was recorded. Figure 8.1.2 shows the magnitude and frequency of partial discharge for that particular circuit section. In the 3 control circuits, which had little detected pre-fault activity, there was little to no partial discharge observed.

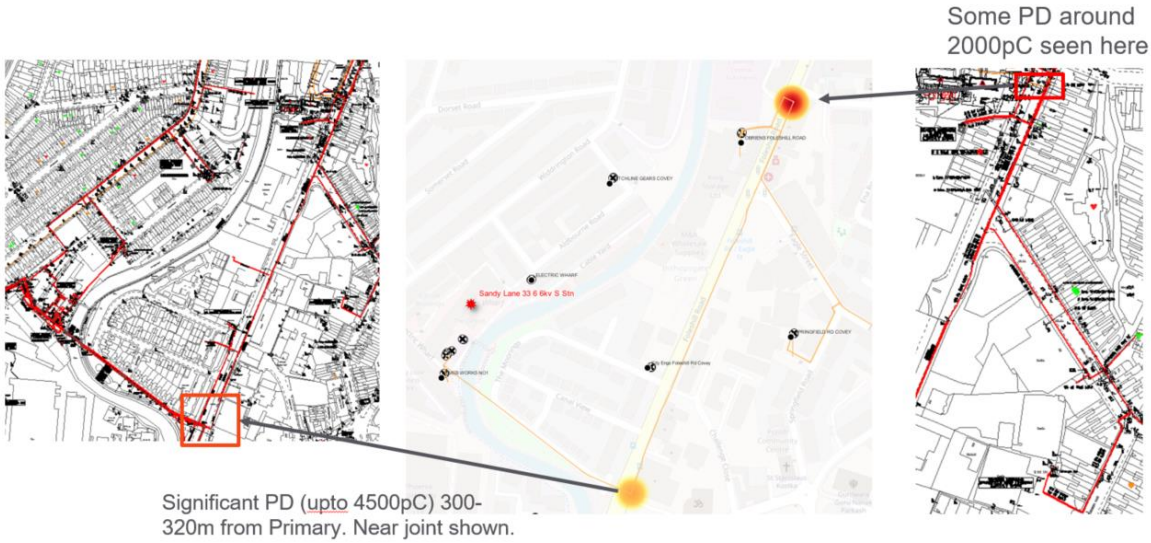

Figure 8.1.1 Pre-Fault Activity (central image) and PD locations (left and right) shown for an underground feeder.

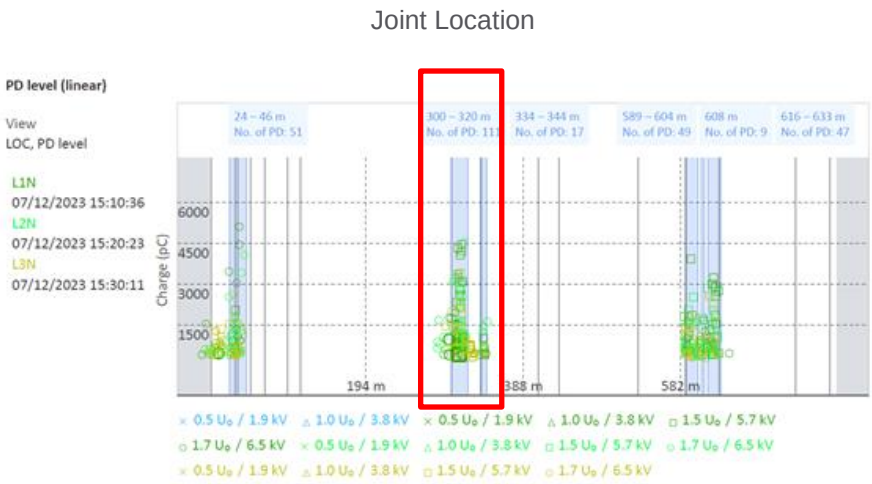

Figure 8.1.2 Partial Discharge level for circuit from figure 8.1.1

From the analysis completed, although there was good correlation regarding location, there was no clear correlation between the current magnitude of pre-fault activity and the partial discharge levels. For example, on one circuit section of a particular feeder where the average peck current magnitude observed was 434A the partial discharge level was 3561 pC, with the average peck current of the adjacent circuit section being 334A and the partial discharge level being 5301pC. There are many factors that could impact this including the fact that the partial discharge testing was completed phase-to earth, whereas the majority of pre-fault activity observed was phase-phase. Due to safety reasons, phase to phase partial discharge testing was not possible. Further testing is required, to understand if any indicators of pre-fault activity correlate to partial discharge levels and what appropriate action would be.

8.1.3. Helicopter Surveys

Specifically for overhead line circuits, another verification method tested during the project was to utilise helicopter surveys to detect issues on the network flagged by the Pre-Fix system. Information gathered by the Pre-Fix system including search zones, predicted locations and defect

classification can be sent through to helicopter units to inform scheduled surveys of OHL circuits. The focus for this can be contact by foreign bodies such as trees or defective insulators. One successful example of this intervention has been shown previously in this report within section 6.2.Towards the end of the project, this method was used more extensively as confidence in the system was gained. For five OHL circuits, where pre-fault activity had been detected and classified, pre-fault locations and predicted causes were passed to NGED's helicopter to patrol. The pre-fault locations were either search zones if the events had only been observed by the OHL FPIs or distance to fault locations, if the event had resulted in protection operating, a successful reclose and the PQube observing the event. On four out of five occasions, the helicopter patrol identified an issue that matched the Pre-Fix waveform classification and matched the location (correct search zone). Three of these were due to contact by trees and one was a damaged insulator. On two of these occasions, where there was a D2F location available, the helicopter unit found the issue 10m and 230m away from the D2F location. On the occasion where pre-fault activity was detected, and the helicopter unit did not identify an issue, the waveform was unknown to the classifier algorithm. At this stage it is difficult to state what the cause might have been and why the helicopter patrol would not have observed this. Further observation of events producing similar waveforms as on this occasion are required to determine the cause and whether it is related to OHL or cable sections of the circuit in question.

It should also be noted that on another occasion where the helicopter was patrolling on one of the circuits monitored by Pre-Fix, there were two insulators identified with hairline cracks present. These were not picked up by the C-DIP. This may suggest that the device settings were not sensitive enough to pick-up on small hairline cracks within insulators on these occasions. Further research is required to understand what device settings are required to enable Pre-Fix to observe these events on OHLs.

8.1.4. Cable Overlay

The ideal situation would be to be able to detect a pre-fault defect and replace the asset as close to failure as possible. This could either be a particular joint or a cable section that has a few critical pre-faults within it. During the project, this intervention has not been tested due to ongoing development of the system and work to increase confidence in the calculations and location predictions before cable overlays are undertaken. To date, pre-fault predictions have landed in the correct circuit section on 11/12 occasions. With this high level of confidence in predicting the correct circuit section, this information can be used to inform decisions regarding which 11kV circuit/sections should be a focus for cable overlay activities. Further research is required to understand criticality of any network anomalies and the time until failure, in order to ensure that proactive cable overlay can take place in a timely manner.

8.1.5. Proactive Switching

Another option when responding to pre-fault location and criticality predictions is to undertake proactive switching on the network. When pre-fault activity has been detected and located to a certain circuit section, before the pre-fault progresses to a fault, the network could be reconfigured through proactive switching to isolate the circuit section in question. There is still uncertainty as to when this proactive switching would need to take place, as there would need to be more certainty that the pre-fault was close to developing into a permanent fault. This could therefore prevent customers from being interrupted and the Pre-Fix system would then indicate if the activity on the circuit is no longer occurring. . This network intervention would be most useful if we could identify the anomaly and track the severity over time, then proactively switch before the anomaly progressed to failure to allow enough time to plan and undertake suitable cable overlay activities or further testing. Further testing, such as PD mapping, could be undertaken to further refine the understanding of the defect location and severity.

8.2. Post-Fault Network Interventions

During the project trial, for most post-fault events suggested network interventions have been hypothetical. Post-fault locations combined with existing pre-fault locations/information can inform both control and field staff, where to switch to reconfigure the network more efficiently and also where to search for the fault. Both of these interventions can help to reduce CMLs. During development of the system, there was a two day delay on data processing and therefore real time information was not available.

Now that the system has been developed and tested, we are at the stage when we can begin to inform staff at the time of fault, regarding both predicted locations and potential causes. This will continue to be monitored as to how many CMLs can be prevented through providing real time information on faults from the Pre-Fix system.

One very recent example is a fault that occurred at the end of February 2024. A number of short interruptions on an OHL feeder had occurred where 939 customers had been interrupted multiple times. Through providing a search zone from the Pre-Fix system, as to where the issue likely was, the network was subsequently reconfigured to transfer the affected section to an adjacent feeder supplying fewer customers.

Subsequently, the fault became permanent and therefore taking customers off supply for longer. However, due to the network reconfiguration aided by Pre-Fix information fewer customers were impacted by this outage, showing that information taken from the C-DIP can be used to make informed and impactful decisions on the network.

8.3. Network Benefit Insights

Towards the end of the trial, once the C-DIP system performance was validated, the results obtained for both pre-fault and post-fault location and classification gave some insight into the potential network benefits that could be gained from deployment of the system into business as usual.

On 3 occasions where a network fault had been detected by the C-DIP, with an automated distance to fault location provided, information was passed to the NGED control room. On these occasions the information was not used for proactive switching but was used to gain valuable feedback from the control engineers on how the information was presented and to gain confidence in the system. Through real time engagement with the control room during these faults, insight was gained into how the information could have been used to reduce outage times. On one occasion, HV fuses had operated meaning that the network had been sectionalised as much as possible and therefore would have been unlikely to have reduced outage times. On another occasion however, the C-DIP provided a fault location that was 400m away from the confirmed fault location. Feedback from the control room indicated that if the information were used to inform switching operations and to direct field staff then the outage time could have been reduced by approximately 60 minutes for 170 customers and by 20 minutes for a further 900 customers. With confidence in the system now established within NGED’s control room, a process is required for how control engineers will receive, process and use the information from the C-DIP to enable these benefits to be realised.

Another approach used towards the end of the trial was to pass information gained from the C-DIP regarding OHL pre-faults was to provide information to operational staff to carry out foot patrols or to proactively reconfigure the network. This approach was used on several occasions where the C-DIP observed successful reclose operations and provided both FPI search zones and distance to fault locations. Operational staff used this information to patrol the areas highlighted by the C-DIP and were able to identify issues that may have been the cause of the protection operation and subsequent successful reclose. Through identifying these issues and repairing the issue or reconfiguring the network, further supply interruptions can be prevented including interruptions that

cause significant time off supply for customers. Confirmation is still required on these circuits that the defect causing the supply interruptions is no longer present through continual monitoring to ensure that the benefits were a direct result of the C-DIP.

As mentioned in section 8.1, helicopter surveys were used to validate some of the defect location and classification predictions made by the C-DIP. On the occasions where the helicopter patrols identified and matched the location predicted by the C-DIP, the information was passed on to operational teams. Through action on these defects and issues, a total of 382 customers will have been prevented from having their supply interrupted. These circuits continue to be monitored for any further activity to ensure that the defects detected by the C-DIP are no longer present and that the benefits can be directly attributed to the insights gained from the C-DIP. Where the pre-fault would be easily observed, such as tree contacts, and D2F locations are available it is likely that the manual foot patrols could find these issues for further intervention. However, the helicopter patrols will still be valuable, through use of thermography, in detecting insulator damage predicted by the C-DIP that is not easily visible from ground level or when the predicted location of the pre-fault activity covers a wider search zone provided by the OHL FPIs.

9. Avenues for Further Research

The following avenues for further research have been identified as a result of Pre-Fix:

- Detection of LV network events using HV network equipment
- Enhance understanding of 3-phase swells and power quality phenomena exhibited by urban (underground cable) HV feeders
- Improving time-to-fail predictions
- Improving overhead-line phase-to-earth fault location accuracy
- Increase confidence in using HV pre-fault information for network interventions
- Assess fault infeeds at primaries with parallel transformers and the impact on D2F calculations
- Understand and classify difference in waveforms from 2-ph spurs and 3-ph sections on OHL
- Handling saturation of CTs (relevant to both NX44s and PQube3s)

Glossary

Abbreviation	Term
3-Ph	Three Phase
ABI	Air Break Isolator
AC	Alternating Current
ADMS	Advanced Distribution Management System
APRS	Automatic Power Restoration System
BaU	Business as Usual
C-DIP	Common Disturbance Information Platform
CI	Customer Interruptions
Class I	Devices that can capture three phase current and voltage waveforms and broadcast the information in operationally useful timescales
Class II	Devices that can capture three phase current waveforms and broadcast the information in operationally useful timescales.
CML	Customer Minutes Lost
CNN	Convolutional Neural Network
CT	Current Transformer
CT	Current Transformer
D2F	Distance to Fault
DC	Direct Current
DP	Driving Point (Voltage)
EMC	Electro-Magnetic Compatibility
FFT	Fast Fourier Transform
FPI	Fault Passage Indicator - A device for tracking abnormal current transients throughout the network
FPI	Fault Passage Indicator
GIS	Geographic Information System
HV	High Voltage. Taken to be 11kV or 6.6kV within this report.

INM	Integrated Network Model
IPR	Intellectual Property Rights
LNER	Liquid Neutral Earth Resistor
LV	Low Voltage. Taken to be 415V within this report.
NER	Neutral Earthing Resistor
NX44	A smart fault passage indicator that is mounted upon a ring main unit
OHL	Overhead Line
PD	Partial Discharge
Ph-E	Phase to Earth
Ph-Ph	Phase to Phase
PowerOn	NGED's control room system for real time management of the network.
PQ	Power Quality
PQM	Power Quality Monitor
RMS	Root Mean Square
RMU	Ring Main Unit
RTU	Remote Terminal Unit
SCADA	Supervisory Control and Data Acquisition
SLD	Single Line Diagram
SN2	Smart Navigator 2.0 – a self-powered overhead line monitoring device
UG	Underground
VT	Voltage Transformer

Appendix

Appendix A: Schneider T300 RMU Pre-fault Detection Test Report

See supplementary document “Appendix A: Schneider T300 RMU Pre-fault Detection Test Report”.

Appendix B: Post-Fault Case Studies

Appendix B contains further case studies on the location of post-faults. Case studies can also be found in Section 7.2.

Case Study: Mixed Topology (OHL/UGC) Network Fault 26/02/2024

An evolving three-phase fault was captured on a mixed topology network at 11:35 on 26th February 2024.

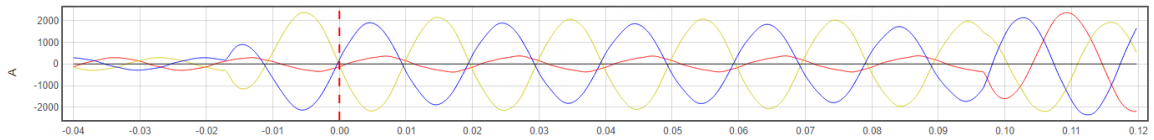

Figure A.1: Fault current profile of network fault on 26/02/2024 showing an evolving 2-Ph to 3-Ph fault.

The Ph-Ph and 3-Ph methodologies were both applied prediction a search zone approximately 500m from the actual fault location (down conductors). For comparison, the total length of the feeder is approximately 21km.

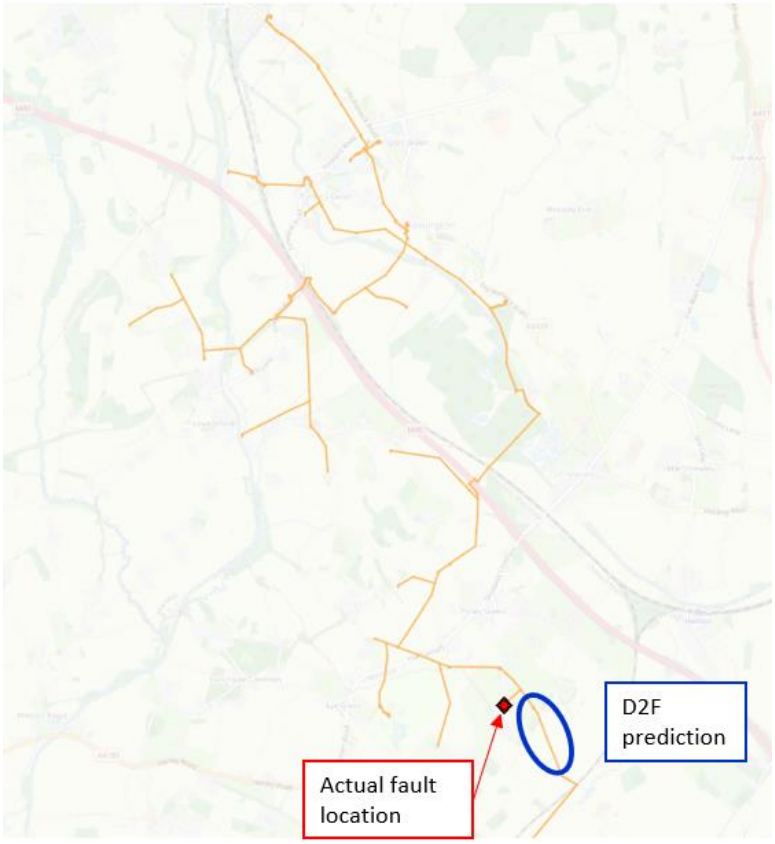

Figure A.2: Fault prediction (blue ring) and actual faulted location (red indicator) for fault on 26/02/2024.

Case Study: Overhead Line Fault 04/09/2023

A Ph-Ph fault was captured on overhead line network at 14:51 on 4th September 2023.

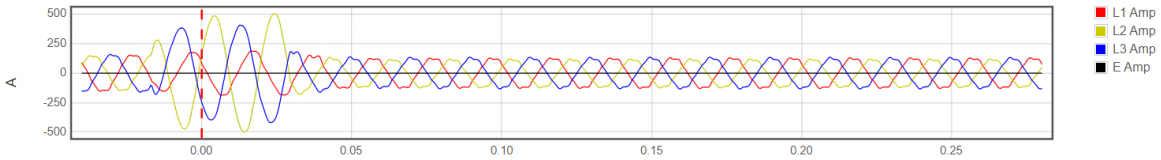

Figure A.3: Fault current observed from PQube for overhead line fault on 04/09/2023.

The Ph-Ph methodology gave several predictions (due to branched nature of network), with one location being approximately 300m from the actual fault location.

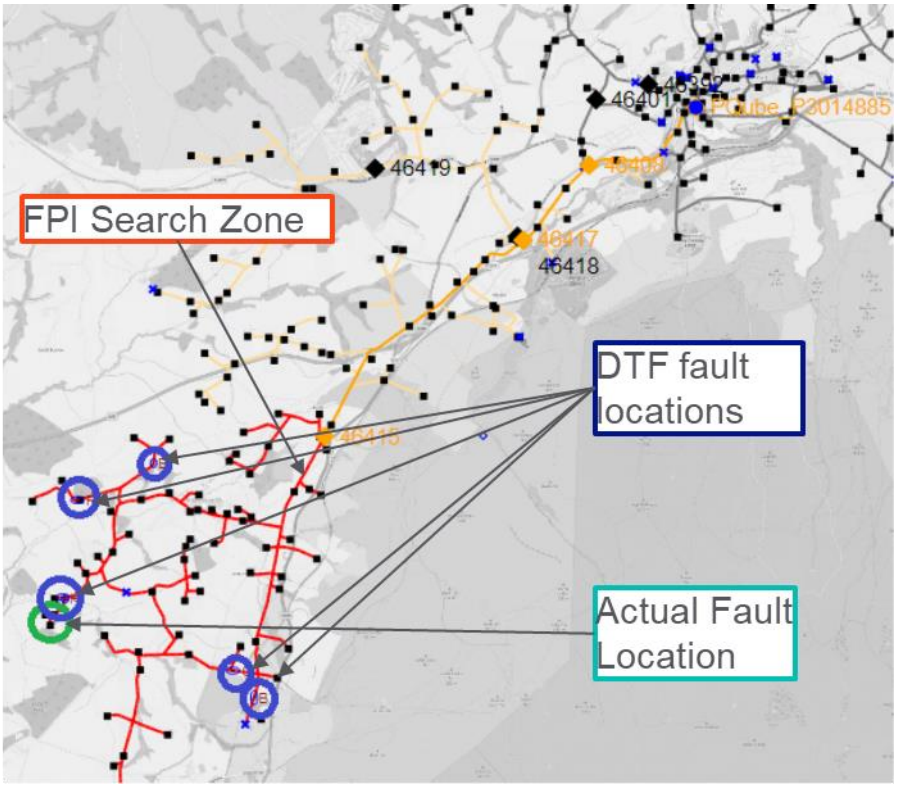

Figure A.4: Fault prediction (blue rings) and actual faulted location (green) for fault on 04/09/2023.

Case Study: Overhead Line Fault 12/04/2023

A Ph-Ph fault was captured on an overhead line network at 17:56 on 12th April 2023.

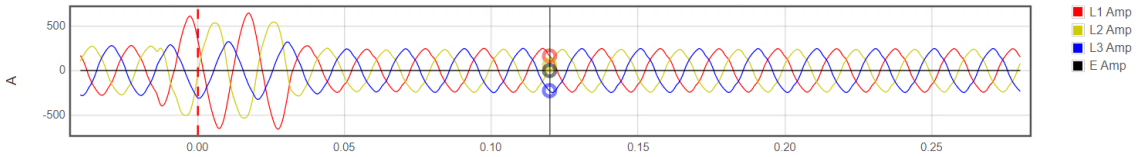

Figure A.5: Fault current observed from PQube for overhead line fault on 12/04/2023.

The Ph-Ph methodology predicted a location approximately 24m from the actual fault location (being downed conductors in this example).

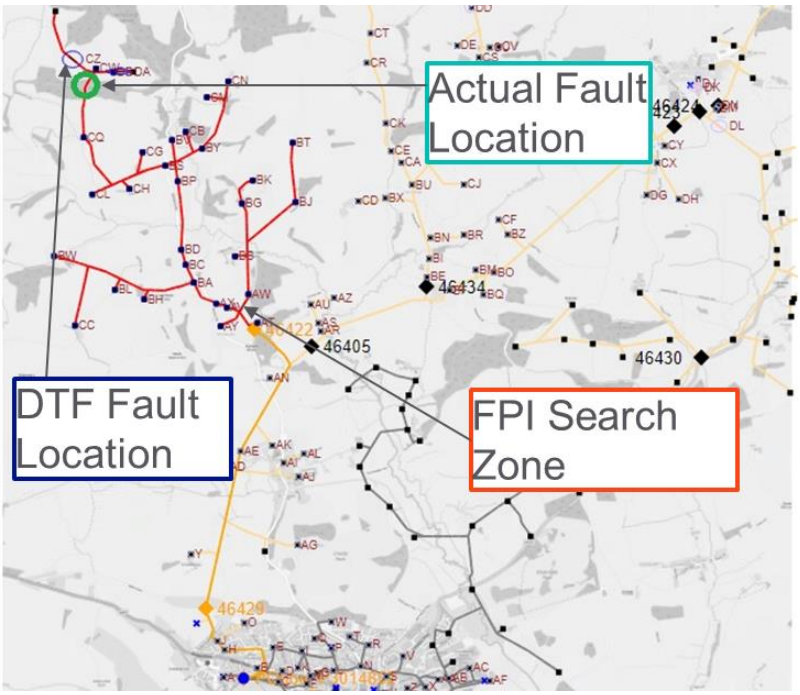

Figure A.6: Fault prediction (blue rings) and actual faulted location (green) for fault on 12/04/2023.

Appendix C: Full Suite of Classified Waveforms

See supplementary document “Appendix C: Full Suite of Classified Waveforms”.

Registered Office: Avonbank, Feeder Road, Bristol BS2 0TB
nationalgrid.co.uk